INTERPRETATION OF RAPID PILE LOAD TESTING

Mr. Van Duc Lam

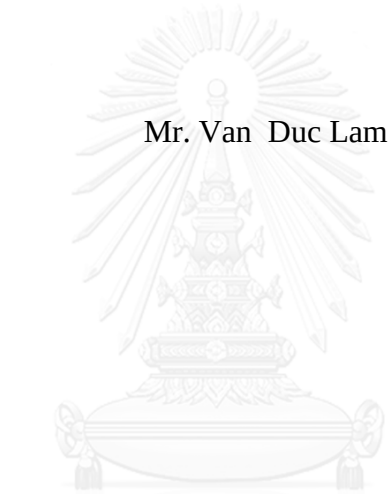

A Dissertation Submitted in Partial Fulfillment of the Requirements
for the Degree of Doctor of Philosophy Program in Civil Engineering
Department of Civil Engineering
Faculty of Engineering
Chulalongkorn University
Academic Year 2016

การประมวลผลสำหรับการทดสอบเสาเข็มแบบเร็ว

นายลาม วัน ดึก

วิทยานิพนธ์นี้เป็นส่วนหนึ่งของการศึกษาตามหลักสูตรปริญญาวิศวกรรมศาสตรดุษฎีบัณฑิต
สาขาวิชาวิศวกรรมโยธา ภาควิชาวิศวกรรมโยธา
คณะวิศวกรรมศาสตร์ จุฬาลงกรณ์มหาวิทยาลัย
ปีการศึกษา 2559

Thesis Title	INTERPRETATION OF RAPID PILE LOAD TESTING
By	Mr. Van Duc Lam
Field of Study	Civil Engineering
Thesis Advisor	Associate Professor Tirawat Boonyatee, Ph.D.

Accepted by the Faculty of Engineering, Chulalongkorn University in Partial Fulfillment of the Requirements for the Doctoral Degree

.....Dean of the Faculty of Engineering
(Associate Professor Supot Teachavorasinskun)

THESIS COMMITTEE

.....Chairman
(Associate Professor Supot Teachavorasinskun, Ph.D.)
.....Thesis Advisor
(Associate Professor Tirawat Boonyatee, Ph.D.)
.....Examiner
(Associate Professor Wanchai Teparaksa, Ph.D.)
.....Examiner
(Associate Professor Boonchai Ukritchon, Ph.D.)
.....External Examiner
(Boonlert Siribumrungwong, Ph.D.)

ลาม วัน ดึก : การประมวลผลสำหรับการทดสอบเสาเข็มแบบเร็ว (INTERPRETATION OF RAPID PILE LOAD TESTING) อ.ที่ปรึกษาวิทยานิพนธ์หลัก: รศ. ฐิรวัตร บุญญะฐี, 143 หน้า.

ปัจจุบันวิศวกรปฐพีได้เริ่มนำการทดสอบเสาเข็มแบบเร็วมาใช้มากขึ้นเนื่องจากสามารถทดสอบได้รวดเร็วและมีประสิทธิภาพมากกว่าการทดสอบเสาเข็มแบบสถิตย์ อย่างไรก็ตามเมื่อทดสอบเสร็จสิ้นแล้วผู้ทดสอบจำเป็นต้องนำค่าที่ตรวจวัดได้มาประมวลผลด้วยวิธีการต่างๆ เสียก่อนจึงจะได้ความสัมพันธ์ระหว่างน้ำหนักบรรทุกกับการทรุดตัวของเสาเข็ม ในบรรดาวิธีการประมวลผลต่างๆ ที่ได้มีผู้นำเสนอไว้นั้น วิธีจุดปล่อยแรงถือได้ว่าเป็นวิธีประมวลผลที่ง่ายและใช้กันอย่างแพร่หลายมากที่สุด แต่จากการศึกษาพบว่าวิธีการนี้ให้ผลการทำนายที่ดีสำหรับการทดสอบในดินทรายเท่านั้นและให้ค่าที่สูงเกินความเป็นจริงเมื่อนำไปใช้กับการทดสอบในดินเหนียว ในงานวิจัยนี้ผู้วิจัยได้เสนอวิธีการประมวลผลแบบใหม่ซึ่งให้ผลการทำนายที่ดีสำหรับการทดสอบในชั้นดินทั้งสองประเภท นอกจากนี้ผู้วิจัยยังได้ใช้โปรแกรมสำเร็จรูป GRLWEAP 2010 เพื่อศึกษาแนวทางในการปรับปรุงวิธีการทดสอบเสาเข็มแบบพลวัตเพื่อให้มีคุณสมบัติเป็นไปตามข้อกำหนดของการทดสอบแบบเร็วด้วย

ภาควิชา วิศวกรรมโยธา ลายมือชื่อนิสิต .....

สาขาวิชา วิศวกรรมโยธา ลายมือชื่อ อ.ที่ปรึกษาหลัก .....

ปีการศึกษา 2559

5671449821 : MAJOR CIVIL ENGINEERING
KEYWORDS: RAPID LOAD TESTING / UNLOADING POINT METHOD / FLEXIBLE PILES

VAN DUC LAM: INTERPRETATION OF RAPID PILE LOAD TESTING. ADVISOR: ASSOC. PROF. TIRAWAT BOONYATEE, Ph.D., 143 pp.

Nowadays, the rapid pile load testing has been used frequently by geotechnical engineers in the world. Comparing to static load testing, the rapid method is quicker and more efficient. However suitable techniques shall be used for obtaining load-displacement curves from rapid load test results. Among methods in literatures, the Unloading Point method can be considered as the simplest and most common. It performs well in sandy soil, but over-predicts the capacity of piles in clayey soils. Therefore, a new technique which performs well in both of sandy and clayey grounds is proposed in this study.

Moreover, the existing dynamic pile load test is modified to approximately meet the requirements of rapid test on driven piles. The modification and illustration of rapid tests on driven piles are carried out by GRLWEAP 2010.

Department: Civil Engineering Student's Signature .....
Field of Study: Civil Engineering Advisor's Signature .....
Academic Year: 2016

ACKNOWLEDGEMENTS

I would like to express my deepest gratitude and sincere appreciation to my supervisor, Associate Prof. Tirawat Boonyatee, who gives me the advice, encouragement and constant guidance throughout my research programme, without him I would not have been able to complete this thesis. Also, I take this opportunity to thank Prof. Suched Likitlersuang and Associate Prof. Boonchai Ukritchon who offered me invaluable help in different ways.

I would like to thank to staff and friends in the Civil Engineering Department for their assistance throughout during studying in here. Many thanks are due to all my friends at Chulalongkorn University.

I am very grateful to all lecturers at Chulalongkorn University for providing general civil engineering backgrounds during my study in PhD level.

I owe greatest debt of gratitude to Chulalongkorn University Scholarship for ASEAN Countries, which supports the finance for my course.

Finally, special thanks are due to my family for their sacrifice and encouragement gave me an opportunity to study in Thailand.

CONTENTS

Page

Page

List of Tables

List of Figures

Notation

A_p the cross-sectional area of a pile

A_s the side surface area of pile

a the pile acceleration

c_p the wave propagation speed of pile material, $c_p = \sqrt{E_p/\rho_p}$

c_c the cushion damping

c_c^* the dimensionless cushion damping

C the damping factor

C_{av} the average damping factor

C_H the hysteretic damping

$C_{H,b}$ the hysteretic damping at the pile base

C_R the radiation damping

$C_{R,b}$ the radiation damping at the pile base

C_V the viscous damping

D the pile diameter/width

D_w the wave length

D_{max} the maximum value of damping ratio

D_r the damping ratio of soil

e the void ratio of soil

E_p the Young's modulus of the pile material

f the frequency

f_1 the first natural frequency

f_n the natural frequency

f_p the force acting in the pile

f_p^* the dimensionless force acting in the pile

f_s the unit skin friction capacity

F the force derived from strain gauge reading

F_a the inertia force

F_p the pore pressure resistance

F_{peak} the maximum force

F_s the static capacity

F_{soil} the soil resistance

$F_{s,corrected}$ the corrected static capacity

$F_{s,ULM}$ the static capacity at the unloading point

F_u the ultimate static resistance

F_v the damping resistance

g the acceleration due to gravity, g = 9.81 m/s^2

G the shear modulus of soil

G_{max} the shear modulus at zero shearing strain amplitude

G_s the secant shear modulus

h the drop height

H the thickness of soil layer

$I_{v\alpha}$ the viscosity index of soil

J the damping constant

J_s the Smith damping factor

j_c the CASE method damping constant

J_G the Gibson damping factor

k the spring stiffness

k_c the cushion stiffness

k_c^* the dimensionless cushion stiffness

k_s the soil stiffness

K the OCR exponent

L the pile length

LL the liquid limit

m_r the hammer mass

m_a the anvil mass

m_a^* the dimensionless anvil mass

M the pile mass

n the dimensionless parameter

N the number of loading cycles

N_w the wave number

p_0' the effective overburden pressure

PI the plasticity index

q the quake, or, displacement at the proportional limit

q_p the unit end bearing capacity

Q_f	the skin friction resistance
Q_p	the total end bearing
Q_u	the total resistance
R	the pile radius
s_u	the undrained shear strength of the soil
t	the time of measurement
t^*	the dimensionless time
t_L	the loading duration
T_r	the relative loading duration
u	the pile displacement
v	the pile velocity
v_{av}	the average velocity
v_{min}	the velocity of the Constant Rate of Penetration Test (CRP)
v_0	the reference velocity
$v_{0,r}$	the velocity of the ram when it strikes the pile
v_{toe}	the velocity of the pile toe
V_s	the shear wave velocity in soil
Z	the pile impedance
α	the viscous parameter
α_R	the Rayleigh damping coefficient
β	the viscous parameter
β_R	the Rayleigh damping coefficient
γ	the shear strain
γ_c	the cyclic shear strain amplitude
η	the rate effect factor
μ	ULM correction factor
ρ	the soil density
ρ_p	the pile density
$\overline{\sigma'_0}$	the mean effective stress
τ	the shear stress
τ_c	the cyclic shear stress amplitude
τ_d	the dynamic shear friction
τ_s	the static shear friction

ω the angular frequency

υ the Poisson's ratio of soil

Δv the relative velocity between the pile and the adjacent soil

Abbreviations

CRP	Constant Rate of Penetration test
DLT	Dynamic Load Test
DULM	Unloading Point method associated with Time Delay
MLT	Maintained Load Test
M-ULM	Modified Unloading Point method
OCR	Over Consolidation Ratio
RLT	Rapid Load Test
SLT	Static Load Test
S-ULM	Segmental Unloading Point method
UK	United Kingdom
ULM	Unloading Point method

Chapter 1: INTRODUCTION

1.1 Background

Pile foundations are constructed based on specification of length and cross section area. The settlement under working load conditions and the ultimate bearing capacity are two main criteria for pile design. Typically, safety factors are used in design to cover uncertainties such as ground variation, qualities of works and accuracies of empirical correlations, etc. The efficiency and reliability design, can be improved by performing pile load tests. The number of tested piles depends on the scale of construction and owner, which is commonly suggested in the national standards.

Nowadays, there are three main load testing methods namely the static load test (SLT), the dynamic load test (DLT), and the rapid load test (RLT). A major difference among them is the velocity of loading. Details of these tests will be discussed in Chapter 2.

An important item to be considered for the interpretation of RLT is the damping or rate effect which enhances the soil resistance during testing. The most widely used interpretation method is the Unloading Point method (ULM) proposed by Middendorp et al. (1992). However, Brown (1994) indicated that the ULM performs well in sandy soils, but over-predicts the pile capacity over 25 to 30% in stiff clayey soils. Therefore, it is necessary to propose a new technique which is more suitable for the latter soil type.

1.2 Aims and objectives

The aim of this study is to verify and apply the rapid load test on clayey and sandy soils. To meet this aim, the following objectives are set:

1. To modify existing dynamic load testing apparatuses to be capable of rapid load testing.

2. To modify existing interpretation method to get a better prediction of equivalent static response from rapid load test results.

1.3 Thesis structure

Literatures related to this study are presented in Chapter 2. This chapter points out the important role of pile load testing and introduces the details of each pile load testing method. The comparisons among tests are also presented in this chapter. Existing interpretation methods for RLT are described in this chapter.

Chapter 3 describes the modification of existing dynamic testing equipment to serve as rapid pile load tests.

Chapter 4 presents the extension of the Unloading Point method (ULM) to consider the delayed response along the pile shaft. The rate-dependent resistance of pile and the velocity at the pile tip are determined from the measurements under rapid loading. The velocities at pile toe and pile head are considered for estimating the velocity of the whole pile. Based on these modifications, a better estimation of load-displacement curves can be obtained from the ULM.

Chapter 5 summaries measured results from static and rapid tests reported in literatures. The collected data consist of three sites in sandy ground and five sites in clayey ground and involve with three pile types which are driven concrete piles, driven steel pipe piles, and drilled piles. The data was used to validate the performance of the proposed method. In addition, the optimum rate effect factors of clayey soils were determined and suggested.

Chapter 6 summarizes the key conclusions of the rate effect factor η for the Unloading Point method and the Unloading Point method associated with Time Delay.

Chapter 7 summarizes some conclusions from this study and makes suggestions for further work.

Chapter 2: LITERATURE REVIEW

2.1 Introduction

In recent decades, estimations of axial pile capacities have been improved significantly. However, almost prediction techniques are heavily based on empirical relationships (Randolph, 2003). It is mentioned in Eurocode 7 that uncertainties in pile design must be verified by static load tests. Poulos (2000) stated that pile testing is a basic part in the design and construction process, and is an effective mean to solve uncertain problems related to pile foundations. Fundamental information which can be known from testing are:

1. The ultimate bearing capacity of piles.
2. The load-displacement behavior of piles.
3. The modulus of soil which can be back analyzed from load-settlement curves.
4. The structural integrity of piles.

The information can be used in many ways, e.g.,

1. Construction quality control.
2. Validation of design assumptions
3. Revise origin designs.

Fundamental pile testing methods are static load tests (SLT), dynamic load tests (DLT) and rapid load tests (RLT). There is also a method called Osterberg Cell or O-Cell (Osterberg, 1998) which is less popular because of some limitations (Schmertmann and Hayes, 1997).

SLT is expensive and time consuming but its analysis and interpretation is quite simple. Conversely, DLT and RLT can be done quickly, but more specialized equipment and complex analyze are required (Brown, 2004).

The content of this chapter consists of

1. Discussion of each pile load testing method.
2. Damping of soil under dynamic loading.
3. The influence of loading rate on rapid test results.
4. Existing methods for interpreting rapid test results.

2.2 Static pile load testing methods

Two common types of static load tests are the maintained load test (MLT) and the constant rate of penetration test (CRP). The former is more common than the latter one (Fleming et al., 2009).

MLT is good for determining the response of piles in clay. It is convenient for the end-bearing piles. However, it is not reasonable for determining the ultimate capacity of piles (Fleming et al., 2009).

CRP is suitable for determining the ultimate resistance of piles because its procedure is similar to the procedure used to obtain the shear strength of soil in laboratory (Fleming et al., 2009).

Static load tests require common reaction systems such as kentledges, reaction piles or ground anchors are shown in Figure 2.1.

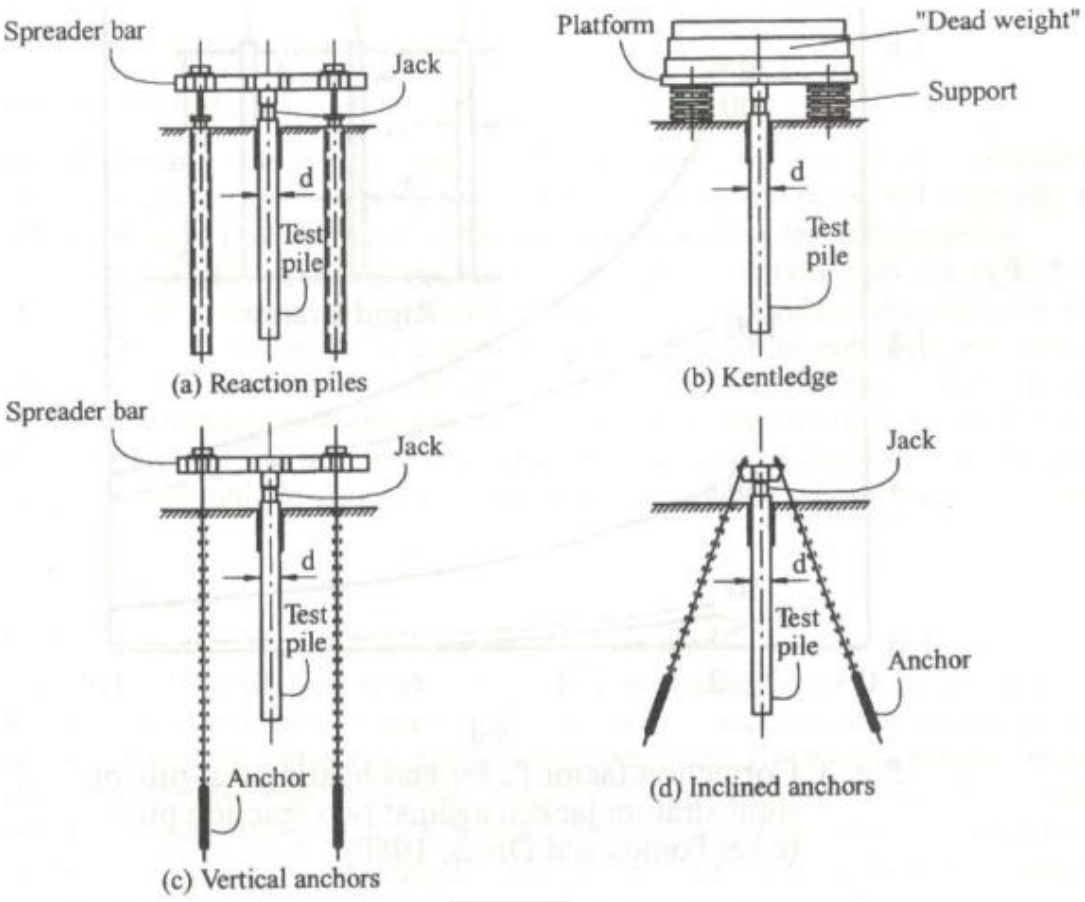

Figure 2.1 Typical reaction systems for static pile load testing (Poulos, 2000).

2.2.1 Maintained load test

The MLT requires a series of loading and unloading increments which are held constant. This test procedure has been developed and specified in various codes, for example, ASTM-D1143 (2013), BS-8004 (1986), the ICE Piling Specification (ICE, 2007). Each increment is hold a minimum specific time before applying the next increment. An example of minimum loading time for each increment and the test result are shown in Table 2.1 and Figure 2.2, respectively. Normally, the ultimate capacity of a pile may be taken when its displacement is equal to 10% of the diameter at pile base (BS-8004, 1986), or when pile plunging occurs.

Table 2.1 Minimum increment loading times for maintained load test (ICE, 2007).

Load*	Minimum time of holding load
25% DVL	30 minutes
50% DVL	30 minutes
75% DVL	30 minutes
100% DVL	6 hour
75% DVL	10 minutes
50% DVL	10 minutes
25% DVL	10 minutes
0	1 hour
100% DVL	1 hour
100% DVL + 25% SWL	1 hour
100% DVL + 50% SWL	6 hour
100% DVL + 25% SWL	10 minutes
100% DVL	10 minutes
75% DVL	10 minutes
50% DVL	10 minutes
25% DVL	10 minutes
0	1 hour

* SWL denotes Specific Working Load; DVL denotes Design Verification Load.

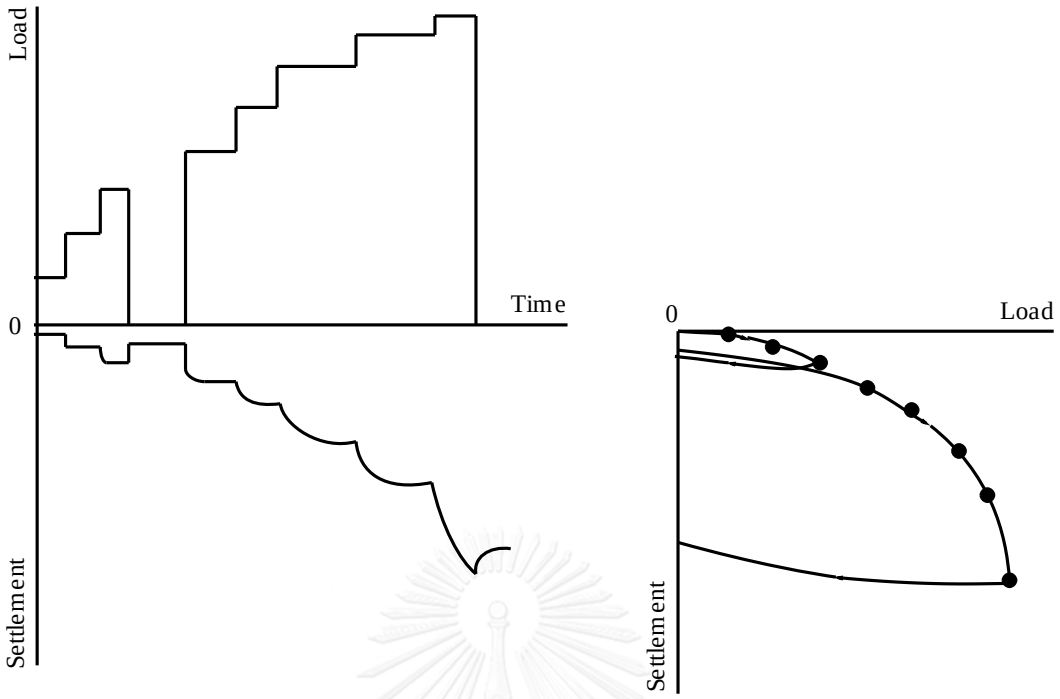

(a) Load and settlement versus time (b) Settlement versus load

Figure 2.2 Relationship between load, settlement and time of maintained load test (BS-8004, 1986).

The limiting rate of axial movement of the pile head is shown in some codes, for example, 0.25 mm/h (BS-8004, 1986; ASTM-D1143, 2013) or 0.1 mm/h when the pile head displacement is less than 10 mm, 1% x pile head displacement/h when the pile head displacement is between 10 mm to 24 mm and 0.24 mm/h when the pile head displacement is greater than 24 mm (ICE, 2007).

The MLT can be used to validate the settlement of piles under working load, which shall be tolerable by superstructures.

MLT is the most reliable pile testing method because it repeats the pile-soil behavior under working load by the superstructure. However, it is also expensive and time consuming. A test requires at least 19h for loading and unloading steps consuming around 5 days to one week when the time for setting up and dismantling are also considered (Nguyen, 2005).

2.2.2 Constant rate of penetration test

On the contrary to the maintained load test, the settlement rate of piles is maintained in the constant rate of penetration test (CRP). ASTM-D1143 (2013) recommends the settlement rate of 0.25 to 1.25 mm/minute for cohesive soil and 0.75 to 2.5 mm/minute for granular soil. British standard (BS-8004, 1986) suggests the settlement rate of 0.75 mm/minute for friction piles in clay and 1.5 mm/minute for end-bearing piles in sand or gravel. ICE Piling Specification (ICE, 2007) requires the settlement rate of 0.01 mm/second for piles in predominantly cohesive soils and 0.02 mm/second for piles in predominantly coarse grained soils. The time for a ARP test is usually shorter than that of a MLT test (Nguyen, 2005).

In the CRP test, piles are loaded to failure point which is defined either as the load at which a pile moves downward continuously without further increase in load, or the load at which the pile settlement is equal to 10% of the diameter at pile base (BS-8004, 1986) or at least 15% of the average pile diameter/width (ICE, 2007; ASTM-D1143, 2013). For very long piles or large diameter piles this criterion is not suitable because the elastic shortening of piles alone is greater 10% of pile base diameter. It is also practically difficult to prepare reaction system for high capacity piles (Nguyen, 2005). For such piles, the assessment of the ultimate capacity should be done based on the response or load-displacement relationship of piles, e.g., the Offset Limit Load (Davisson, 1972), the Brinch-Hansen Failure Criterion (Brinch-Hansen, 1961), the Chin Failure Criterion (Chin, 1970), the De Beers method (Fellenius, 1980), etc.

2.3 Dynamic pile load testing methods

On the contrary to static tests which load piles over duration of 2 ~ 72 hours (Horvath et al., 1993), loading durations of dynamic tests are as short as 3 to 10 milliseconds (Horvath et al., 1993; CGS, 2006; Hyde and Brown, 2008). Dynamic loading is generated by dropping a ram on the pile head (Figure 2.3). The weight of rams are determined based on criteria such as 2% of the maximum test load (Middendorp et al., 2000), 50% of the pile weight or 1.5% of the working load of piles (Long, 2007).

Figure 2.3 Dynamic pile load tests by a drop weight, (a) with a guiding system [1], (b) without a guiding system [2].

The response of piles under impact loading is usually measured by accelerometers and strain gauges mounted to the pile shaft at the distance more than two pile diameter below the pile head (Figure 2.4). Normally, accelerometers and strain gauges are installed in pair on opposite sides of the shaft to check whether the pile is loaded evenly across the section or not (Randolph, 2003). The measurement is then used to derive the applied load and velocity of the pile during testing. The former is derived by multiplying the measured strains with the cross-sectional rigidity of the pile and the latter is calculated from the integration of accelerations.

[1] http://www.civil.ist.utl.pt/sw2008/invitation4.htm
[2] http://www.indiamart.com/proddetail/high-strain-dynamic-load-testing-pda-2526958288.html

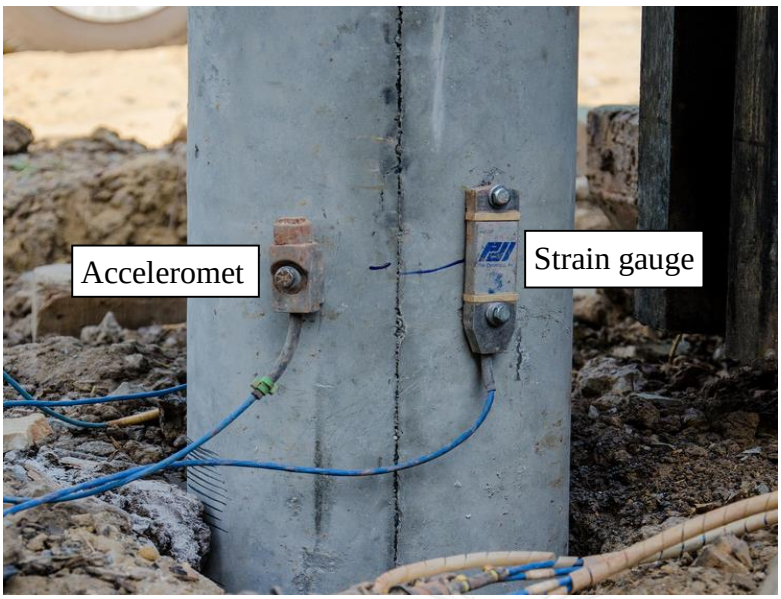

Figure 2.4 Installation of sensors to a precast concrete pile for DLT [3].

The stress wave created by impact loading travels down along the pile shaft as shown in Figure 2.5.

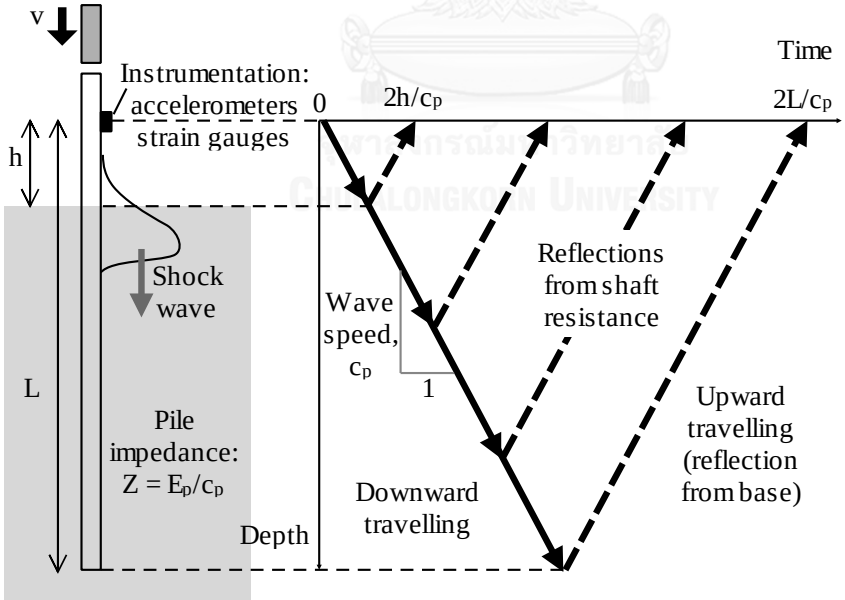

Figure 2.5 Schematic of the propagation of stress wave in pile (Randolph, 2003).

[3] http://www.bhumisiam.com/dynamic-load-test

The force and velocity are related by:

$$F = Z \cdot v \tag{2.1}$$

where

F = the force derived from strain gauge reading;

Z = the pile impedance, $Z = A_p \cdot E_p \cdot c_p$;

A_p = the cross-sectional area of the pile;

E_p = the Young's modulus of the pile;

c_p = wave speed in the pile, $c_p = \sqrt{\frac{E_p}{\rho_p}}$;

ρ_p = the density of the pile material;

v = the pile velocity.

While a wave travels down along the pile shaft, the development of the shaft friction along the shaft or any change in pile section such as at the pile base, which will cause reflection waves which move up to the pile head. The total resistance of the pile during moving of the stress wave down and up of the pile is equal to the sum of the downward travelling wave force plus the upward travelling wave force that arrives at the instrumentation at a time *2L/c*, *L* is the pile length, after the initial peak load (Rausche et al., 1985; Randolph, 2003).

Dynamic test results can be interpreted by various methods, e.g., visual inspection, pile driving formulas, signal processing, numerical models and frequency domain analyses (Holeyman, 1992). A simple signal processing for estimating the static capacity in the field is the CASE method (Rausche et al., 1985). This analysis uses closed form solutions of the one-dimensional wave propagation theory and empirical correlates to static pile load tests. The static resistance can be determined by:

$$F_s(t) = \frac{1}{2}(1 - j_c)\left[F(t) + \frac{M \cdot c_p}{L} v(t) \right] + \frac{1}{2}(1 + j_c)\left[F(t + \frac{2 \cdot L}{c_p}) - \frac{M \cdot c_p}{L} v(t + \frac{2 \cdot L}{c_p}) \right] \quad (2.2)$$

where

F_s = the pile static capacity;

t = the time of measurement;

j_c = the CASE method damping constant (Table 2.2);

M = the pile mass;

L = the length of pile below the instrumentation point.

Table 2.2 Suggested values for CASE damping coefficient (Rausche et al., 1985).

Soil type	Suggested range, j_c	Correlation value, j_c
Sand	0.05 ~ 0.20	0.05
Silty sand or sandy silt	0.15 ~ 0.30	0.15
Silt	0.20 ~ 0.45	0.30
Silty clay and clayey silt	0.40 ~ 0.70	0.55
Clay	0.60 ~ 1.10	1.10

The derived static capacity of a pile depends on the selection of the CASE damping value. The increase of j_c will decrease the estimated static capacity. Therefore, the high value of j_c may be used when there is little available experiences for providing a marginal safety to the designer (Rausche et al., 1985).

A more reliable technique to interpret the stress wave data is done by modelling the pile as a series of elements embedding in the ground with varying properties. The simulation is done in iterative manner by adjusting input parameters until the computed

signal matches with the measured data, such as the force or velocity at the pile head. Examples of this process can be seen in Goble et al. (1980). Popular commercial packages are such as CAPWAP (CAse Pile Wave Analysis Program) by Rausche et al. (1985) and TNOWAVE by Bielefeld and Middendorp (1995).

Dynamic methods are widely used due to a number of advantages including

- Short execution and set up time, e.g., testing with load around 10 MN can be done two times within one day (Middendorp et al., 2000).
- The testing cost is around half of an equivalent static load test (Randolph, 2003).

The dynamic method also has some disadvantages such as

- The complexity of analyzing procedure which only suitable for experts (Brown, 2004).
- The dependency of the derived static capacity on the justifications of the viscous damping constant and pile material properties such as the length, mass, density and Young's modulus (Middendorp et al., 2000).
- Damages that may occur due to tension stresses during testing (Middendorp et al., 2000).

2.4 Rapid pile load testing methods

The earliest rapid testing, called Dynatest, was proposed by Gonin et al. (1984). They used a heavy mass to strike on soft coil springs attached to the pile head (Figure 2.6). The springs have an important role to lengthen the duration of the force pulse which is in a range of 100 to 150 ms for the maximum load of 4 MN (Holeyman, 1992).

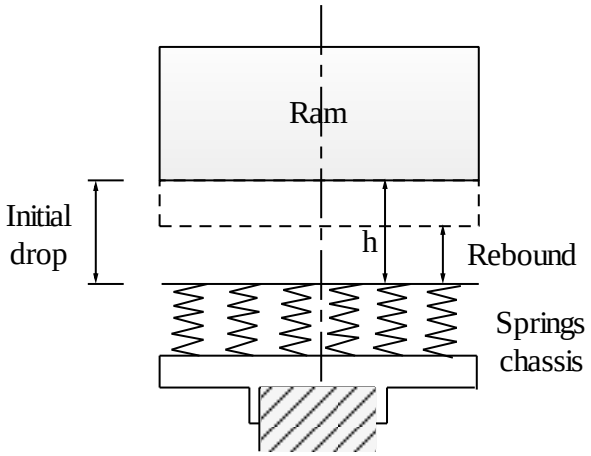

Figure 2.6 Dynatest apparatus (Holeyman, 1992).

Bermingham and Janes (1989) developed another loading system called Statnamic (Figure 2.7). The apply force in this method is generated by gas pressure of a solid fuel burned in a combustion chamber. The force associated with this gas accelerates the reaction mass upward at 20 g, producing an equal force on the pile. In other words, the reaction mass required for the test weights approximately 5% of the maximum test load (Justason et al., 1998; van Ginneken and Middendorp, 2000). Loading duration of Statnamic tests is typically 100 to 200 ms (Matsumoto et al., 2000; Turner, 2006).

Figure 2.7 Statnamic device [4].

Schellingerhout and Revoort (1996) developed a similar equipment called Pseudo-Static Load Tester (PSPLT) by attaching a set of non-linear springs to the bottom of the falling mass (Figure 2.8). The non-linear springs were essential to create a slow-rising and long-lasting force to the pile head (Huy, 2010).

[4] http://www.allnamics.eu/services-new/pile-testing-2/pile-testing-statnamic-load-testing-stn

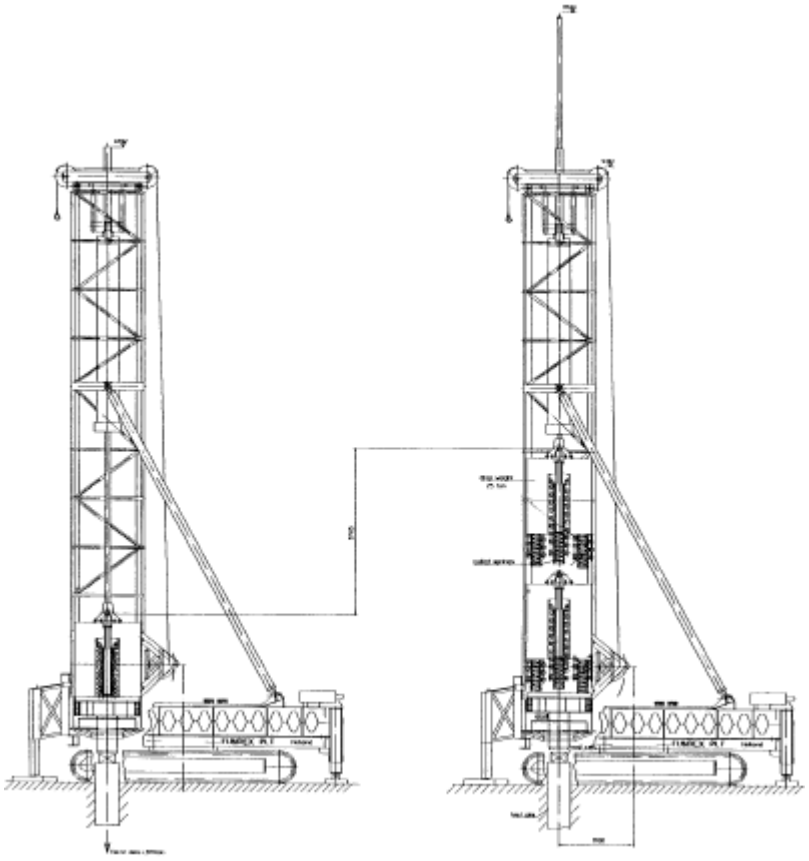

Figure 2.8 Drawing of the Pseudo Static Pile Load Tester (Schellingerhout and Revoort, 1996).

Kanazawa University and Marubeni Material Lease Corporation (Matsumoto et al., 2004) developed another RLT method called Spring Hammer Method (SHM). The loading mechanism of the SHM is similar to that of the PSPLT but the spring hammer unit, made from arrays of coned disk springs, was placed on the pile head instead of attaching to the falling mass (Figure 2.9). The loading characteristic of a spring hammer unit can be adjusted by changing the hammer mass, the spring value as well as the falling height of the hammer. One of the advantages of the SHM is that repetitive loading can be done easily.

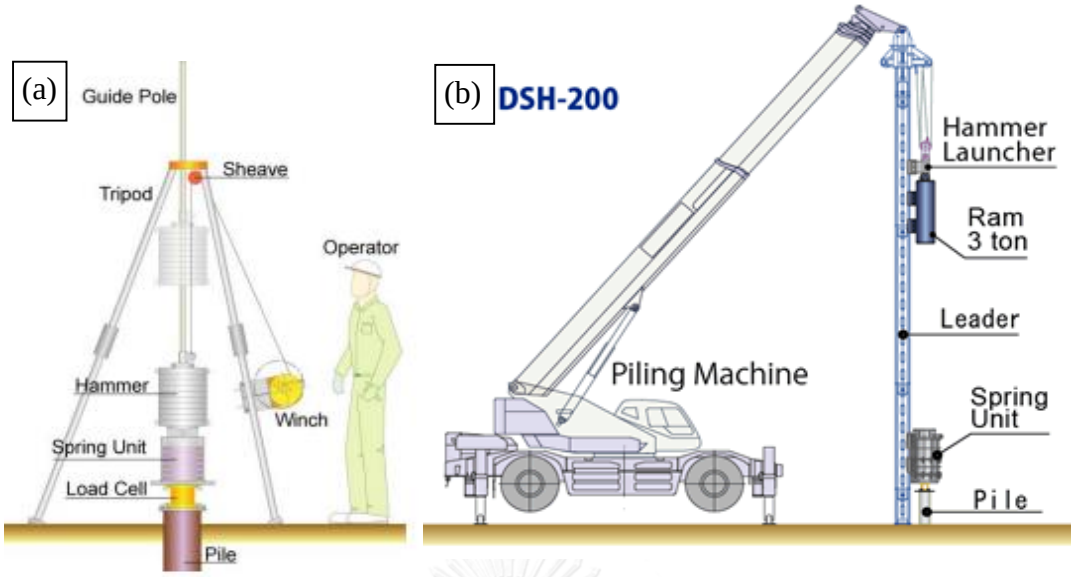

Figure 2.9 Spring hammer test device, (a) portable type, (b) machine-mounted type (Matsuzawa et al., 2008).

Miyasaka et al. (2008) proposed another rapid loading system called Hybridnamic Load Test (HLT) (Figure 2.10). HLT loads a pile by dropping a mass on the Hybridnamic cushion, which is a composite sheet consists of a steel plate, air cell, and an elastomer layer. During unloading process, the recovery to the original configuration of the cushion is delayed due to the effect of the negative pressures acting on the air cell. This mechanism gives low repulsion of the drop ram, and small rebound. Moreover, the lateral deformation of the elastomer layer is restrained by the steel plate which also prevents the stress in the elastomer layer to go beyond its maximum limit and prolong the useful life under repeating uses.

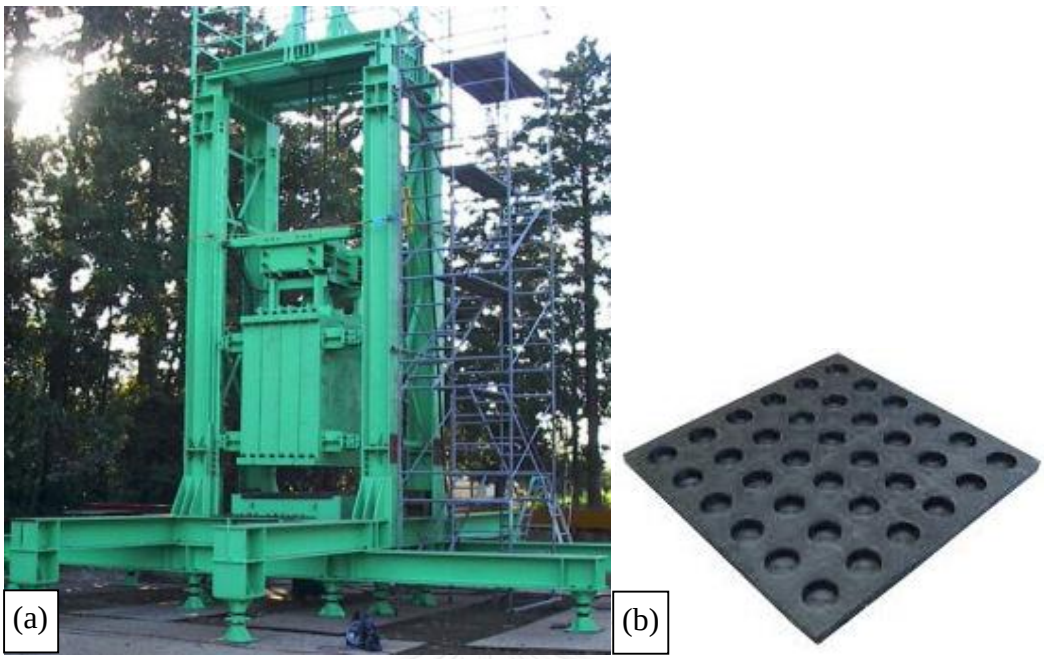

Figure 2.10 Hybridnamic system, (a) test equipment, (b) cushion (Miyasaka et al., 2008).

Another rapid test named StatRapid was developed by Cape Holland and Allnamics (Chew et al., 2015). As is shown in Figure 2.11, the device consists of the top frame (A), the bottom frame with hydraulically adjustable legs (B), the container for modular drop weight assembly (C), a set of rubber springs (D), the impact plate equipped with load cells (E), the internal lifting tool for continuous adjustment of the drop height (F), and the brake system for catching the rebounding drop hammer after impacting (G). The magnitude and duration of loading can be adjusted by varying the hammer mass, the drop height and the spring stiffness. The catch mechanism can prevent the repetition of loading after the first impact.

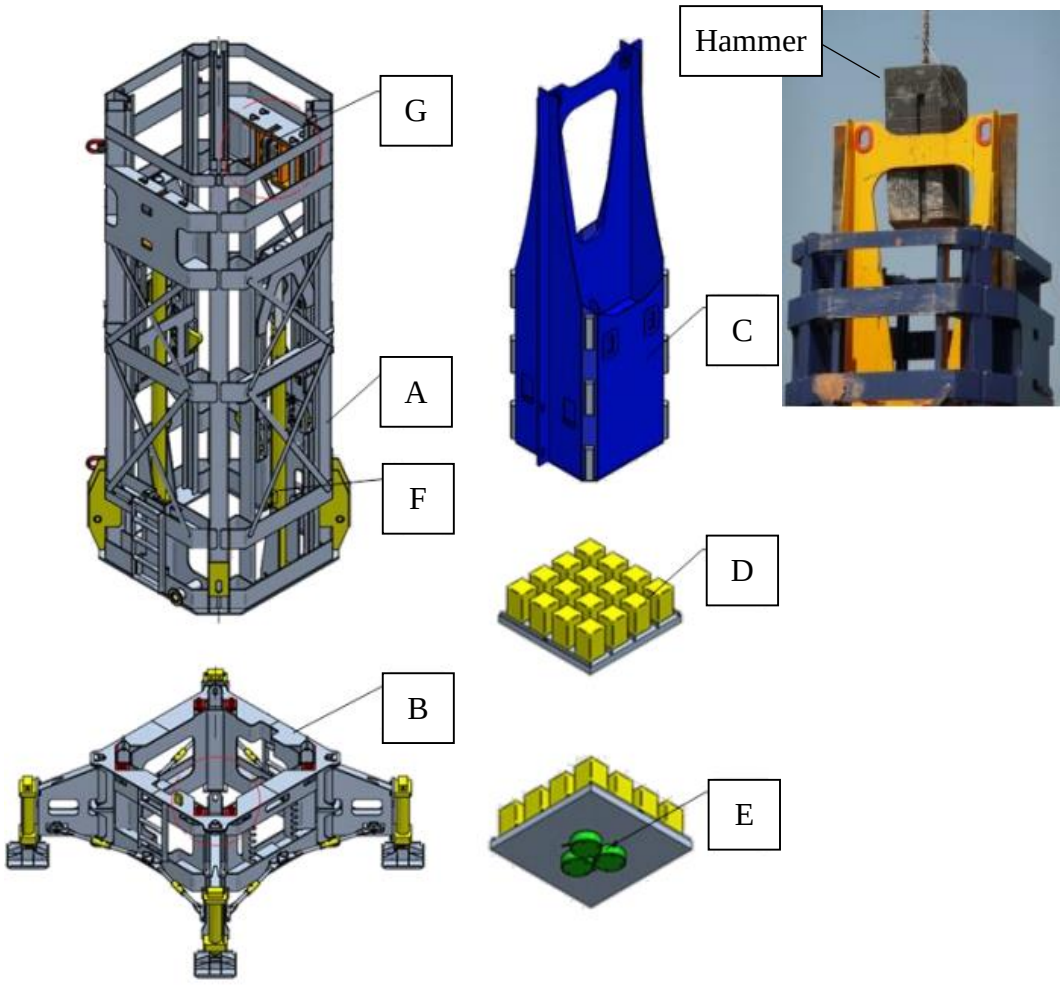

Figure 2.11 StatRapid setup (Chew et al., 2015).

Loading mechanisms of RLT can be divided into two types which are falling mass type and combustion type (Statnamic). The falling mass type seems to have more advantages than combustion type in the following aspects (Matsumoto et al., 2008):

- Preparation time is short.
- Repetitive tests can be done easier.
- Loading duration can be adjusted by varying hammer and spring stiffness.
- Maximum load can be adjusted by varying the drop height.
- Cost of the test is cheaper.

Poulos (2000) offered a number of advantages of Statnamic testing as follows;

- The testing is quick and the device is easy to mobilize.

- The test can be done for high loading capacity.

- The loading is centered and can be applied to either single piles or group piles.

- The test does not require any pre-installation of loading equipment.

- Statnamic can easily apply for lateral loading.

- The damage due to tensile stress during testing is not likely to occur because of the long loading duration.

- The test can be carried out on either the un-instrumented and instrumented piles.

- The applied load can be measured directly by a calibrated load cell which does not depend on the pile material and cross-sectional properties.

The typical loading duration of RLT ranges between 80 ms to 300 ms (CGS, 2006). JGS-1815 (2002) suggested that the relative loading duration, T_r, as defined be equation (2.3), is between 5 and 500.

$$T_r = \frac{t_L}{2L / c_p} \tag{2.3}$$

where

T_r = the relative loading duration;

t_L = the loading duration;

L = the pile length;

c_p = the wave velocity, $c_p = \sqrt{E_p/\rho_p}$;

E_p, ρ_p = the Young's modulus and density of the pile material, respectively.

2.5 Analytical consideration of hammer impact

2.5.1 The effect of drop height

Schellingerhout and Revoort (1996) used a simple model for the simulation of the Pseudo Static Pile Load Tester (PSPLT). The magnitude of loading can be estimated by

$$F_{peak} = m_r \cdot g \cdot \left[\sqrt{\left(\frac{2 \cdot k \cdot h}{m_r \cdot g} + 1 \right)} + 1 \right] \tag{2.4}$$

In which,

F_{peak} = the maximum force;

m_r = the mass of the drop weight;

k = the spring stiffness;

h = the drop height;

g = the acceleration due to gravity, g = 9.81 m/s^2.

An example, which considers a mass of 25 tons and a spring stiffness of 8 MN/m is shown in Figure 2.12.

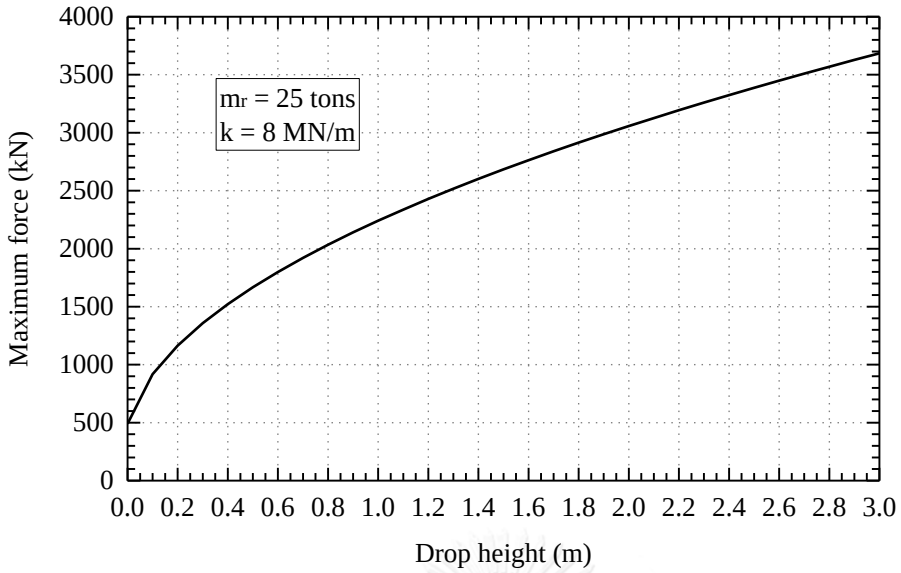

Figure 2.12 Maximum force as a function of the drop height (Schellingerhout and Revoort, 1996).

The influence of the drop height to the duration of loading is plotted in Figure 2.13.

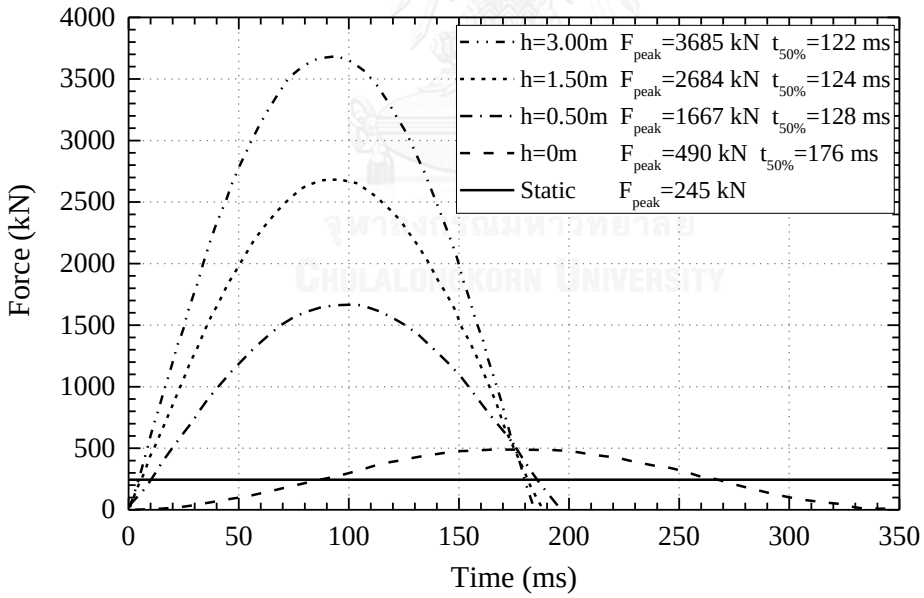

Figure 2.13 The influence of the drop height on the force-time history (Schellingerhout and Revoort, 1996).

Note: $t_{50\%}$ = the duration where the force exceeds 50 % of the maximum force.

The graphs show that the variation of the drop height has little effect to the duration of force.

2.5.2 The ram/pile model

Deeks and Randolph (1993) proposed a simple model consisted of an impacting mass and a pile (Figure 2.14a). In their model, the pile is represented by a dashpot with the impedance of

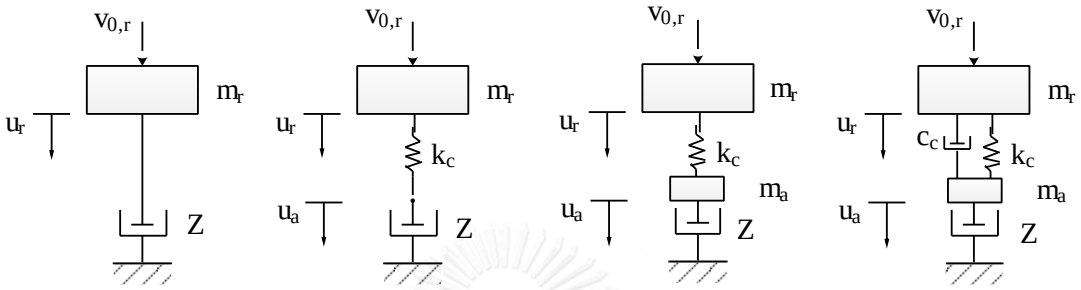

Figure 2.14 Analytical pile hammer models (Deeks and Randolph, 1993).

$$Z = \frac{E_p \cdot A_p}{c_p} \tag{2.5}$$

where

E_p, A_p = Young's modulus and cross-sectional area of the pile, respectively;

c_p = axial wave velocity in the pile, $c_p = \sqrt{\frac{E_p}{\rho_p}}$.

The dimensionless force exerted on the pile, f_p^*, is defined by

$$f_p^* = \frac{1}{e^{t^*}} \tag{2.6}$$

The force acting on the pile, f_p, is given by

$$f_p = f_p^* \cdot Z \cdot v_{0,r} \tag{2.7}$$

where $v_{0,r}$ = the velocity of the ram when it strikes the pile.

The dimensionless time, t^*, is defined by

$$t^* = \frac{Z}{m_r} \cdot t \tag{2.8}$$

where t = the time of measurement.

The result of this simulation is shown in Figure 2.15, denoted by the infinite cushion stiffness. It can be seen that the dimensionless force increases instantaneously to unity at time zero and then degrades exponentially with the dimensionless time constant of unity.

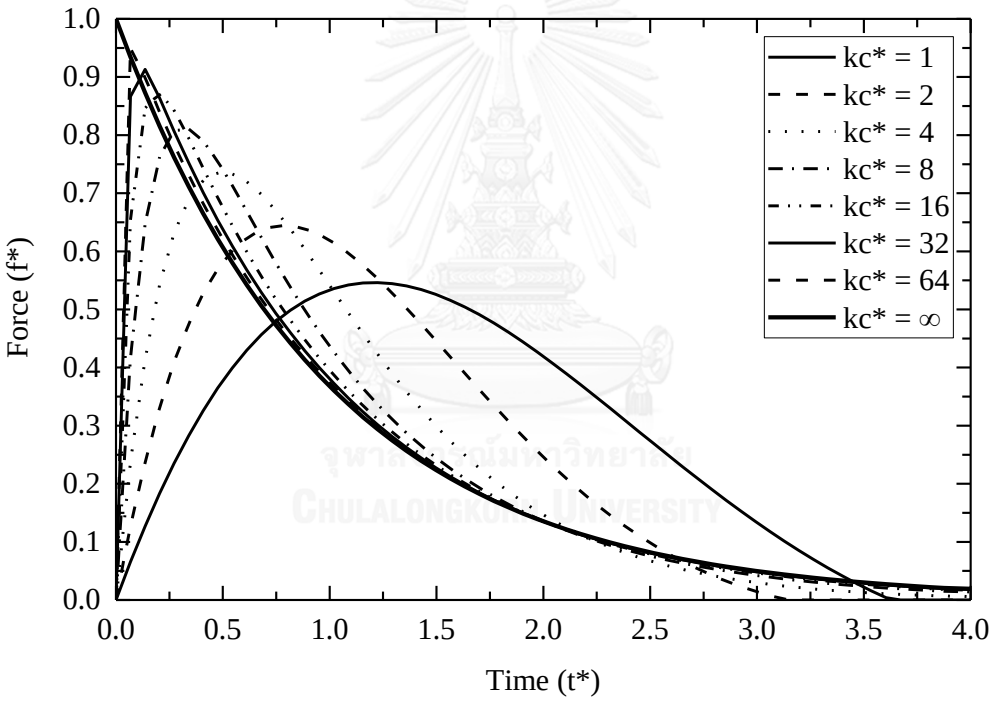

Figure 2.15 The influence of the cushion stiffness on the force-time history (Deeks and Randolph, 1993).

2.5.3 The ram/cushion/pile model

To consider the cushion between the ram and the pile, the model described earlier can be modified by adding a linear spring as shown in Figure 2.14b (Deeks and Randolph, 1993).

The dimensionless stiffness, k_c^*, of the cushion is defined by

$$k_c^* = \frac{k_c \cdot m_r}{Z^2} \tag{2.9}$$

where k_c = the cushion stiffness.

If k_c^* is greater than 4, the dimensionless force, f_p^*, exerted on the pile is

$$f_p^* = \frac{1}{e^{(k_c^*/2)t^*}} \frac{k_c^*}{\mu} \sinh(\mu t^*) \tag{2.10}$$

If k_c^* is equal to 4,

$$f_p^* = \frac{t^*}{e^{(k_c^*/2)t^*}} \tag{2.11}$$

If k_c^* is less than 4,

$$f_p^* = \frac{1}{e^{(k_c^*/2)t^*}} \frac{k_c^*}{\mu'} \sin(\mu' t^*) \tag{2.12}$$

where

$$\mu = \sqrt{\frac{k_c^{*2}}{4} - k_c^*} \tag{2.13}$$

$$\mu' = \sqrt{k_c^* - \frac{k_c^{*2}}{4}} \tag{2.14}$$

The effect of the cushion stiffness on the dynamic force at pile head are shown in Figure 2.15. A soft cushion lengthens the rise time whereas a hard cushion shortens the rise time. When the stiffness grows to infinity, the solution becomes similar to the ram/pile model in Section 2.5.2.

2.5.4 The ram/cushion/anvil/pile model

Deeks and Randolph (1993) introduced a finite anvil mass to the hammer model (Figure 2.14c), the additional term can improve the accuracy of the model. The anvil mass is represented by a dimensionless unit as

$$m_a^* = \frac{m_a}{m_r} \tag{2.15}$$

where m_a = the anvil mass.

The dimensionless force exerted on the pile head are presented by

$$f_p^* = F_p \cdot e^{-c_1 \cdot t^*} \left[1 - e^{-c_2 \cdot t^*} \frac{\cos(\omega \cdot t^* - \phi)}{\cos\phi} \right] \tag{2.16}$$

where

$$a_0 = \frac{k_c^*}{m_a^*} \; ; \; a_1 = k_c^* \left(\frac{1}{m_a^*} + 1 \right) \; ; \; a_2 = \frac{1}{m_a^*} \tag{2.17}$$

$$\alpha = \frac{a_1 a_2}{6} - \frac{a_0}{2} - \frac{a_2^3}{27} \; ; \; \beta = \sqrt{\frac{a_1^3}{27} - \frac{a_1^2 a_2^2}{108} - \frac{a_0 a_1 a_2}{6} + \frac{a_0^2}{4} + \frac{a_0 a_2^3}{27}} \tag{2.18}$$

$$b_1 = \frac{a_2}{3} - (\alpha + \beta)^{1/3} - (\alpha - \beta)^{1/3} \; ; \; b_2 = \frac{a_2}{3} + \frac{1}{2}\left[(\alpha + \beta)^{1/3} + (\alpha - \beta)^{1/3} \right] \tag{2.19}$$

$$\omega = \frac{\sqrt{3}}{2}\left[(\alpha + \beta)^{1/3} - (\alpha - \beta)^{1/3} \right] \tag{2.20}$$

$$c_1 = b_1 \; ; \; c_2 = b_2 - b_1 \; ; \; \phi = \arctan\frac{c_2}{\omega} \; ; \; F_p = \frac{a_0}{\omega^2 + c_2^2} \tag{2.21}$$

The ram will separate from the top of the cushion at time t_s^*, which is determined by the following relation;

$$e^{c_2 \cdot t_s^*} = \frac{\cos(\omega \cdot t_s^* - \theta)}{\cos\theta} \tag{2.22}$$

where

$$\theta = arc\tan\left[\frac{c_2(a_2 - c_1 - c_2) - \omega^2}{\omega(a_2 - c_1)}\right] \tag{2.23}$$

The dimensionless velocity of the anvil when it separates from the ram is denoted by v_s^*. This velocity relates to the dimensionless force by

$$f_p^* = v_s^* \cdot e^{-(t^* - t_s^*)/m_a^*} \tag{2.24}$$

The effect of the anvil mass on the force exerted on the pile head is shown in Figure 2.16. As seen from the figure, the rise time increases with the anvil mass. However, the peak force only increases in a range of m_a^*, then decreases after m_a^* exceeds a certain value.

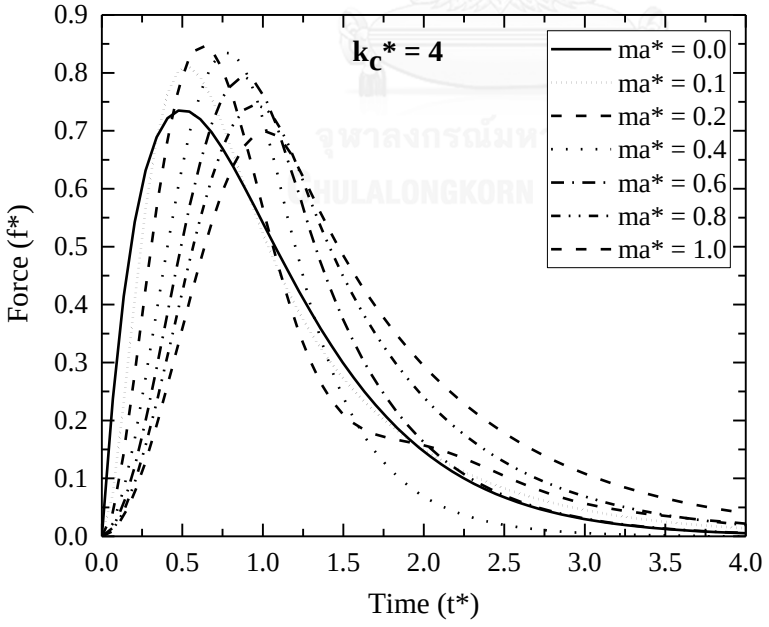

Figure 2.16 The effect of the anvil mass on the force-time history (Deeks and Randolph, 1993).

2.5.5 The damped cushion model

Since the cushion deforms non-linearly and absorbs energy under impact loading, a dashpot is introduced to the model explained earlier for obtaining the model shown in Figure 2.14d. Deeks and Randolph (1993) concluded that this model was adequate for simulating the behavior of real pile hammers.

The additional dimensionless cushion damping, c_c^*, is given by

$$c_c^* = \frac{c_c}{Z} \tag{2.25}$$

where c_c = the cushion damping.

The dimensionless force exerted at the pile head is expressed as

$$f_p^* = F_p \cdot e^{-c_1 \cdot t^*} \left[1 - e^{-c_2 \cdot t^*} \frac{\cos(\omega \cdot t^* - \phi)}{\cos\phi} \right] \tag{2.26}$$

where

$$a_0 = \frac{k_c^*}{m_a^*} \; ; \; a_1 = k_c^* \left(\frac{1}{m_a^*} + 1 \right) + \frac{c_c^*}{m_a^*} \; ; \; a_2 = c_c^* \left(\frac{1}{m_a^*} + 1 \right) + \frac{1}{m_a^*} \tag{2.27}$$

$$c_0 = \frac{c_c^*}{m_a^*} \; ; \; b_4 = \frac{k_c^*}{c_c^*} \tag{2.28}$$

$$c_1 = b_1 \; ; \; c_2 = b_2 - b_1 \; ; \; c_4 = b_4 - b_1 \tag{2.29}$$

$$\phi = \arctan \frac{c_2(c_4 - c_2) - \omega^2}{\omega \cdot c_4} \; ; \; F_p = \frac{c_0 \cdot c_4}{\omega^2 + c_2^2} \tag{2.30}$$

The ram will separate from the top of the cushion at time t_s^* as

$$e^{c_2 \cdot t_s^*} = A_s \frac{\cos(\omega \cdot t_s^* - \theta)}{\cos\theta} \tag{2.31}$$

where

$$A_s = \frac{\frac{1}{m_a^*} - b_2 + \gamma \cdot \omega}{\frac{1}{m_a^*} - b_1} \tag{2.32}$$

$$\theta = arct\,\mathrm{an}\left(\frac{\frac{\gamma}{m_a^*} - \omega - \gamma \cdot b_2}{\frac{1}{m_a^*} - b_2 + \gamma \cdot \omega} \right) \tag{2.33}$$

$$\gamma = \frac{(c_4 - c_2)c_2 - \omega^2}{\omega \cdot c_4} \tag{2.34}$$

Figure 2.17 shows the effect of the dimensionless cushion damping on the force at the pile head. It can be seen that the increase of the damping will reduce the oscillation and the maximum value of the applying force.

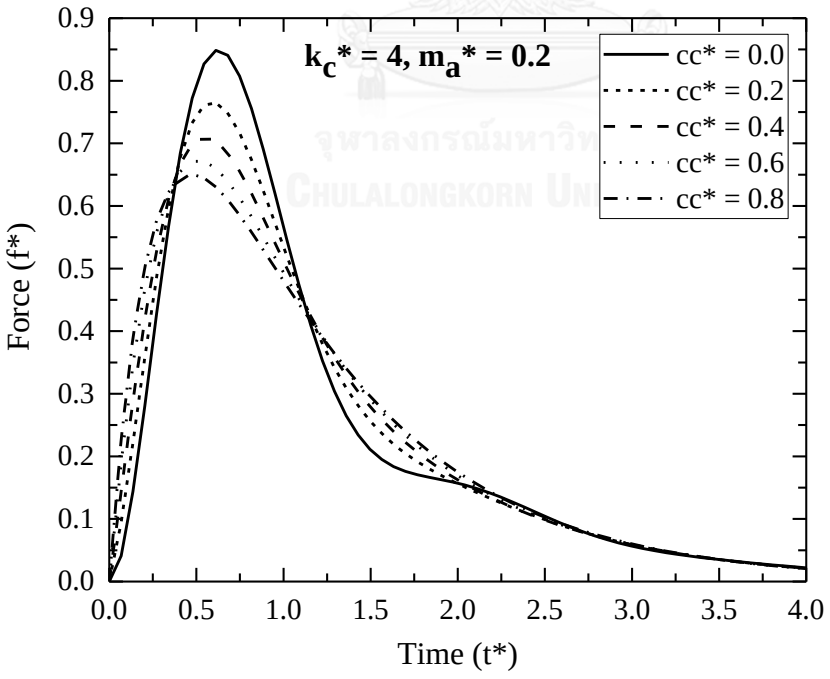

Figure 2.17 The effect of the cushion damping on the force-time history (Deeks and Randolph, 1993).

2.6 Damping of soil

When driving a pile, impact energy transforms to stress waves which transmits through the pile and the soil. The energy in stress waves is stored by elastic deformation, absorbed by plastic deformation or dissipated by hysteretic damping of the soil.

2.6.1 Hysteretic damping

Hysteretic damping is caused by the nonlinear stress-strain behavior of the soil. The loss of mechanical energy is increased through the expansion the hysteretic loop (Yoshida, 2015).

Hysteretic damping can be evaluated by laboratory tests or field tests (Tien, 1987). It can be estimated by Eq. (2.35)

$$C_H = 2\pi \cdot R \cdot L \cdot D_r \sqrt{\rho \cdot G} = D_r \cdot C_R \tag{2.35}$$

where

C_H = the hysteretic damping;

R, L = the radius and length of the pile, respectively;

ρ, G, D_r = the density, shear modulus and damping ratio of soil, respectively;

C_R = the radiation damping.

The damping ratio can be estimated by Eq. (2.36) (Hardin and Drnevich, 1972).

$$\frac{D_r}{D_{\max}} = 1 - \frac{G}{G_{\max}} \tag{2.36}$$

where

D_{max} = the maximum value of the damping ratio;

G_{max} = the shear modulus at zero shearing strain amplitude (Figure 2.18).

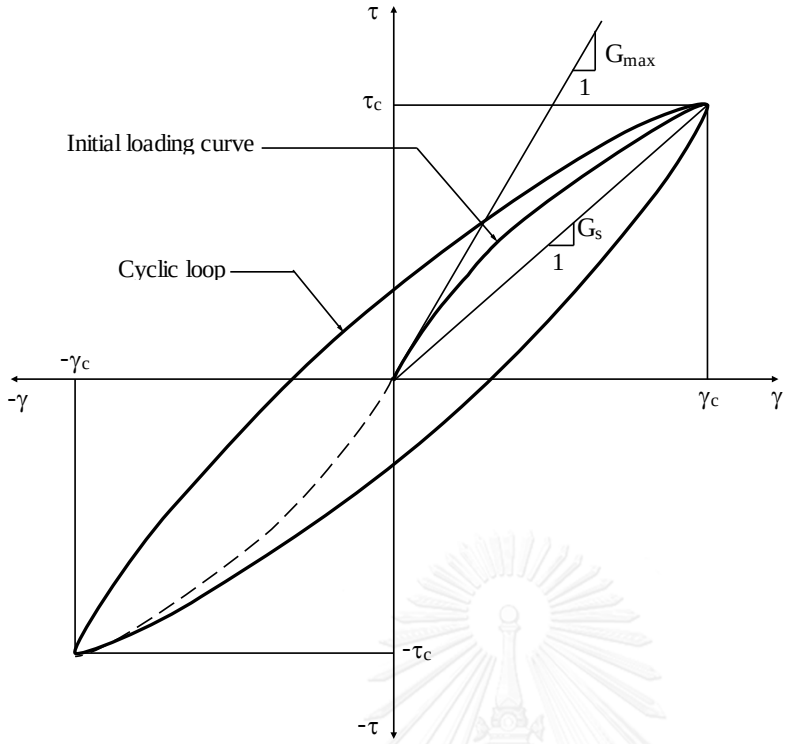

Figure 2.18 Idealized first cycle symmetric stress-strain loop (Lanzo et al., 1997).

Notes: τ = the shear stress, γ = the shear strain, τ_c = the cyclic shear stress amplitude, γ_c = the cyclic shear strain amplitude and G_s = the secant shear modulus corresponding to γ_c.

The maximum value of damping ratio for cohesive soils can be estimated by

$$D_{\max} = 31 - (3 + 0.03f)\sqrt{\bar{\sigma}_0'} + 1.5\sqrt{f} - 1.5\log N \qquad (2.37)$$

where

f = the frequency of shearing in cycles per second;

$\bar{\sigma}_0'$ = the mean effective stress in kg/cm^2;

N – the number of loading cycles.

The maximum shear modulus, G_{max}, can be estimated for any soils by

$$G_{\max} = 1230 \frac{(2.973 - e)^2}{1 + e} \sqrt{\bar{\sigma}_0'} \cdot (OCR)^K \tag{2.38}$$

where

e = the void ratio of soil;

OCR = the over-consolidation ratio;

K = the OCR exponent depends on the plasticity index, PI, of the soil and can be interpolated from the values given in Table 2.3;

$\bar{\sigma}_0'$, G_{max} = are in pounds per square inch, 1 pound/in^2 = 6.895 kPa.

Table 2.3 The value of the OCR exponent, K (Hardin and Drnevich, 1972).

Plasticity index, *PI*, %	Exponent, *K*
0	0
20	0.18
40	0.30
60	0.41
80	0.48
≥ 100	0.50

An approximate value of the maximum shear modulus of normally consolidated clays (zero internal friction angle) is given by Brinkgreve et al. (2016a) as:

$$G_{\max} = 33 \frac{(2.97 - e)^2}{1 + e} \quad [MPa] \tag{2.39}$$

Hysteretic damping at the pile base is suggested by Tien (1987):

$$C_{H,b} = 4 \cdot R \cdot D_r \frac{\pi \cdot G \cdot L \cdot \rho_p}{1-\nu} \tag{2.40}$$

where v = the Poisson's ratio of the soil.

2.6.2 Viscous damping

Viscous damping is the damping that varies proportionally to the velocity. Viscous damping can be estimated by Eq. (2.41) (Lai-bing, 2000; Zhang et al., 2001).

$$C_V = F_s \cdot J_s \tag{2.41}$$

where

C_V = the viscous damping;

J_s = the Smith damping factor (Table 2.4);

F_s = the static resistance.

Table 2.4 Smith damping constant of soils (Rausche et al., 2010).

Soil type	Smith damping factor, J_s
Shaft	
Sand	0.15 s/m (0.05 s/ft)
Clays	0.65 s/m (0.20 s/ft)
Clayey silt / Sandy clay	0.50 s/m (0.15 s/ft)
Sandy silt / Clayey sand	0.33 s/m (0.10 s/ft)
Toe	
All soils	0.50 s/m (0.15 s/ft)
Hard rock	0.15 s/m (0.05 s/ft)

$$F_s = \begin{cases} k_s \cdot u, & u < q \\ F_u, & u \geq q \end{cases} \tag{2.42}$$

k_s = the soil stiffness;

u = the pile displacement;

F_u = the ultimate static resistance;

q = the quake, or, displacement at the proportional limit (Table 2.5).

Table 2.5 Quakes at the shaft and toe of piles.

Reference	Quake for shaft, q_s, mm	Quake for toe, q_t, mm
Smith (1960)	2.54	2.54
Coyle et al. (1973)	Clay: 2.54	Clay: 2.54
	Sand: Loading: 5.1	Sand: Loading: 10.2
	Unloading: 2.54	Unloading: 2.54
Hannigan et al. (1997)	2.54	Very dense/hard soil: D/120
		Soft soil: D/60

Note: D = the diameter or width of piles.

2.6.3 Radiation damping

Radiation damping (also called as geometric damping, geometric attenuation or inertial damping) is the reduction in amplitude of stress waves when propagate away from piles because of the spreading of energy over a greater volume of soil (Kramer, 1996).

Radiation damping from the pile shaft can be evaluated according to Randolph and Simons (1986); Randolph (1991):

$$C_R = 2 \cdot \pi \cdot R \cdot L \cdot \sqrt{\rho \cdot G} \tag{2.43}$$

Radiation damping from the pile tip is estimated by

$$C_{R,b} = \frac{3.4R^2}{1-\nu}\sqrt{\rho \cdot G} \tag{2.44}$$

2.6.4 Rayleigh damping

Damping in dynamic calculations can occur due to various factors, e.g., the viscous properties of soil, the friction and the development of irreversible strains. Although some of them may be simulated by the use of elasto-plastic soil models, an additional damping called Rayleigh damping is still required to fully simulate the damping characteristic of the soil (Brinkgreve et al., 2016b).

Rayleigh damping is a numerical damping which is composed from the mass matrix, *M*, and the stiffness matrix, *K*, by

$$C = \alpha_R \cdot M + \beta_R \cdot K \tag{2.45}$$

where α_R, β_R = the Rayleigh damping coefficients.

The parameter, α_R, represents the influence of mass in the damping of the system. The higher α_R is, the more the lower frequencies are damped. The parameter, β_R, represents the influence of stiffness in the damping of the system. The higher β_R is, the more the higher frequencies are damped.

Rayleigh damping coefficients can be linked to the damping ratio, ξ, by the following relationship:

$$\alpha_R + \beta_R \cdot \omega^2 = 2 \cdot \omega \cdot \xi \tag{2.46}$$

where

ω = the angular frequency, $\omega = 2 \cdot \pi \cdot f$;

f = the frequency.

Based on Eq. (2.46), α_R and β_R, can be determined when target damping ratios are specified at two different frequencies.

$$\alpha_R = 2\omega_1\omega_2 \frac{\omega_1\xi_2 - \omega_2\xi_1}{\omega_1^2 - \omega_2^2} \quad ; \quad \beta_R = 2\frac{\omega_1\xi_1 - \omega_2\xi_2}{\omega_1^2 - \omega_2^2} \tag{2.47}$$

The relationships in Eq. (2.46) and (2.47) can be shown by Figure 2.19.

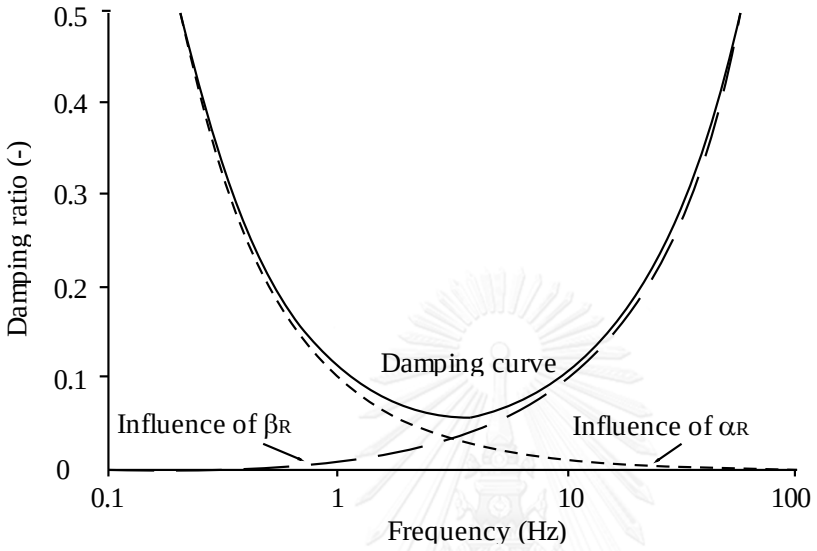

Figure 2.19 Rayleigh damping parameter influences (Brinkgreve et al., 2016b).

Hudson et al. (1994); Brinkgreve et al. (2007); Phillips and Hashash (2009) suggested that the target frequencies must be selected in the range of the natural frequency of the system, f_n and the dominant loading frequency. The former is usually estimated by

$$f_n = (2n-1)\frac{V_s}{4 \cdot H} \tag{2.48}$$

where

V_s = the shear wave velocity in the soil;

H = the thickness of soil layer.

They suggested to select the first target frequency as the first natural frequency of the soil profile, f_1,

$$f_1 = \frac{V_s}{4 \cdot H} \tag{2.49}$$

while the second target frequency, f_2, is a higher mode that corresponds to the predominant frequency of the input motion.

Yoshida (2015) mentioned that the Rayleigh damping, α_R, works proportional to the absolute velocity whereas the Rayleigh damping, β_R, works with the relative value of the velocity. The stiffness proportional component may be used to simulate hysteretic damping (Salgado et al., 2015).

Cai et al. (2002); Hashash and Park (2002); Wilson (2005); Fakharian et al. (2014); Yoshida (2015) showed that the stiffness proportional damping, β_R, is more important than the mass proportional damping, α_R. Therefore, the latter may be neglected, which leading to a simpler relationship as follows;

$$C = \beta_R \cdot K \tag{2.50}$$

and

$$\beta_R = \frac{2 \cdot \xi}{\omega} \tag{2.51}$$

The typical duration of applying force in this study is 0.1 second which corresponded to the period of 0.2 seconds or the angular frequency ω of 31.416 rad/sec. By substituting this number into Eq. (2.51), the relationship is simplified to

$$\beta_R = 0.064\,\xi \tag{2.52}$$

Biggs and Testa (1964) (as cited in Charatpangoon et al. (2014)); Richart et al. (1970); Hashash and Park (2002) suggested the damping ratio, ξ, in the range of 2 ~ 5% for all soil types. Moreover, Massarsch (1993); Salgado et al. (2015) suggested using the damping ratio of 5% when the soil deformation is in the elastic range.

2.7 Interpretation methods for rapid pile load test

Rapid load testing may be used to investigate the dynamic and static response of piles. Several interpretation methods have been proposed for this purpose.

2.7.1 Analysis using concentrated mass models with linear velocity

Middendorp et al. (1992) suggested a simple method called the Unloading Point method (ULM). The method was formulated by the observation on rapid test results that the velocity at pile head reduces to zero when the displacement of the pile head reaches its maximum value and about to rebound, or in the other words, the unloading point.

Middendorp (2000) indicated three primary assumptions of the ULM for determining of the damping *C*. Firstly, the static resistance of the pile is maintained at its ultimate value during plunging. Secondly, the stress wave phenomena can be neglected when loading durations are longer than 10 ~ 12 of traveling time of stress waves from the head to the tip of a pile (Middendorp and Bielefeld, 1995; Nishimura and Matsumoto, 1998; JGS-1815, 2002; ASTM-D7383-10, 2010). Thirdly, piles are assumed to be rigid.

The model, as shown in Figure 2.20(a), consists of a spring, a dashpot and a concentrated mass. The spring represents the static resistance, F_s, and the dash pot represents the rate effect the system, F_v. The pile can be modelled as a rigid body on which various forces are acting on as shown in Figure 2.20(b). In this figure, the displacement dependent forces consist of the static soil resistance, F_s, and pore pressure resistance, F_p which relates with the volume of displaced soil under the pile tip. Velocity dependent force, F_v, represents the soil damping and the acceleration dependent force, F_a, represents the inertia force acting on the pile mass.

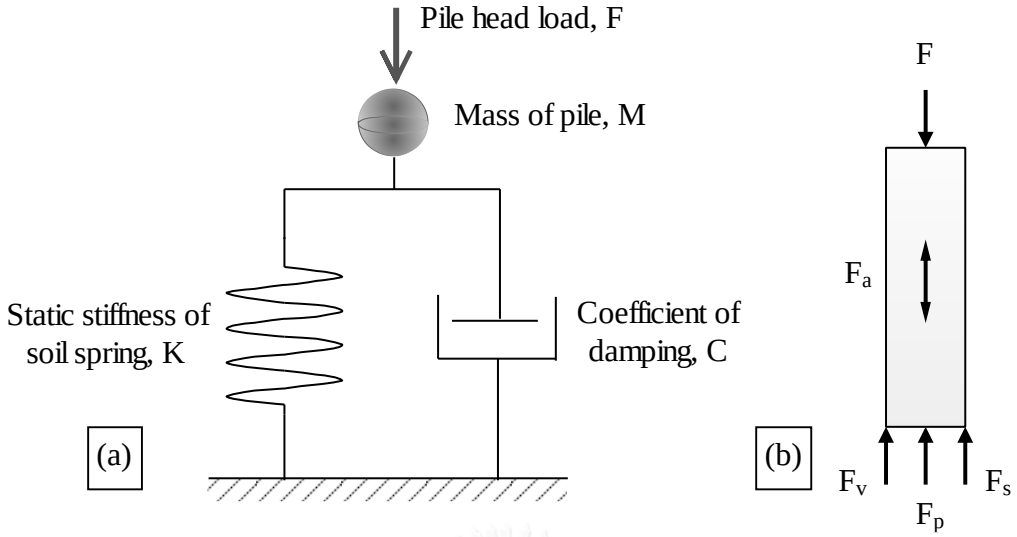

Figure 2.20 Concentrate mass model (a) (Yamashita et al., 1995) and Equilibrium of forces (b)(Middendorp et al., 1992).

The force equilibrium of the pile - soil system is expressed by:

$$F(t) = F_s(t) + F_v(t) + F_a(t) + F_p(t) \tag{2.53}$$

or

$$F(t) - F_a(t) = F_{soil}(t) = F_s(t) + F_v(t) + F_p(t) \tag{2.54}$$

Since the pore pressure resistance can be considered as a part of the damping (Middendorp et al., 1992), Eq. (2.54) can be reduced further to

$$F_{soil}(t) = F_s(t) + F_v(t) \tag{2.55}$$

or

$$F(t) = F_s(t) + C \cdot v(t) + M \cdot a(t) \tag{2.56}$$

where

t = the time of measurement;

F = the measured rapid load;

F_s = the static resistance of soil;

F_v = the damping force of soil, $F_v(t) = C \cdot v(t)$;

C = the damping factor;

v = the pile velocity;

u = the pile displacement;

a = the pile acceleration;

F_a = the inertia force, $F_a(t) = M \cdot a(t)$;

M = the pile mass;

F_p = the pore pressure resistance.

The governing equation (2.56) is in determinate. Since the spring stiffness, k, and damping factor, C, are two remaining unknowns which cannot be measured directly. To solve this equation, Middendorp assumed that the damping becomes zero at the unloading point. As a result, the force equilibrium at the unloading point can be written as

$$F_s(t_{u,\max}) = F(t_{u,\max}) - M \cdot a(t_{u,\max}) \tag{2.57}$$

or

$$F_s(t_{u,\max}) = F_{soil}(t_{u,\max}) \tag{2.58}$$

Based on assumptions that the static resistance is constant during pile plunging and the damping is constant during testing, the damping C can be estimated by Eq. (2.59) (Middendorp, 2000).

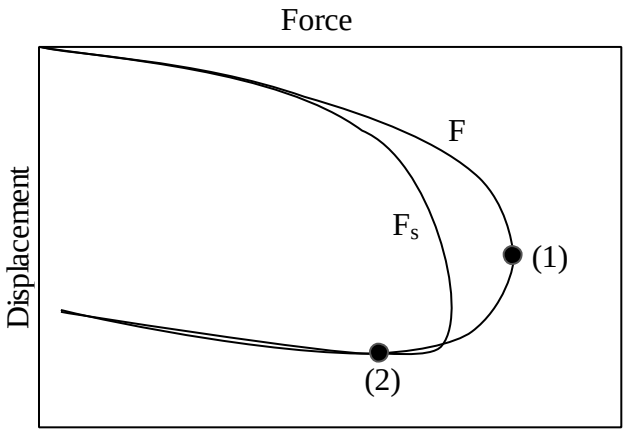

Figure 2.21 Time window for determining the damping constant (Mullins et al., 2002).

$$C(t) = \frac{F(t) - F_{soil}(t_{u,\max}) - M \cdot a(t)}{v(t)} \tag{2.59}$$

Middendorp and Bielefeld (1995); Middendorp (2000); Mullins et al. (2002) suggested that the damping value is fairly constant between the maximum rapid load (point (1) in Figure 2.21, 2.22) and the unloading point (point (2) in Figure 2.21, 2.22). Hence, the damping constant can be approximated from the average over this range as shown in Figure 2.22.

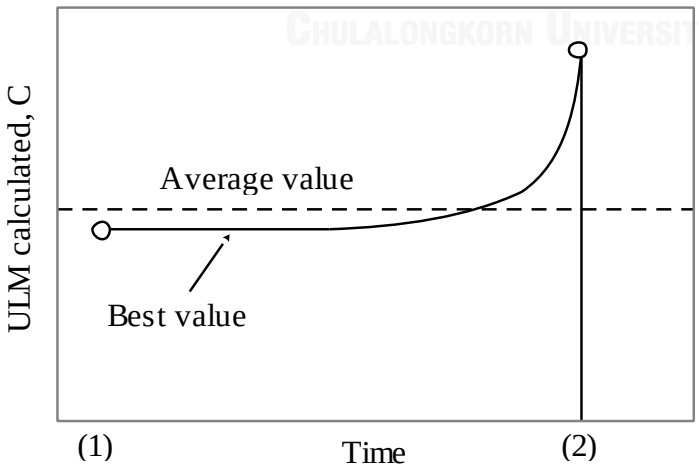

Figure 2.22 Variation of the ULM damping C from point (1) to point (2) (Mullins et al., 2002).

Once the value of *C* has been determined from Eq. (2.59), the derived static soil resistance can be computed by

$$F_s(t) = F(t) - M \cdot a(t) + C \cdot v(t) \tag{2.60}$$

Since the ULM assumes piles to be rigid, the variation in displacement does not occur along the pile. However, an appreciable delay of movements can occur between the head and toe of long piles, hence, negating the rigid body assumption. This situation becomes prevalent for end-bearing piles, when the lower portion of piles is prevented from moving jointly with the top one (Mullins et al., 2002).

Middendorp and Bielefeld (1995) defined the "Wave number", N_w, to quantify the applicability of the ULM (Figure 2.23).

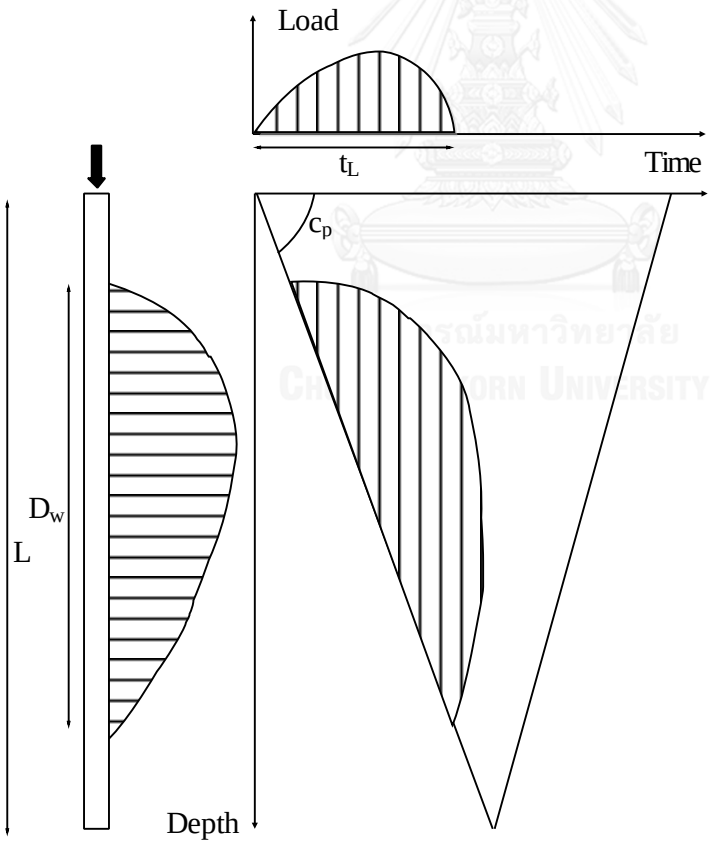

Figure 2.23 Relationship between the wave number, N_w, the loading duration, t_L and the wave length, D_w (Middendorp and Bielefeld, 1995).

The wave number is calculated by dividing the wave length, D_w, by the pile length, L. This wave length, D_w, is obtained by multiplying the wave speed, c_p, with the loading duration, t_L.

$$N_w = \frac{D_w}{L} = \frac{c_p \cdot t_L}{L} \tag{2.61}$$

Based on the wave number, N_w, a pile load test can be categorized as follows:

- If $N_w > 1000$, the test is considered as static load test.

- If $12 < N_w \leq 1000$, the test is considered as rapid load test, and no need to correct for the stress wave phenomena.

- If $6 \leq N_w \leq 12$, the test is considered as pseudo rapid load test, and the correction for the stress wave phenomena is required.

- If $N_w < 6$, the test is considered as dynamic load test.

When a pile is socked into rock or driven to dense bearing strata, its resistance may not be mobilized fully during testing (Mullins et al., 2002). As a consequent, pile responses (i.e. acceleration, velocity, and displacement) between the top and the tip are significantly different. To overcome this problem, an additional accelerometer should be installed at the pile tip for determining the response at the pile tip. In this case, the entire pile is still assumed to be a single mass, but the acceleration and velocity of this mass are now defined by the average of values from the pile head and toe. This method is referred to as the Modified Unloading Point method (M-ULM) by Justason (1997) .

Although the M-ULM is more refined than the ULM, it still not suitable for the tests with $N_w < 12$. To solve it, Middendorp (2000); Mullins et al. (2002) developed another method called the Segmental Unloading Point method (S-ULM). The S-ULM divides a pile into multiple segments where additional strain gauges are installed. Each segment is assumed as a rigid body. Its calculation is similarly to that of M-ULM with the average values measured from the upper and lower positions of each unit. The static response of the whole pile can be calculated by summing the static resistance of the individual segments.

The S-ULM can be implemented only when the test was planned prior to the construction phase because the strain gages, accelerometers, or other transducers have to be embedded beforehand.

Brown (1994) analyzed the Statnamic tests by the ULM and suggested that the ULM produced excellent agreement in sandy soils, but over-predict capacity by as much as 25 to 30% in stiff, over-consolidated clays. To overcome this shortcoming, the rate effect factor η was proposed to improve the ULM for the rapid load tests on piles embedded in clays, such as 0.65 (McVay et al., 2003; Paikowsky, 2006), or, 0.47 (Weaver and Rollins, 2010). However, these rate effect factors were based on a very limited data set with several pile types in some soil condition. Thus, the further analyses are expected to obtain the approximate rate effect factors for the different piles in varying soil layers (Powell and Brown, 2006; Weaver and Rollins, 2010).

2.7.2 Non-linear velocity dependent technique

The simple linear damping relationship is suitable for sand when the rate effect has a minor role to dynamic pile response. However, more sophisticated models are required for clay because of its sensitivity to the rate of loading (Hyde et al., 1998).

Based on of triaxial test results at Texas A&M University, Gibson and Coyle (1968); Coyle and Gibson (1970) suggested that the total resistance varies exponentially to the pile velocity which can written by

$$F = F_s\left(1 + J_G \cdot v^n\right) \tag{2.62}$$

where

F = the measured force;

F_s = the static capacity;

J_G = the Gibson damping factor;

v = the pile velocity;

n = the dimensionless parameter drawn from the test results which was 0.18 for clays and 0.2 for sands.

Litkouhi and Poskitt (1980) performed tests on model piles (10 mm diameter, 260 mm length with a 120^0 cone tip) in fine-grained soil at velocities from $3x10^{-4}$ m/s to 1.66 m/s. They suggested the non-linear viscous law for describing the dynamic friction as follows;

$$F = F_s(1 + J \cdot v^n) \tag{2.63}$$

where

J = the damping constant;

n = the dimensionless parameter, n = 0.2 for clays.

Randolph and Deeks (1992) tested a closed-ended pipe pile with a diameter of 0.96 m. The pile was seated in clay soil with shear modulus, G = 45 MPa, and shear strength, s_u = 330 kPa. They suggested that the dynamic shear resistance can be estimated by

$$\tau_d = \tau_s \left[1 + \alpha \left(\frac{\Delta v}{v_0} \right)^{\beta} \right] \tag{2.64}$$

where

τ_d = the dynamic shear friction;

τ_s = the static shear friction, defined at a very low slip velocity, 0.01 ~ 0.1 mm/s;

Δv = the relative velocity between the pile and the adjacent soil;

v_0 = a reference velocity of l m/s;

α, β = the viscous parameters, β = 0.2 (Gibson and Coyle, 1968; Heerema, 1979; Litkouhi and Poskitt, 1980), α = 0.1 for sandy soils and 1.0 for clayey soils (Randolph and Deeks, 1992).

Hyde et al. (1998) collected data from previous researchers which were either penetration or shear tests at different rates on clay soils. Based on these data, they modified the equation of Randolph and Deeks (1992) to be

$$\frac{\tau_d}{\tau_s} - 1 = \alpha \left(\frac{\Delta v}{v_0} \right)^{\beta} - \alpha \left(10^{-6} \right)^{\beta} \tag{2.65}$$

where

β = viscous parameter, $\beta = 0.2$;

α = viscous parameter which varies over with a large range as shown in Figure 2.24. It can be seen that a relatively small change of the parameter α gives considerable variation in the predicted dynamic resistance ratio.

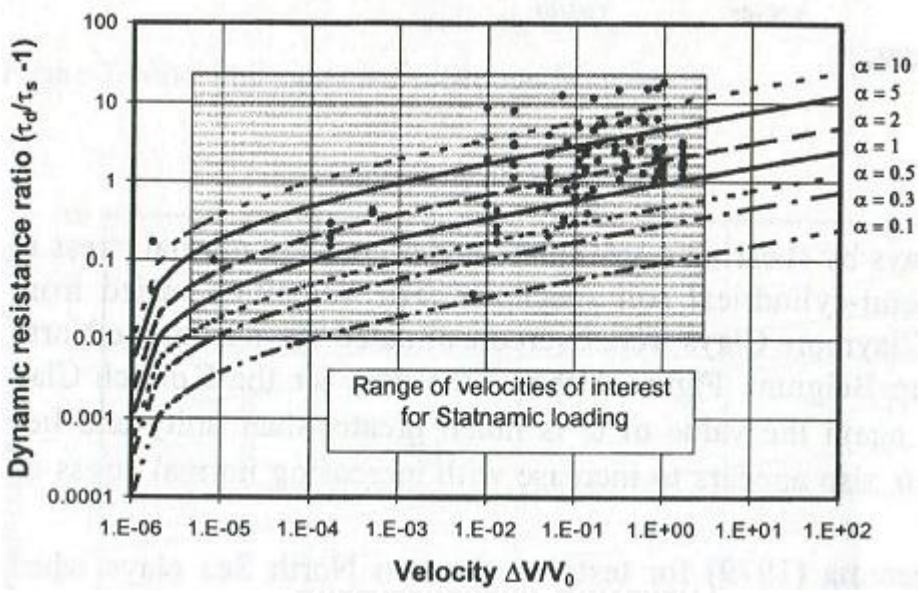

Figure 2.24 Ratio of dynamic resistance ratio versus velocity of pile in RLT (Hyde et al., 1998).

Balderas-Meca (2004) tested full scale Statnamic tests in Grimsby glacial till. He predicted the static pile resistance from Statnamic data from a nonlinear damping model shown below.

$$F_s = \frac{F - M \cdot a}{1 + \alpha \left[\left(\frac{v}{v_0} \right)^{0.2} - \left(\frac{0.01}{v_0} \right)^{0.2} \right]} \tag{2.66}$$

where

M = pile mass;

a = acceleration at the pile head;

α = damping coefficient, this value is a function of pile displacement and varies linearly from zero when the pile displacement is zero to 0.9 when the pile displacement is 1% of the pile diameter and remains constant after that.

Schmuker (2005) proposed an alternative analysis based on the viscosity index, $I_{v\alpha}$, of the soil (as cited in Brown and Powell (2012)).

$$F_s = (F - M \cdot a) \cdot \left(\frac{0.02mm/min}{v} \right)^{I_{v\alpha}} \tag{2.67}$$

where $I_{v\alpha}$ = the viscosity index which depends on soil types (Table 2.6).

Table 2.6 The viscous index, $I_{v\alpha}$, for several soil types (Middendorp et al., 2008).

Soil type	Viscosity index, $I_{v\alpha}$
Sandy silt	0.018
Silt	0.025 ~ 0.032
Clayey silt	0.015 ~ 0.038
Silty clay	0.017 ~ 0.034
Clay, medium plasticity	0.03
Clay, high plasticity	0.04
Clay	0.06
Peat	0.07

Brown and Hyde (2008) carried out experiments on an augered cast in situ pile (12 m long and 600 mm diameter) installed in Glacial Till, and suggested the following formula

$$F_s = \frac{F - M \cdot a}{1 + \left(\frac{F}{F_{peak}} \right) \cdot \alpha \cdot (\Delta v)^{0.2} - \left(\frac{F}{F_{peak}} \right) \cdot \alpha \cdot (v_0)^{0.2}} \tag{2.68}$$

where

F_{peak} = the maximum applied load;

α = a damping parameter, α = 0.92.

Brown and Powell (2013) modified the ULM and Schmuker methods by allowing rate parameters to vary with pile settlement. The study was based on RLT results in two clay sites. The ground in the first case was made of high plasticity Quaternary London clay and the one in the second case was made of low to medium plasticity glacial till. The CFA piles in the first case were 450 mm in diameter and installed to 9.5 m below ground level, whereas the CFA piles in the second site were 600 mm in diameter and installed to 10.4 m below ground surface. The modified ULM formula can be written as

$$F_{s,corrected} = F_s \left[1 + (\mu - 1) \frac{F_s}{F_{s,ULM}} \right] \tag{2.69}$$

where

$F_{s,corrected}$ = the corrected static resistance;

$F_{s,ULM}$ = F_s at the unloading point;

μ = ULM reduction factor, $\mu = -0.0033 \cdot LL + 0.69$;

LL = the liquid limit of clays.

Schmuker method was also modified as:

$$F_s = (F - M \cdot a) \cdot \left(\frac{0.02mm/min}{v} \right)^{\left[I_{v\alpha} \times \left(F / F_{peak} \right) \right]} \tag{2.70}$$

However, they suggested that further verifications are required for the existing viscosity parameter, $I_{v\alpha}$.

Moreover, Brown and Powell (2013) modified a nonlinear velocity-dependent method by Brown and Hyde (2008) to be the equation shown below;

$$F_s(t) = \frac{F(t) - M \cdot a(t)}{1 + \left[\frac{F(t)}{F_{peak}}\right]\alpha\left[\frac{v(t)}{v_0}\right]^{0.2} - \left[\frac{F(t)}{F_{peak}}\right]\alpha\left[\frac{v_{\min}}{v_0}\right]^{0.2}} \quad (2.71)$$

where

v_{min} = the velocity of the Constant Rate of Penetration Test (CRP) which is assumed to be 10^{-5} m/s as shown in the guidance of ICE (2007);

α = the rate parameter of 0.9 (Balderas-Meca, 2004) or 1.0 for clayey soil and 0.1 for sandy soil (Randolph and Deeks, 1992).

Powell and Brown (2006) proposed a relationship between the rate parameter with the plasticity index *PI* as shown by

$$\alpha = 0.03\,PI + 0.5 \quad (2.72)$$

However, this formula was based on limit numbers of studies on clays with the plasticity index mainly in the range of 14 ~ 20%. Brown and Powell (2013) modified this formula by considering the test results on high to very high plasticity clays. The improved formula is shown by

$$\alpha = 0.033\,PI + 0.55 \quad (2.73)$$

The expression above can be linked to the liquid limit *LL* of soils as follows;

$$\alpha = 0.027\,LL + 0.25 \quad (2.74)$$

2.7.3 One-dimensional stress wave analysis (wave matching analysis)

Smith (1960) is the first person who simulate pile driving by a series of pile segments which are supported by three components as shown by Figure 2.25.

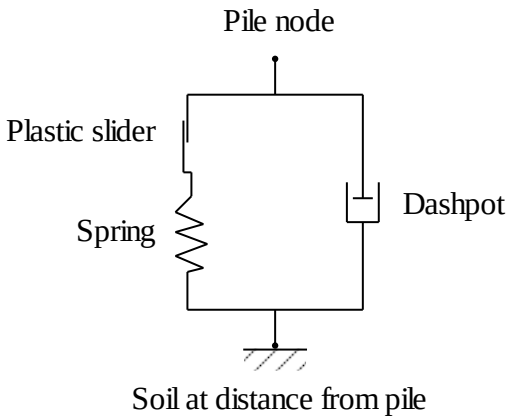

Figure 2.25 Soil models for each pile segment in the pile driving analysis of Smith (Randolph and Deeks, 1992).

Software that has been developed following Smith's idea are GRLWEAP (Rausche et al., 1992), CAPWAP (Rausche et al., 2000), TNOWAVE (Middendorp, 2004).

EI-Naggar and Novak (1992); Ochiai et al. (1997); Nishimura and Matsumoto (1998) applied a technique similar to wave matching analysis to Statnamic test results and found that the interpreted results agreed well with the measurement.

2.7.4 Finite element method

Finite element method (FEM) can be applied to complex boundary conditions which are not possible for concentrate mass models. Moreover, it can also consider the changes in drainage conditions explicitly.

Applications of FEM to the interpretation of RLT have been demonstrated by Yamashita et al. (1995); Horikoshi et al. (1998); Matsumoto (1998); Boonyatee and Kimura (2000).

2.8 Coefficient of determination

The correlation between the derived static curve from RLT and the static curve from SLT can be evaluated by the coefficient of determination, R^2. [5]For example, a data set of the derived static curve from RLT has n values marked $y_1, y_2, \ldots, y_n$, each associated with a desired value of the static curve from SLT as $f_1, f_2, \ldots, f_n$. The data varies from the initial loading point to the unloading point (the point of the maximum pile head displacement) during rapid loading.

The mean value of the calculated data from RLT as follows;

$$\bar{y} = \frac{1}{n}\sum_{i=1}^{n} y_i \tag{2.75}$$

The total sum of squares is calculated by

$$SS_{tot} = \sum_{i=1}^{n} (y_i - \bar{y})^2 \tag{2.76}$$

The sum of squares of residuals is computed by

$$SS_{res} = \sum_{i=1}^{n} (y_i - f_i)^2 \tag{2.77}$$

The coefficient of determination is expressed by

$$R^2 = 1 - \frac{SS_{res}}{SS_{tot}} \tag{2.78}$$

[5] https://en.wikipedia.org/wiki/Coefficient_of_determination

Chapter 3: DEVELOPMENT OF THE RAPID TEST EQUIPMENT

3.1 Introduction

Impact loading can be generated either by freely released or unspooled drop hammers. The energy losses of the latter are higher than the former due to various factors, e.g., the winch inertia, the operator is attempt to catch the ram just before the impact for maintaining stability (Rausche et al., 2010), the misalignment (Rausche, 2000), etc.

In this study, freely released drop hammer system is combined with the hammer cushion to create the rapid load on the pile head. On the other hand, the existing dynamic test equipment is modified for rapid load testing by an additional hammer cushion putted at the pile head.

3.2 Scope of study

Three components considered in this study are the pile, hammer cushion and drop mass. The effects of them to the force-time history are investigated individually in the later sections. Sensors (strain gauges, accelerometers) are assumed to be installed at about two times of pile diameter below the pile head.

The ultimate capacity of piles in this study ranges between 20 tons and 80 tons which is typical for driven piles in civil engineering.

The cushion used in this study is shown in Figure 3.1. Its dimensions are 300 mm x 300 mm with the thickness varying in the range of 25 ~ 300 mm. According to Lee Leon Lowery et al. (1967), the average elastic modulus is determined at one-half of the maximum strain, hence the Young modulus of the cushion is about 0.00053 ton/mm2 (Figure 3.2) which is based on 50 mm of thickness of the current sample. The coefficient of restitution of the cushion is assumed to be 0.5.

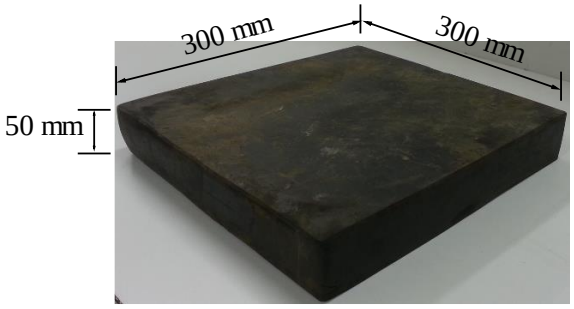

Figure 3.1 Rubber cushion.

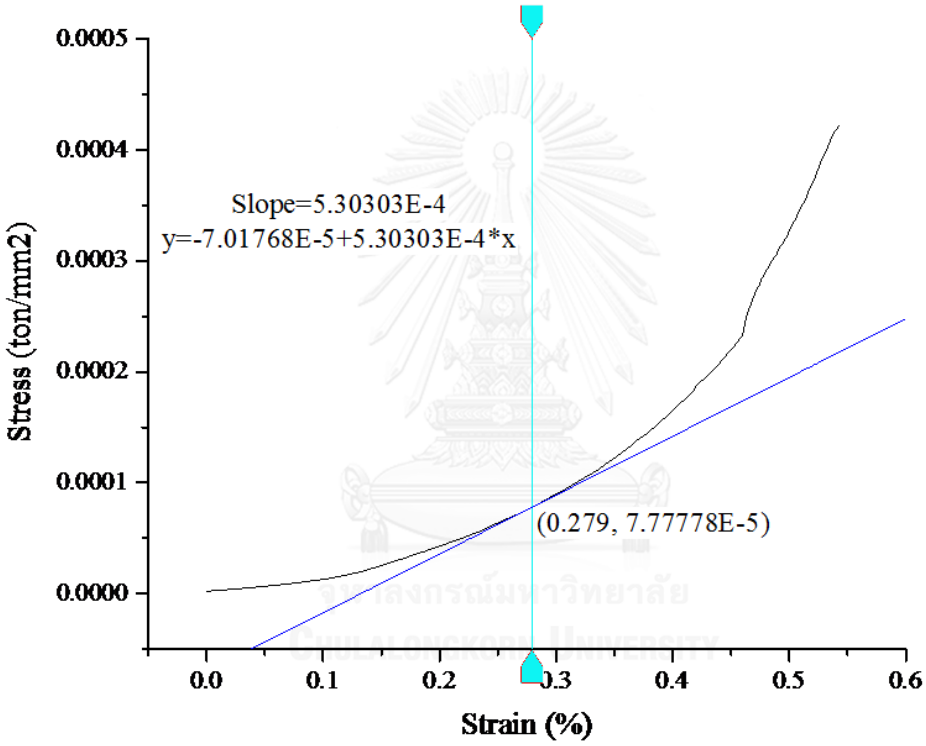

Figure 3.2 Stress-strain curve for a rubber cushion.

The suitable weight of drop hammers should be selected before rapid testing. Justason et al. (1998); Middendorp et al. (2000) mentioned that the reaction mass in Statnamic is around 5% of the maximum test load. Therefore, the same ratio is also employed in this study.

The drop height in this study is in the range of 0.5 ~ 3.0 m. Additionally, the drop mass is set to 2.5 ~ 25 tons, which can be operated by a common crane. The efficiency of drop hammers is assumed to be 0.67 as suggested by Rausche et al. (2010).

Brown et al. (2006) proposed the minimum applied load during rapid load testing in clayey soils to be higher than 1.7 times the design ultimate static capacity. Although this criterion does not be linked directly with the yielding of soil, it is easier for applying in the practice than others criteria which based on the percentage of the pile diameter.

The analyses in this research were carrying out in this study on a 400 kN capacity pile with 2.1 m of the drop height, 5 tons of hammer mass and 150 mm of the hammer cushion thickness. This ultimate resistance is estimated from the square driven concrete pile, which is 0.3 m in edge and 12 m embedded in soil. It is noted that the peak of rapid load must be mobilized up to 680 kN, which is equivalent to 1.7 of the design ultimate static resistance.

The program used to simulate the hammer-cushion-pile system is GRLWEAP version 2000 (GRL's Wave Equation Analysis of Pile Driving) which was developed by Rausche et al. (1988) for analyzing the drivability of piles. In this study, the program is used to consider the effects of the mass and drop height of hammer, the thickness of hammer cushion and the pile capacity on the characteristic of generated load.

3.3 Effect of the pile capacity

This section tries to study the effect of the pile capacity on the shape of generated load. Except the pile capacity, other parameters are kept constant to the following conditions; pile length = 12 m, square concrete section of 300 x 300 mm, hammer mass = 5 tons, drop height = 2.1 m and the thickness of hammer cushion = 150 mm. The variation of pile capacity was made by changing the shear strength, s_u, of a homogeneous clayey ground in a range of 25 ~ 167 kN/m^2, corresponding to capacity between 200 kN and 800 kN (Figure 3.3).

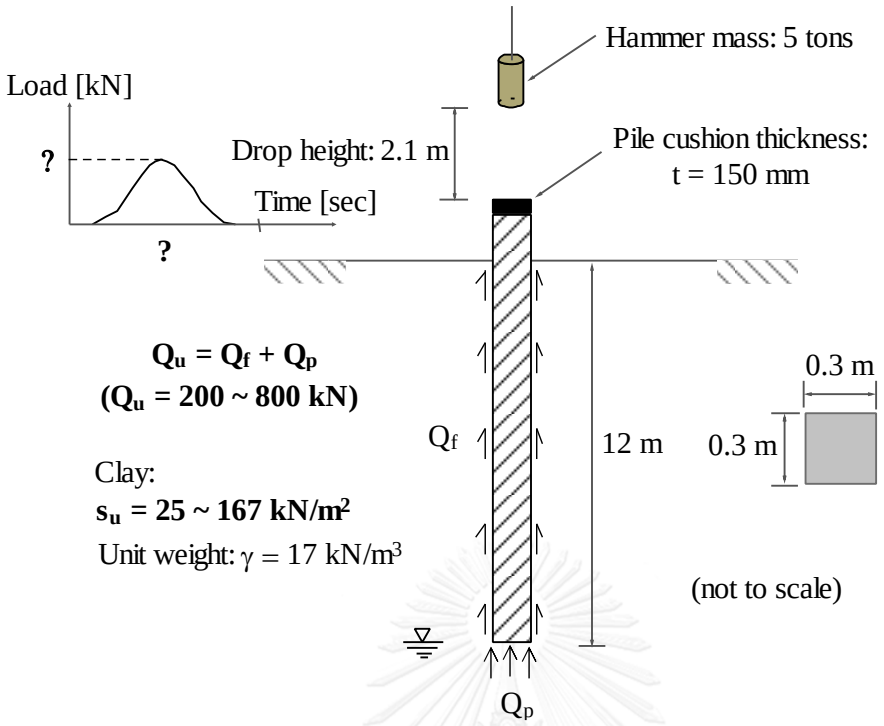

Figure 3.3 Input parameters for determining the effect of the pile capacity on the generated impact load.

It is noted that the pile capacity is estimated by the API method as follows,

$$Q_u = Q_f + Q_p \tag{3.1}$$

where

Q_u = the total resistance;

Q_f = the skin friction resistance, $Q_f = f_s \cdot A_s$;

Q_p = the total end bearing, $Q_p = q_p . A_p$;

f_s = the unit skin friction capacity;

q_p = the unit end bearing capacity;

A_s, A_p = the side surface area and the cross section end area of a pile, respectively;

Unit skin friction capacity in cohesive soils is calculated by

$$f_s = \alpha \cdot s_u \tag{3.2}$$

where

α = a dimensionless factor computed by

$$\begin{aligned} &\alpha = 0.5\psi^{-0.5} && \text{for } \psi \le 1.0 \\ &\alpha = 0.5\psi^{-0.25} && \text{for } \psi > 1.0 \\ &\alpha \le 1.0 && \text{for all } \psi \end{aligned} \tag{3.3}$$

$\psi = s_u/p_0'$

p_0' = the effective overburden pressure;

s_u = the undrained shear strength of the soil.

For end bearing piles in cohesive soils, the unit end bearing capacity is calculated by

$$q_p = 9 \cdot s_u \tag{3.4}$$

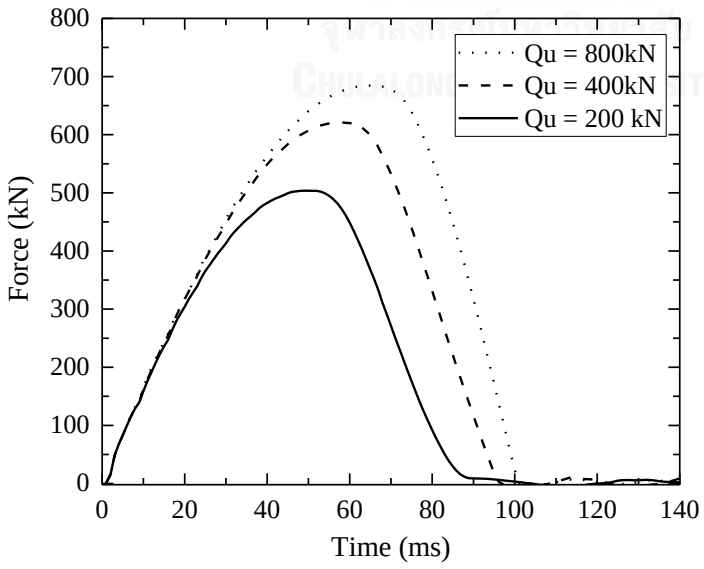

Figure 3.4 The effect of the pile capacity on the generated impact load.

The variation of the maximum and duration of loading against the pile capacity are summarized in Table 3.1. Based on the Figure 3.4 and Table 3.1, the peak force and the loading duration increase with increasing of the pile capacity.

Table 3.1 Simulation results by varying the pile capacity.

Pile capacity, Q_u *(kN)*	Peak force, F_{peak} *(kN)*	Loading duration, t_L *(ms)*
200	504	88
400	621	96
800	685	100

It can be seen from Figure 3.5 that the exponential functions can be used to express the relationship between the peak force, the loading duration and the pile capacity.

The relationships are summarized as follows;

$$F_{peak} = 158.83\, Q_u^{0.221} \tag{3.5}$$

$$t_L = 54.4\, Q_u^{0.092} \tag{3.6}$$

where

F_{peak} = the peak force;

t_L = the loading duration;

Q_u = the pile capacity in the range of 200 ~ 800 kN.

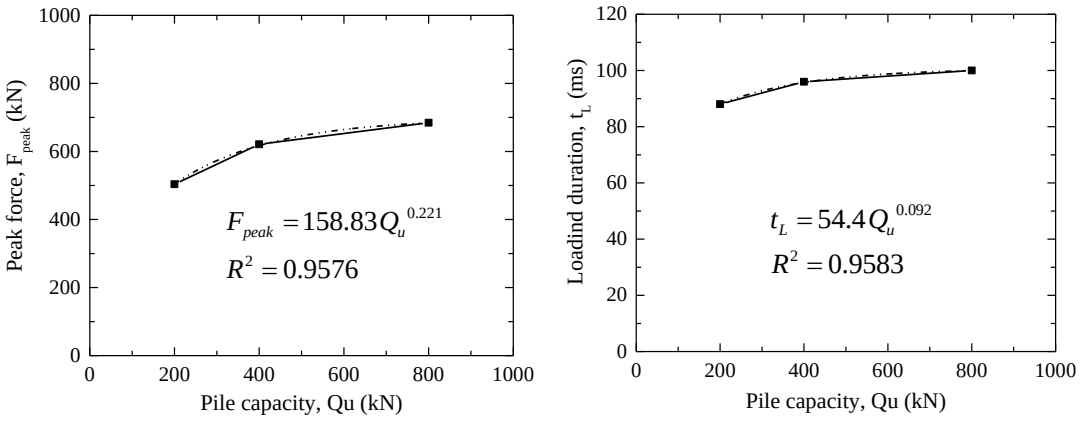

Figure 3.5 Relationships between the pile capacity, the peak force and the loading duration.

3.4 Effect of the hammer mass

The hammer mass is varied between 2.5 tons and 25 tons while others parameters as shown in Figure 3.6 are kept constant. Results from simulations are shown in Figure 3.7.

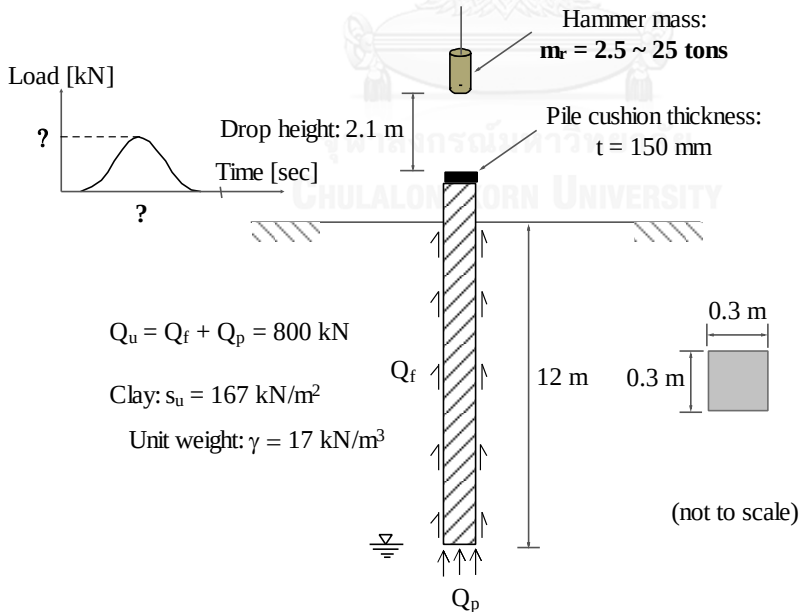

Figure 3.6 Input parameters for determining the effect of the hammer mass on the generated impact load.

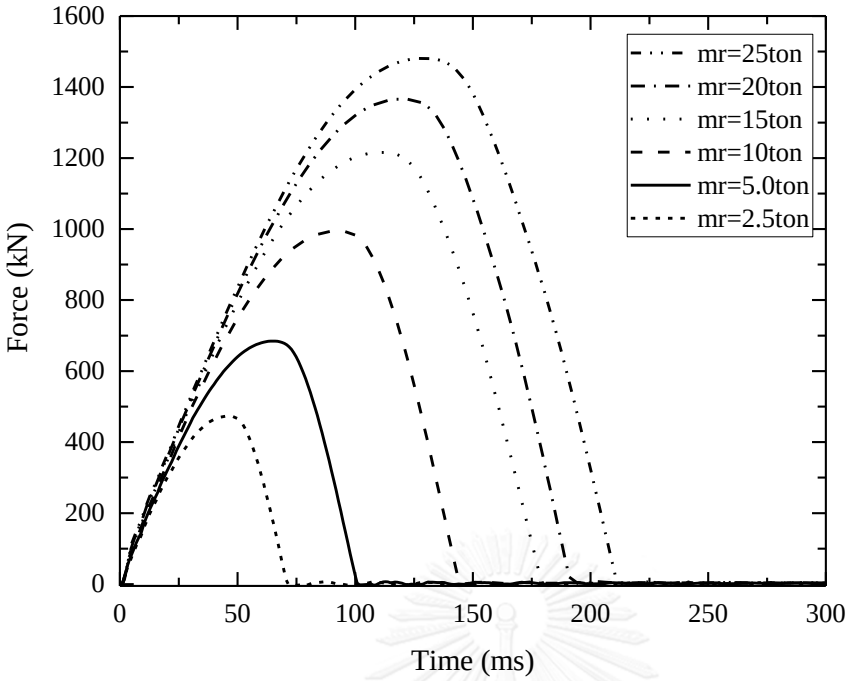

Figure 3.7 The effect of the hammer mass on the generated impact load.

The variation of the maximum and duration of loading against the ram mass are summarized in Table 3.2. Based on the Figure 3.7 and Table 3.2, the peak force and the loading duration increase with increasing of the hammer mass.

Table 3.2 Simulation results by varying the hammer mass.

Hammer mass, m_r *(ton)*	Peak force, F_{peak} *(kN)*	Loading duration, t_L *(ms)*
2.5	473	71
5	684	100
10	995	144
15	1216	179
20	1366	191
25	1481	211

It can be seen from Figure 3.8 that the exponential functions can be used to express the relationship between the peak force, the loading duration and the hammer mass.

The relationships are summarized as follows;

$$F_{peak} = 320\ m_r^{0.483} \tag{3.7}$$

$$t_L = 49\ m_r^{0.46} \tag{3.8}$$

where m_r = the hammer mass in the range of 2.5 ~ 25 tons.

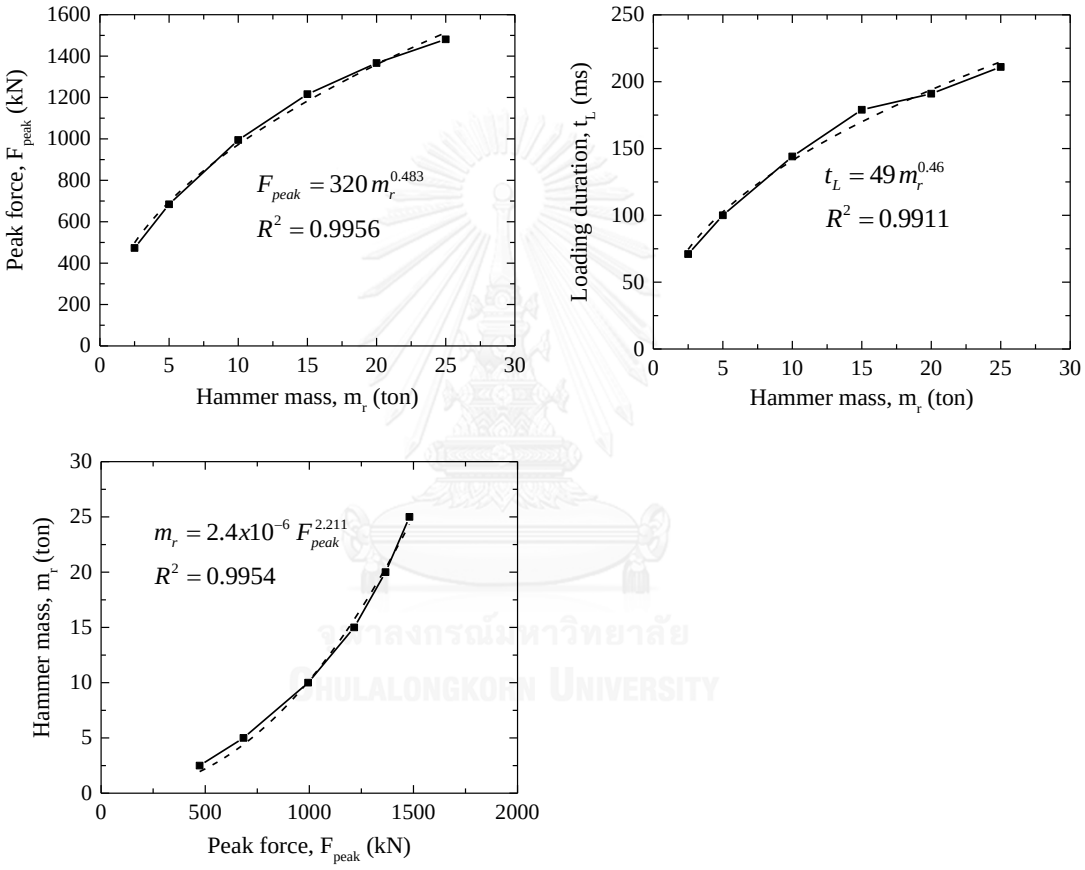

Figure 3.8 Relationships between the hammer mass, the peak force and the loading duration.

3.5 Effect of the drop height

The parametric study was carried out by varying the drop height in the range of 0.25 ~ 3.0 m while maintaining other parameters to the values shown in Figure 3.9.

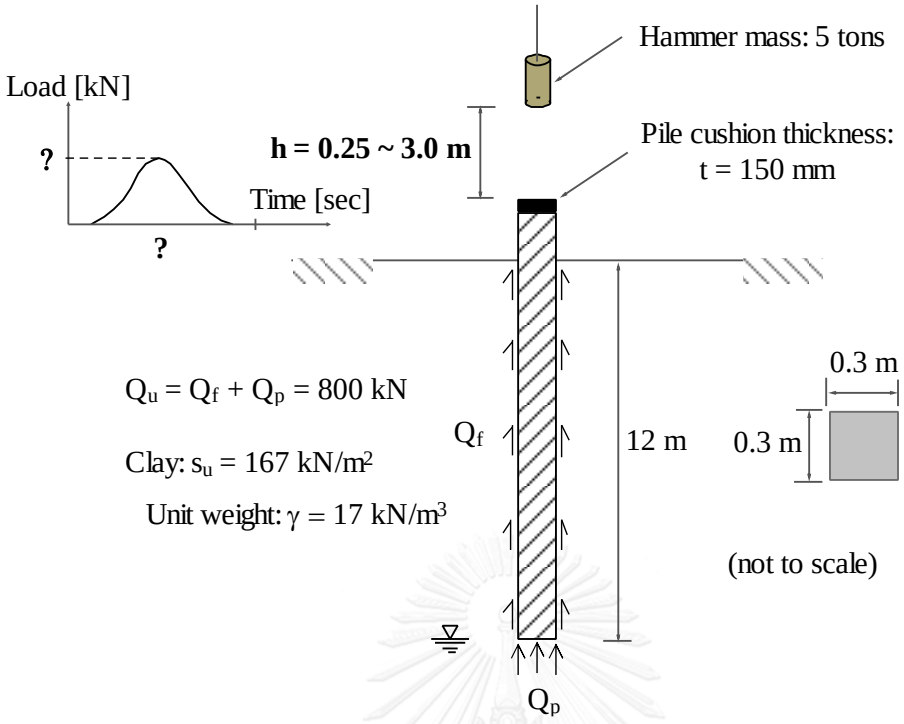

Figure 3.9 Input parameters for determining the effect of the drop height on the generated impact load.

Analysis results in Figure 3.10 show that the drop height rarely affects the loading duration, but has a significant influence to the peak force. The latter effect is summarized in Table 3.3. The relationship between the drop height and the peak force can be expressed by

$$F_{peak} = 492\ h^{0.447} \tag{3.9}$$

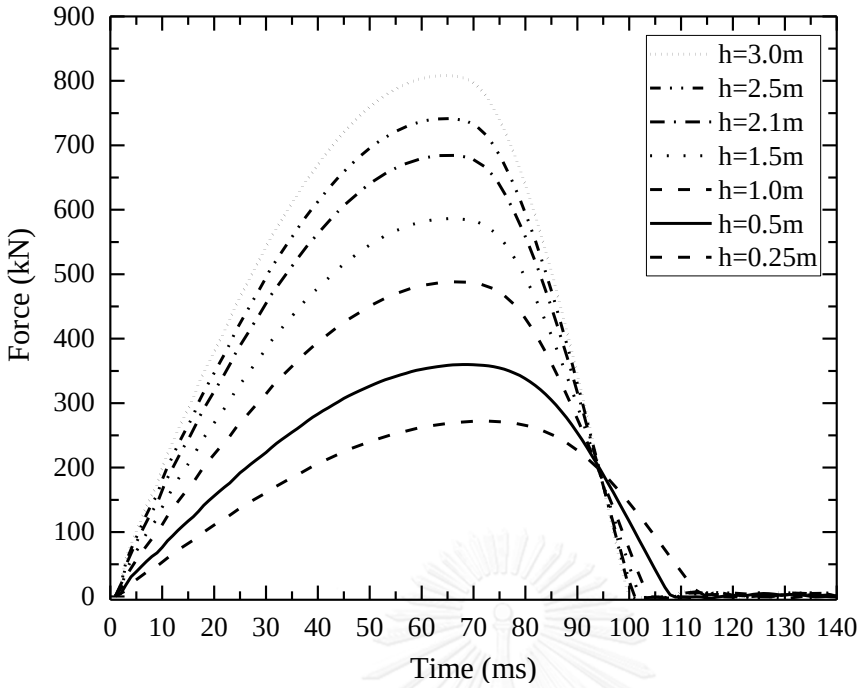

Figure 3.10 The effect of the drop height on the generated impact load.

Table 3.3 Simulation results by varying the drop height.

Drop height, *h (m)*	Peak force, F_{peak} *(kN)*
0.25	272
0.5	360
1	488
1.5	586
2.1	684
2.5	742
3	808

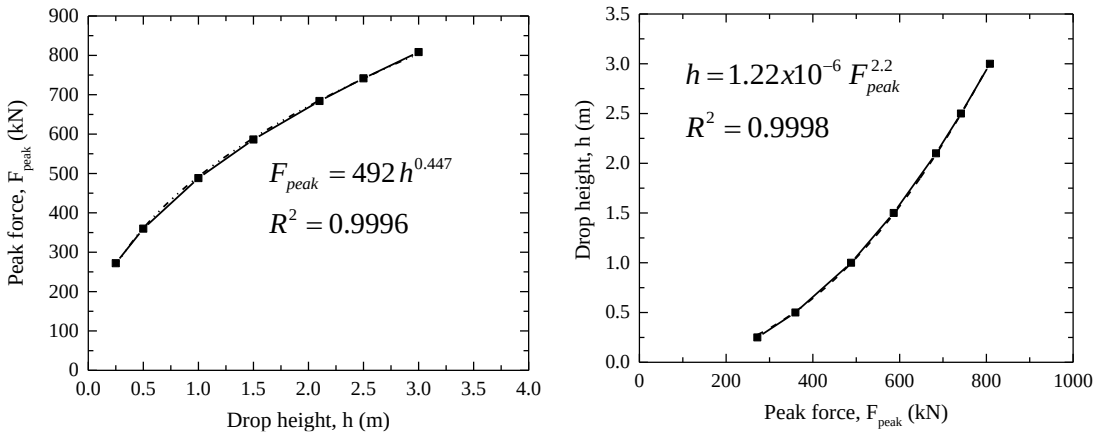

Figure 3.11 Relationship between the peak force and the drop height.

3.6 Effect of the pile cushion thickness

It has been known that the cushion stiffness significantly affects the force-time history. The stiffness of cushions depends not only on the elastic modulus but also the cross-section area and the thickness. Among the three parameters, the thickness is the easiest choice for stiffness tuning purpose. In this study, the cushion thickness is varied in the range of 25 ~ 300 mm while maintaining other parameters to the values in Figure 3.12.

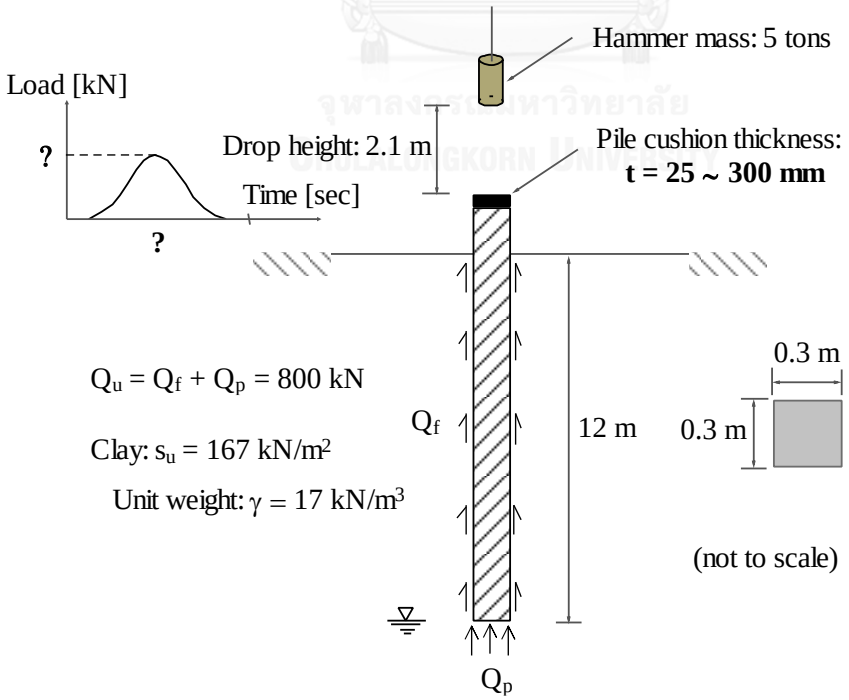

Figure 3.12 Input parameters for determining the effect of the pile cushion thickness on the generated impact load.

Analysis results in Figure 3.13 show that the pile cushion thickness significant affects to the peak force and the loading duration. These effects are summarized in Table 3.4 and Figure 3.14. The relationships of the cushion thickness with the peak force and the loading duration can be expressed by equations that follow;

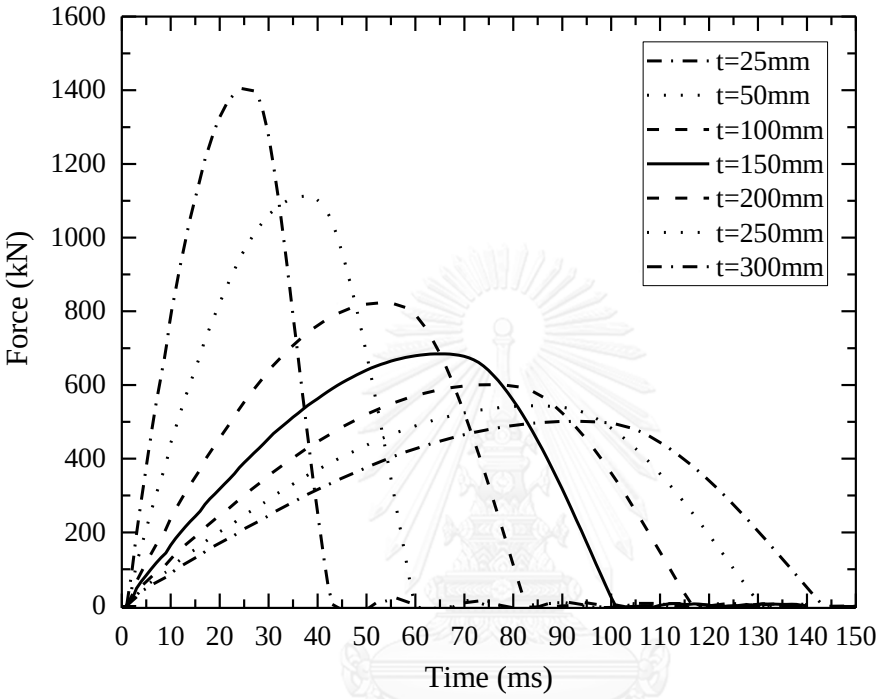

Figure 3.13 The effect of the pile cushion thickness on the generated impact load.

Table 3.4 Simulation results by varying the pile cushion thickness.

Cushion thickness, *t (mm)*	Peak force, F_{peak} *(ton)*	Loading duration, t_L *(ms)*
25	1407	43
50	1112	59
100	823	82
150	685	100
200	601	116
250	543	130
300	501	143

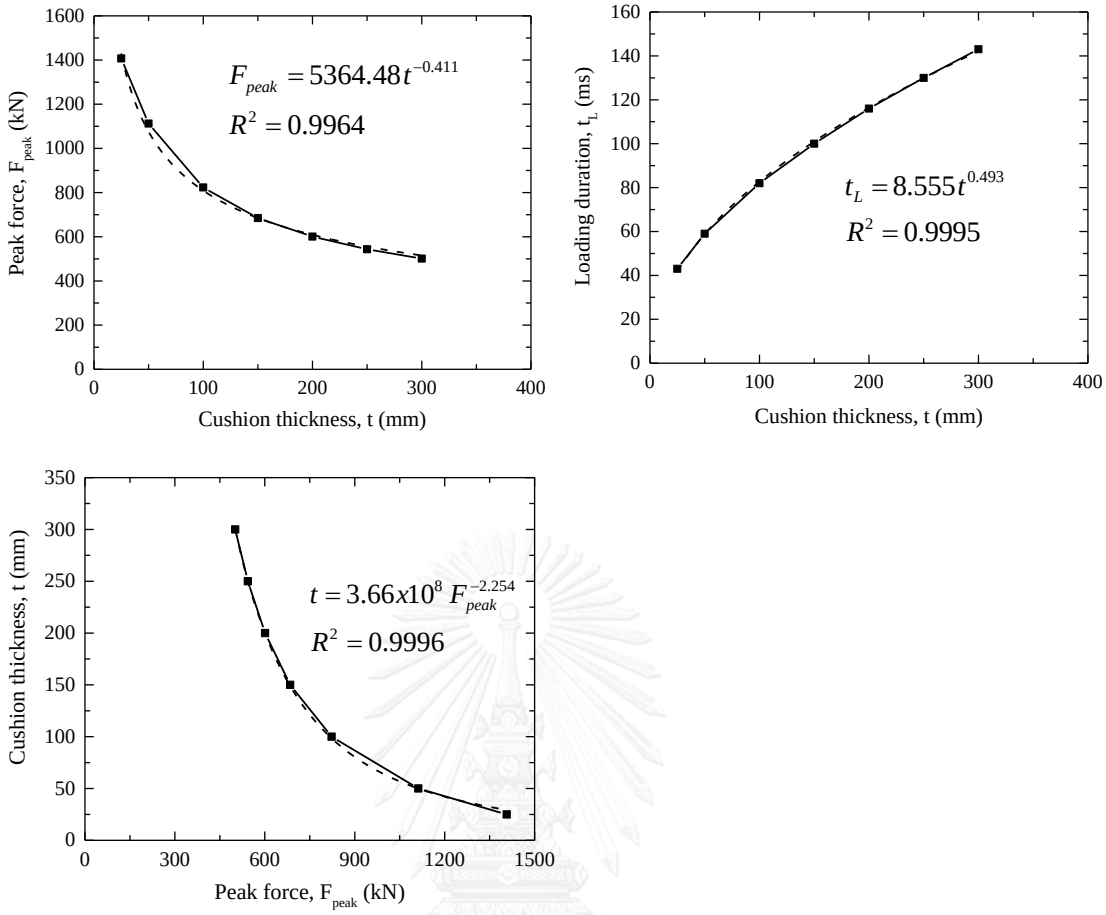

Figure 3.14 Relationships between the peak force, the loading duration and the pile cushion thickness.

$$F_{peak} = 5364.48\ t^{-0.411} \tag{3.10}$$

$$t_L = 8.555\ t^{0.493} \tag{3.11}$$

3.7 The summary of the main points

Based on the research in this Chapter, the relationships between the peak force, the loading duration, the hammer mass, the drop height and the pile cushion thickness are summarized in Figure 3.15, Figure 3.16 and Figure 3.17.

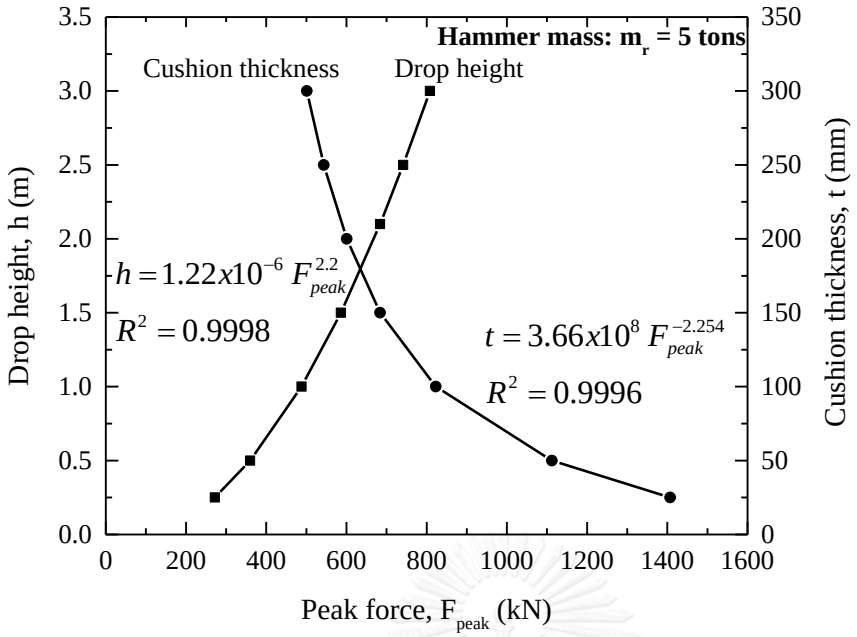

Figure 3.15 Relationships between the peak force, the drop height and the pile cushion thickness.

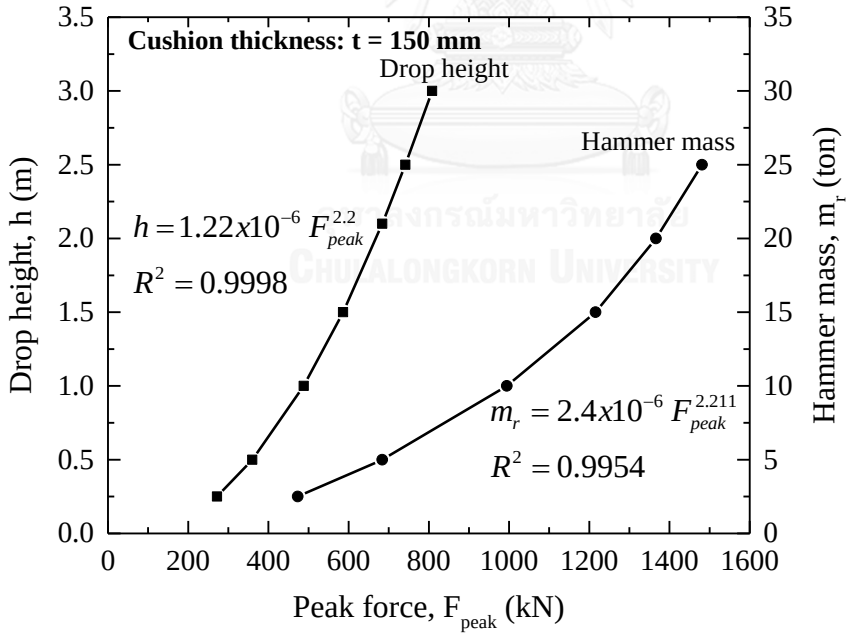

Figure 3.16 Relationships between the peak force, the drop height and the hammer mass.

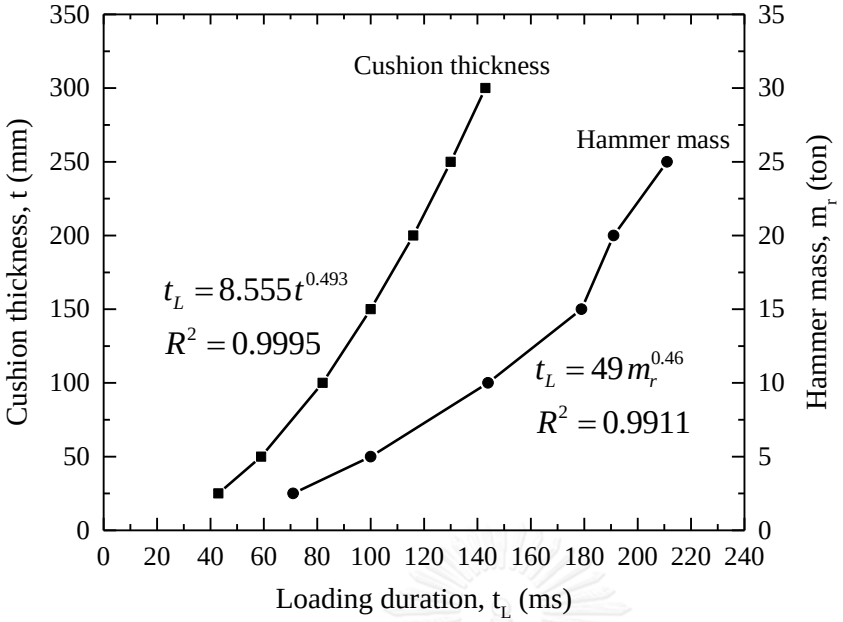

Figure 3.17 Relationships between the loading duration, the pile cushion thickness and the hammer mass.

With the philosophy is that the testing equipment including the hammer mass, the drop height and the pile cushion thickness, should be reasonably adjusted to mobilize the desired maximum force on the pile head.

For example, it is desired that the maximum force on the pile head is 600 kN. From Figure 3.15 and Figure 3.16 indicate that one of three equipment sets below is available.

$$\begin{cases} h = 1.6\,m \\ m_r = 5\,tons \\ t = 150\,mm \end{cases} \quad or \quad \begin{cases} h = 2.1\,m \\ m_r = 5\,tons \\ t = 200\,mm \end{cases} \quad or \quad \begin{cases} h = 2.1\,m \\ m_r = 3.4\,tons \\ t = 150\,mm \end{cases}$$

which h = the drop hammer, m_r = the hammer mass, t = the pile cushion thickness.

Chapter 4: UNLOADING POINT METHOD ASSOCIATED WITH TIME DELAY

4.1 Estimation of pile resistance by stress wave theory

A new interpretation technique is introduced in this study. The proposed method uses only the force and velocity that are measured at the pile head and the stress wave theory to estimate the response of the pile-soil during testing. The delay in response along the pile length is then taken into the consideration for determining the static response of piles.

Goble et al. (1975); Rausche et al. (1985) suggested a formula for estimating the resistance of piles as

$$F_{soil}\left(t+\frac{L}{c_p}\right)=\frac{1}{2}\left[F\left(t\right)+F\left(t+\frac{2L}{c_p}\right)\right]+\frac{M\cdot c_p}{2\cdot L}\left[v\left(t\right)-v\left(t+\frac{2L}{c_p}\right)\right] \quad (4.1)$$

where

F_{soil} = the soil resistance;

F = the force at the pile head;

v = the velocity at the pile head;

c_p = the wave propagation speed of pile material, $c_p = \sqrt{E_p/\rho_p}$;

M = the pile mass;

L = the pile length;

$2L/c_p$ = the time interval after impact.

It can be seen that the calculated soil resistance consists of two terms, which are the average of two forces over a time interval of $2L/c_p$ and the inertial force deduced from the change in velocity over the period of $2L/c_p$.

4.2 Unloading Point method associated with Time Delay (DULM)

As mentioned by Middendorp (2000), the estimation of the damping is more accurate when the average velocity is used instead of the velocity at the pile top. Inherit the concept of the Modified Unloading Point method, the stress wave theory is used to estimate the velocity at pile toe instead of embedding the accelerometer. The velocity of concentrate pile mass is represented by the average of the top and toe velocities by Eq. (4.2).

$$v_{av}(t) = \frac{1}{2}\left[v(t) + v_{toe}(t)\right] \tag{4.2}$$

where v_{toe} = the velocity at the pile tip computed by Eq.(4.3).

Because the stationary point in the concentrate pile mass occurs at a short period of time after the unloading point of the pile head, the time that the average velocity became zero after the zero pile top velocity is called the time delay.

The pile toe velocity can be determined according to Goble et al. (1975); Rausche et al. (1985) as

$$v_{toe}\left(t + \frac{L}{c_p}\right) = v(t) + \frac{c_p}{E_p \cdot A_p}\left[F(t) - F_{soil}(t)\right] \tag{4.3}$$

where F_{soil} = the soil resistance is calculated by Eq.(4.1).

Once the resistance time history of soil has been determined and the average velocity has been determined from Eq. (4.3), the calculation similar to the ULM is used to determine the damping constant, C_{av} (Figure 2.21, Eq. (2.59)).

Finally, the static capacity can be determined by

$$F_s(t) = F_{soil}(t) - C_{av} \cdot v_{av}(t) \tag{4.4}$$

Chapter 5: VALIDATION OF THE UNLOADING POINT METHOD ASSOCIATED WITH TIME DELAY

5.1 Introduction

To validate the performance of the Unloading Point method associated with Time Delay (DULM), case studies are carried out on RLT results in literatures that the force and motion (displacement, acceleration) were directly measured. All data of static load tests and rapid load tests are digitized from the corresponding papers.

There are fifteen rapid tests on eleven piles consisting of two steel pipe piles with concrete grouting, three concrete driven piles, five drilled piles and one auger bored cast in-situ pile. The piles were carried out at different six sites. Four of the sites are clayey ground and the remaining ones are sandy ground.

As mentioned earlier, the rate effect factor η is also considered in this study, but it should be corrected as the optimum rate effect factor to get the best result for each rapid load test.

The performance of the DULM were compared with the non-linear velocity-dependent method as referencing to the corresponding static test results.

5.2 Tests in sandy ground

5.2.1 Case study no.1, drilled pile, College Station, Texas, USA

Ballouz et al. (1991) and Brown (1994) performed the test in a sandy ground at the east side of the Riverside campus, the Texas A&M University, College Station, Texas. The pile was 0.9 m in diameter, 11.4 m long and embedded 10.4 m in the ground which consisted of medium dense, fine sands and silty sand. The plasticity index *PI* of the ground varied between 1.8% and 29.7%.

The static load testing was performed prior to the Statnamic test. Statnamic test results and static test results are shown in Figure 5.1 and Figure 5.2, respectively.

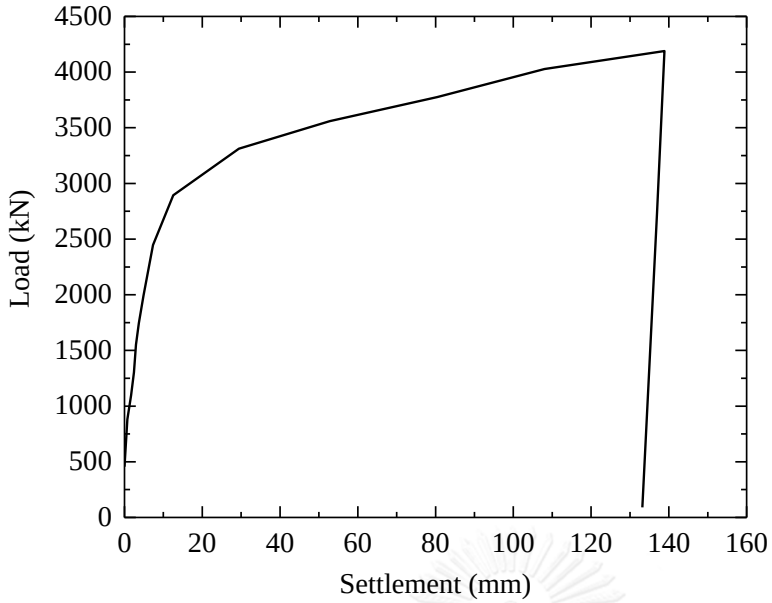

Figure 5.1 Static test result in sandy ground, drilled pile, College Station, Texas, USA (Brown, 1994).

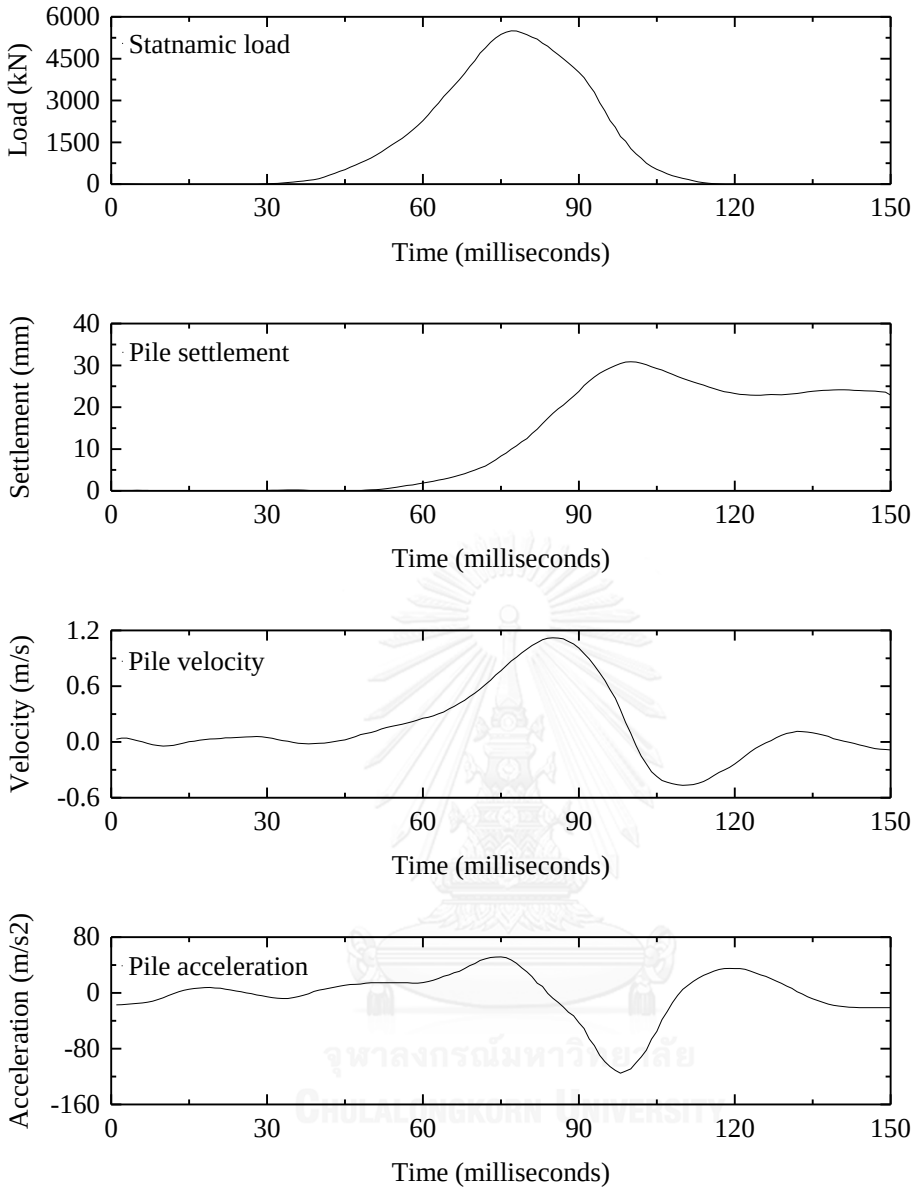

Figure 5.2 Statnamic test results in sandy ground, drilled pile, College Station, Texas, USA (Brown, 1994).

As seen in Figure 5.1, the failure did not occur even the displacement was as large as which is equivalent to 15.4% of pile diameter. This is a typical behavior of piles in sandy soil.

Parameters involving with the calculation are summarized in Table 5.1.

Table 5.1 Parameters used in the case study no.1.

Items	Value
Length of pile, L	11.4 m
Radius of pile, R	0.45 m
Density of pile material, ρ_p	2.4 ton/m^3
Young's modulus of pile material, E_p	25.53 GPa
Wave speed in pile, $c_p = \sqrt{E_p/\rho_p}$	3,262 m/s
Return period, $2L/c_p$	0.008 sec
Cross-sectional area of pile, $A_p = \pi \cdot R^2$	0.636 m^2
Impedance of pile, $Z = A_p \cdot E_p/c_p$	4,980 kN.s/m
Mass of pile, $M = A_p \cdot L \cdot \rho_p$	17.4 tons

Firstly, the damping constants, from the peak rapid load to the maximum displacement (c.f. point (1) and (2) of Figure 2.21), were determined by the ULM and the DULM. Their variations are shown in Figure 5.3. The average factor C from the ULM and DULM were 1613 kN.s/m and 1446 kN.s/m, respectively.

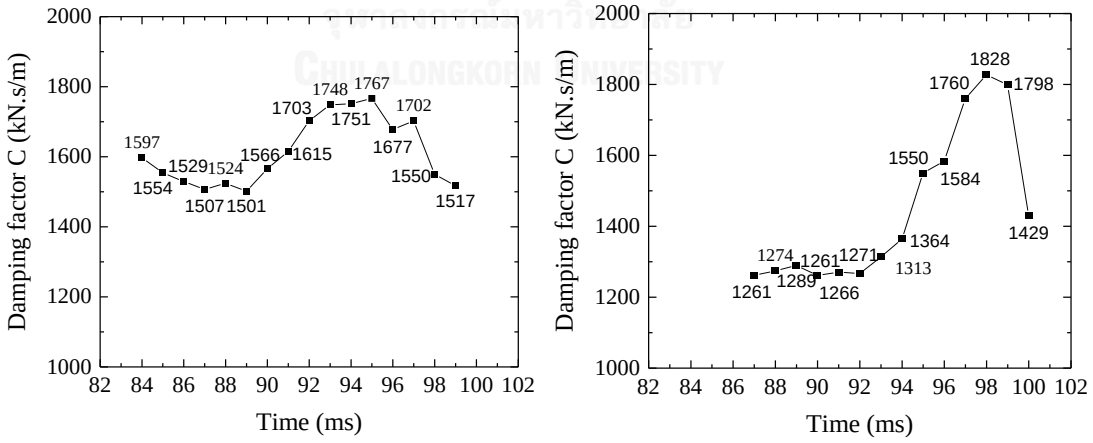

a) ULM b) DULM

Figure 5.3 Variation of the damping factor C.

Derived static responses, rapid and static test results are shown in Figure 5.4. Based on the ULM and DULM, the failure occurred at around 5 mm, corresponding to the derived static load of 3000 kN.

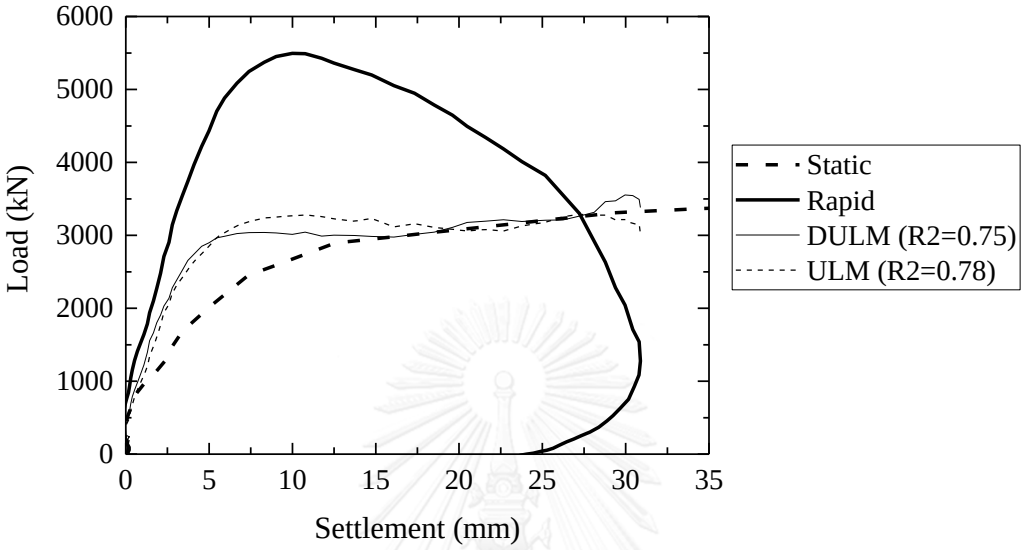

Figure 5.4 Comparison of predicted static capacity with measured, drilled pile in sandy ground, College Station, Texas, USA.

The estimated static curve from the ULM is slightly better than the DULM because R^2(ULM) = 0.78 is slightly greater than R^2(DULM) = 0.75.

5.2.2 Case study no.2, drilled pile, Cupertino, California, USA

Brown (1994) presented a Statnamic test on the drilled shaft No.4. The pile is 0.9 m in diameter and 9.1 m long. The ground consists of alternating layers of very dense clayey and sandy gravels to the depth of 10 m and underlain by dense silty sands.

The static load testing was performed prior to the Statnamic test. Statnamic test results and static test results are shown in Figure 5.5 and Figure 5.6, respectively.

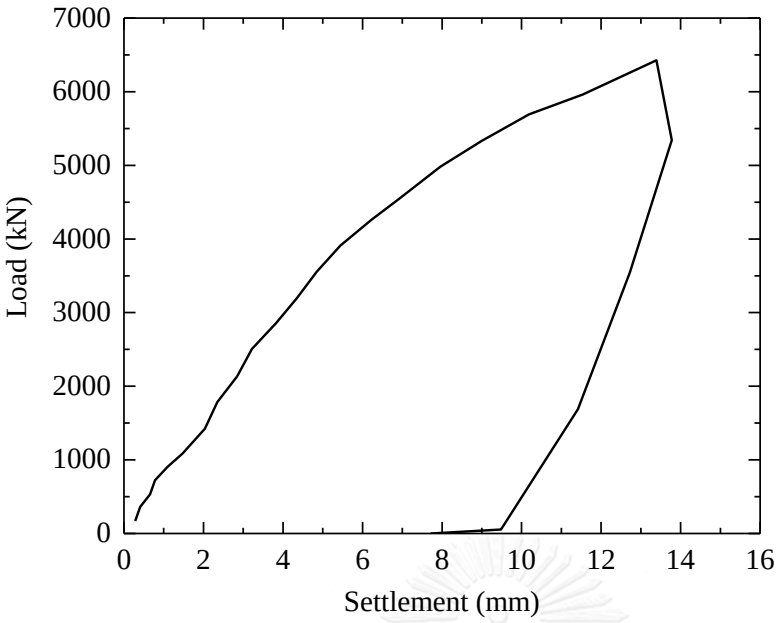

Figure 5.5 Static test result in sandy ground, drilled pile, Cupertino, California, USA (Brown, 1994).

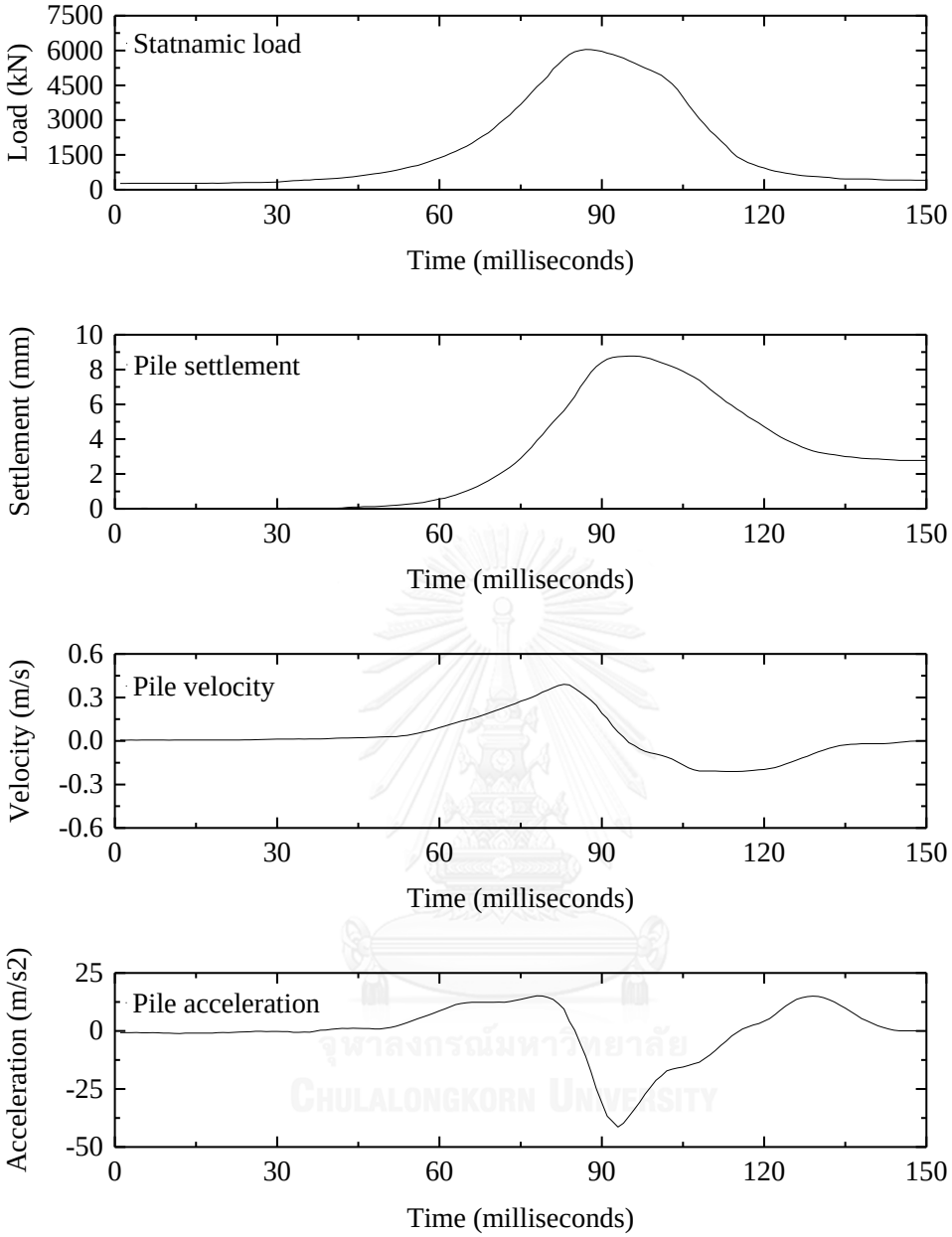

Figure 5.6 Statnamic test results in sandy ground, drilled pile, Cupertino, California, USA (Brown, 1994).

Under static loading, the pile was loaded to the maximum value of 6427 kN. The corresponding displacement was 13.4 mm which is equal to 1.5 % of pile diameter. It is considered that the pile had not been mobilized to its ultimate capacity and was still in its elastic stage.

Parameters involving with the calculation are summarized in Table 5.2.

Table 5.2 Parameters used in the case study no.2.

Items	Value
Length of pile, *L*	9.1 m
Radius of pile, *R*	0.45 m
Density of pile material, ρ_p	2.4 ton/m^3
Young's modulus of pile material, E_p	30.00 GPa
Wave speed in pile, $c_p = \sqrt{E_p/\rho_p}$	3,536 m/s
Return period, $2L/c_p$	0.006 sec
Cross-sectional area of pile, $A_p = \pi \cdot R^2$	0.636 m^2
Impedance of pile, $Z = A_p \cdot E_p/c_p$	5,398 kN.s/m
Mass of pile, $M = A_p \cdot L \cdot \rho_p$	13.9 tons

Similar to the earlier case, the damping factors from the ULM and the DULM are shown in Figure 5.7. The average values of the ULM and DULM are 1448 kN.s/m and 4811 kN.s/m, respectively. It can be seen that the latter is around three times of the former. The reasons for this signification change are two folds; 1) the difference in marking the point of zero velocity (the unloading point) and 2) the difference in determining the resistance of soil (Eq. (4.1)).

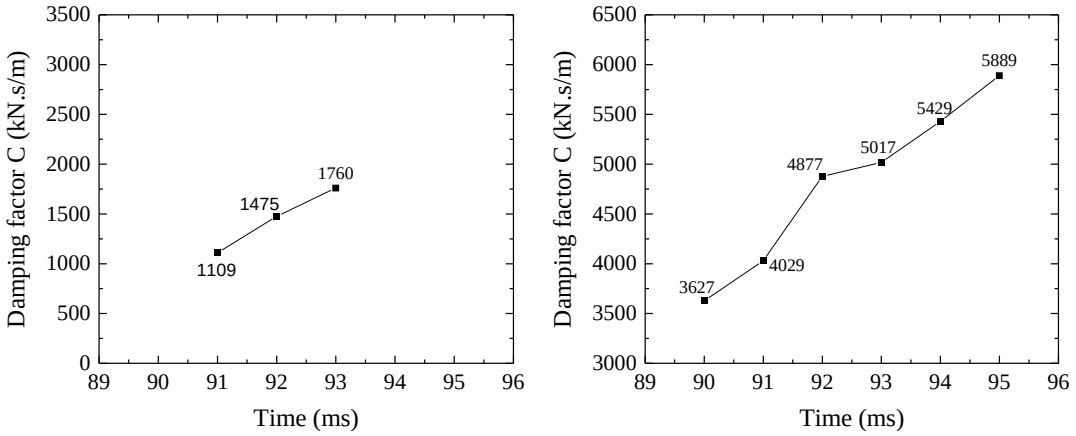

a) ULM b) DULM

Figure 5.7 Variation of the damping factor C.

Derived static responses, rapid and static test results are shown in Figure 5.8. Since the derived static load is only 6% of the static capacity observed in the SLT, the pile was still in elastic stage under this rapid loading.

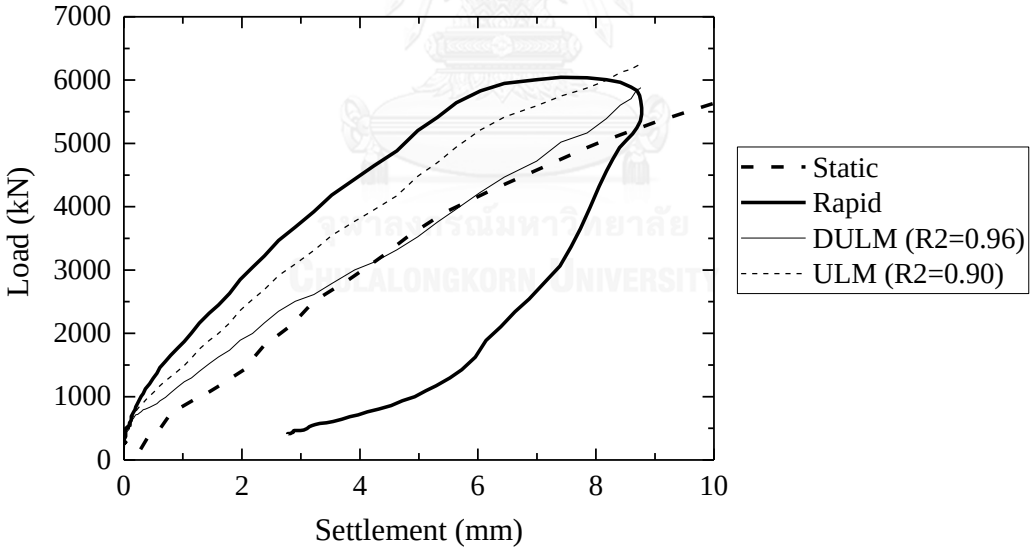

Figure 5.8 Comparison of predicted static capacity with measured, drilled shaft in sandy ground, Cupertino, California, USA.

The derived static curves from ULM and DULM were quite linear. However, the proposed technique was closer to the verified curve than the ULM one because R^2(DULM) = 0.96 was greater than R^2(ULM) = 0.90.

5.2.3 Case study no.3, driven pre-stressed concrete pile, Florida, USA

Static and Statnamic tests were carried out by Justason et al. (1998) on a pre-stressed concrete pile #15. The pile was a 0.6 m square pile with the length of 10.5 m. The test site was at the Bayou Chico Bridge Project in Pensacola, Florida. The soil profile was comprised of medium to dense, poorly graded sand with some silty sand.

The static test was conducted 50 days prior to the Statnamic test. Statnamic test results and static test results are shown in Figure 5.9 and Figure 5.10, respectively. The pile was tested under three static loading cycles which the peak loads increased from 3675 kN to 4123 kN. As plunging failure was not observed, the ultimate resistance could not be determined from these tests.

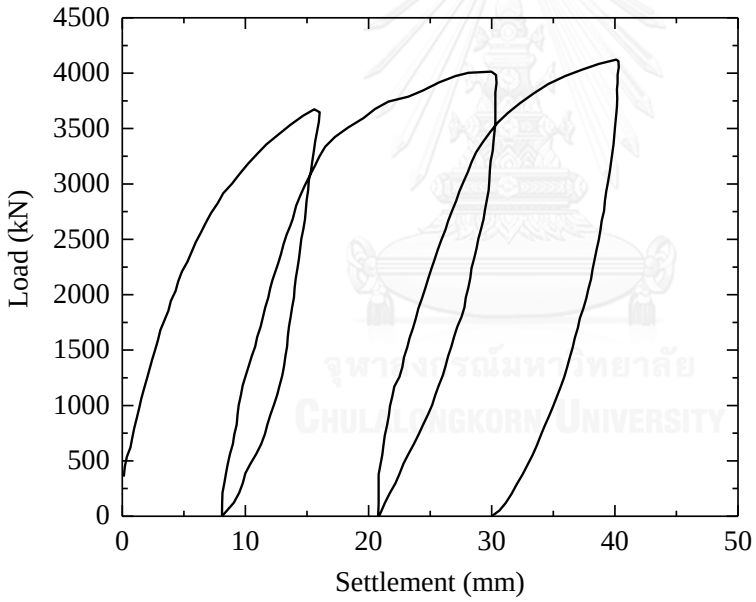

Figure 5.9 Static test result, driven pre-stressed concrete pile, Florida, USA (Justason et al., 1998).

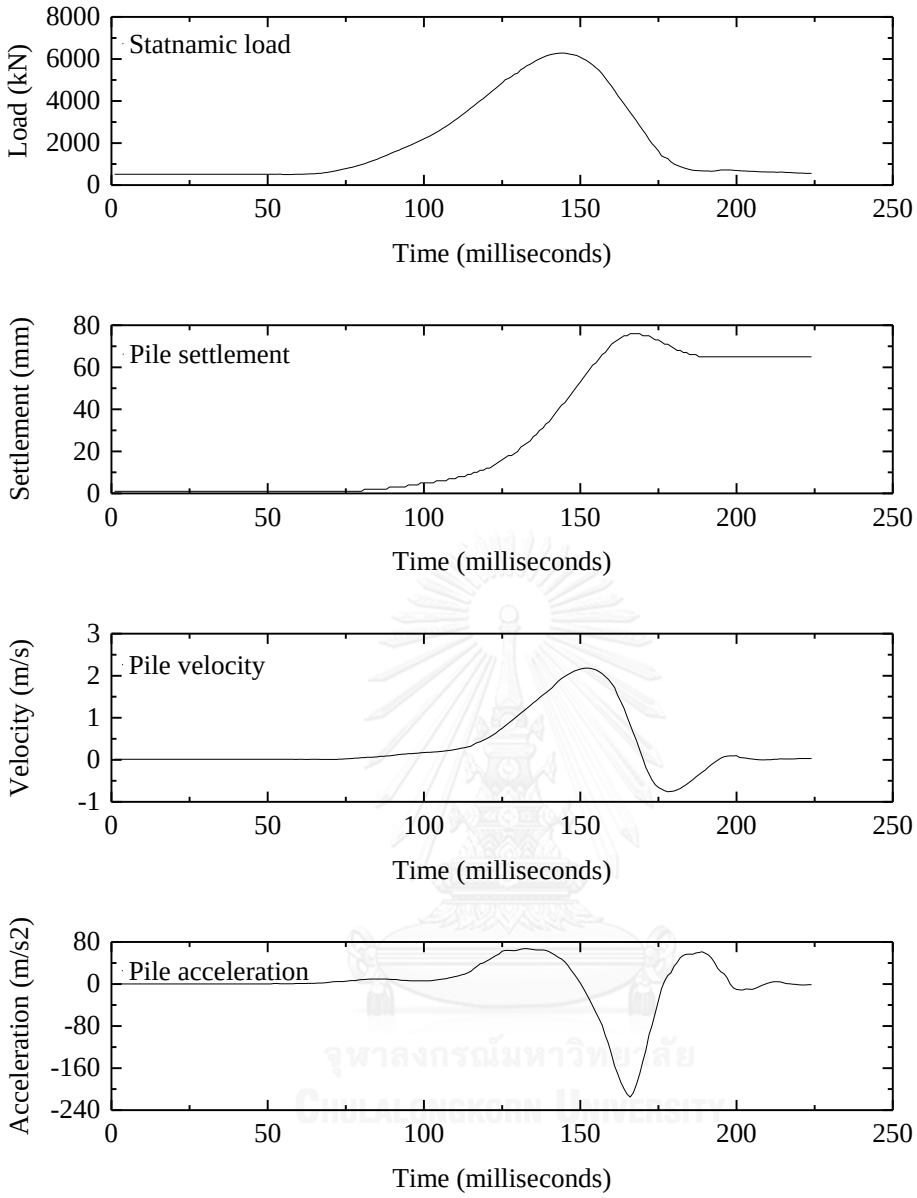

Figure 5.10 Statnamic test results in sandy ground, driven pre-stressed concrete pile, Florida, USA (Justason et al., 1998).

Parameters involving with the calculation are summarized in Table 5.3.

Table 5.3 Parameters used in the case study no.3.

Items	Value
Length of pile, L	10.5 m
Edge of pile, a	0.6 m
Density of pile material, ρ_p	2.4 ton/m^3
Young's modulus of pile material, E_p	30.00 GPa
Wave speed in pile, $c_p = \sqrt{E_p/\rho_p}$	3,536 m/s
Return period, $2L/c_p$	0.006 sec
Cross-sectional area of pile, $A_p = a \times a$	0.360 m^2
Impedance of pile, , $Z = A_p \cdot E_p/c_p$	3,055 kN.s/m
Mass of pile, $M = A_p \cdot L \cdot \rho_p$	9.1 tons

Similar to the earlier case, the damping factors from the ULM and the DULM are shown in Figure 5.11. The average values of the ULM and DULM are 1273 kN.s/m and 782 kN.s/m, respectively. It can be seen that the latter is around three times of the former. The reasons for this signification change are two folds; 1) the difference in marking the point of zero velocity (the unloading point) and 2) the difference in determining the resistance of soil (Eq. (4.1)).

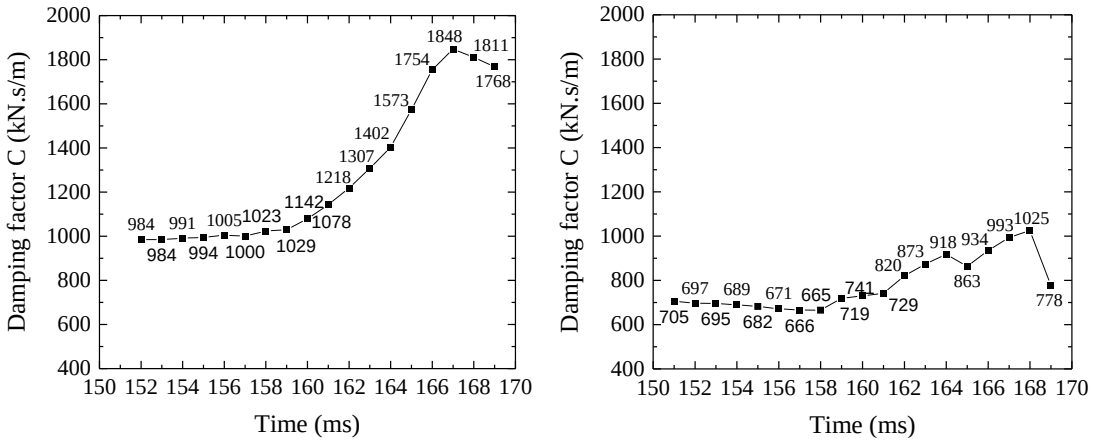

a) ULM b) DULM

Figure 5.11 Variation of the damping factor C.

Results from the ULM, DULM and load test results are shown in Figure 5.12. It can be seen that the DULM line is close to the static line than the ULM. The ultimate capacities observed from the DULM was 4100 kN which was similar to the static one. On the contrary, the ultimate value from the ULM is 3300 kN, or, around 80% of the SLT result.

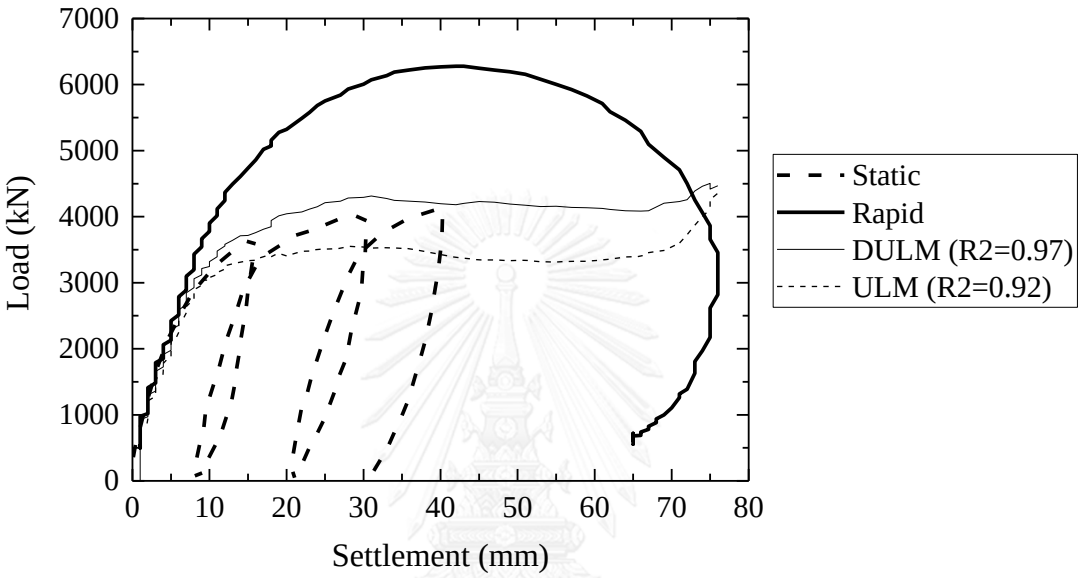

Figure 5.12 Comparison of predicted static capacity with measured, driven pre-stressed concrete pile in sandy ground, Florida, USA.

From the three RLTs in sandy soils, some conclusion can be made as follows;

1. The results derived from the standard ULM were not consistent. For example, the result from the ULM was good in Figure 5.4, over-predicted or under-predicted in Figure 5.8 and Figure 5.12, respectively.

2. The coefficient of determination, R^2, calculated from DULM are 0.96 and 0.97 higher than ones from the ULM as 0.90 and 0.92 in the case study no.2 and 3, respectively. Although the R^2 value of the ULM is 0.78 slightly higher than one of the DULM as 0.75 as in the case study no.1, it can be said that the DULM performed better than the ULM.

5.3 Tests in clayey ground

5.3.1 Case study no.1, drilled pile, College Station, Texas, USA

Ballouz et al. (1991) and Brown (1994) conducted the test on the west side of the Riverside campus of the Texas A&M University, College Station, Texas. The test site mainly consisted of stiff clays with the plasticity index *PI* varied from 31% to 50% along the pile length. The test pile was 0.92 m in diameter and 10.7 m in length embedded 9.5 m into the ground.

The static test was performed four days prior to the Statnamic test. The test results are shown in Figure 5.13 and Figure 5.14.

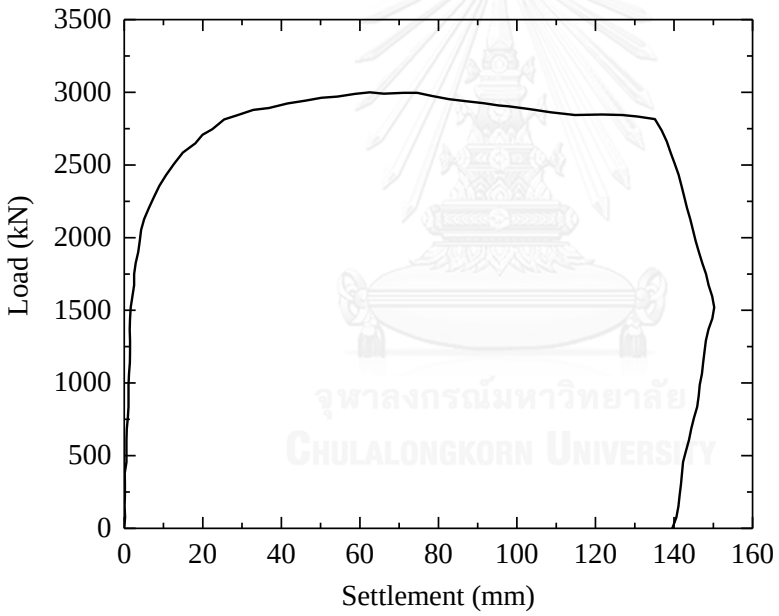

Figure 5.13 Static test result in clayey ground, drilled pile, College Station, Texas, USA (Brown, 1994).

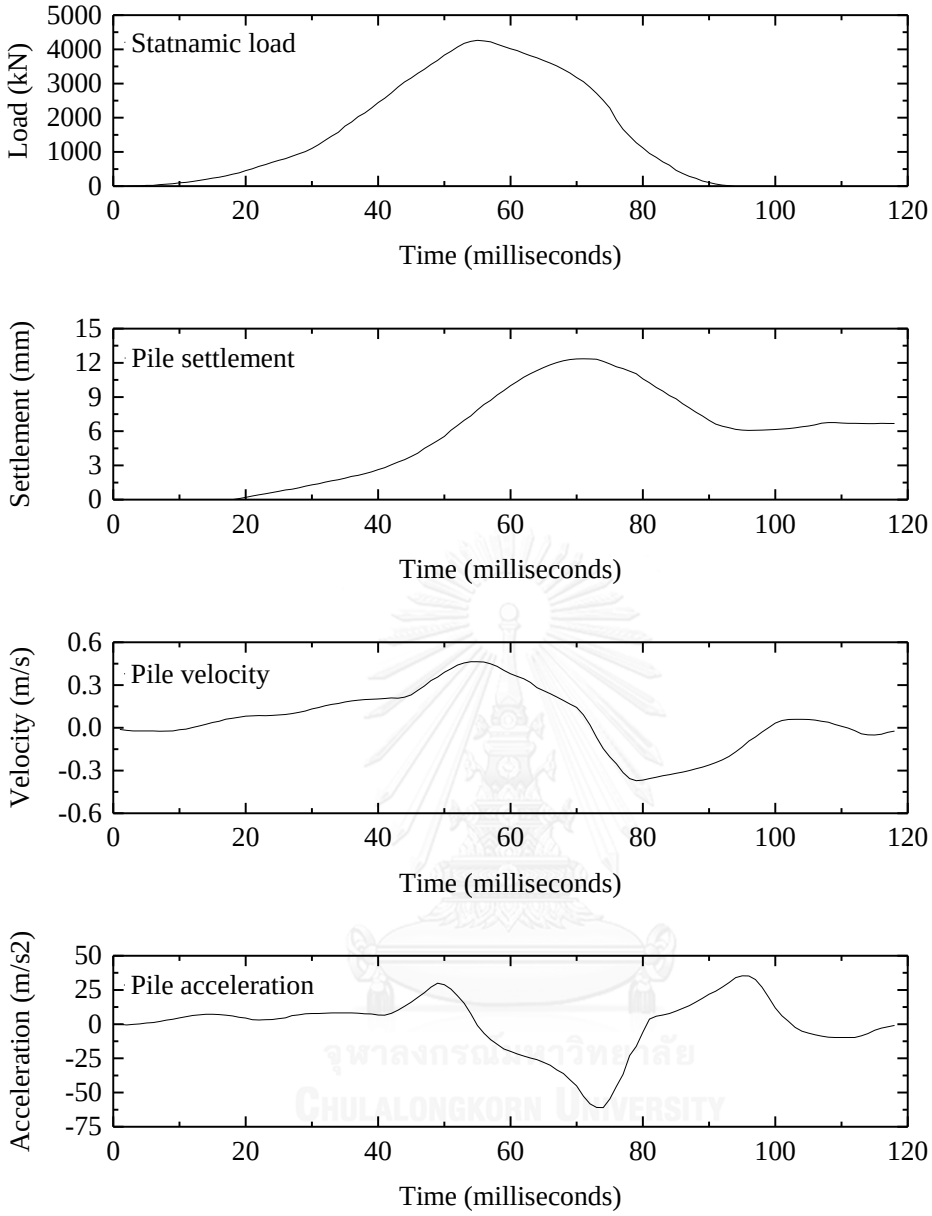

Figure 5.14 Statnamic test results in clayey ground, drilled pile, College Station, Texas, USA (Brown, 1994).

Based on the test result in Figure 5.13, it can be concluded that the pile failed under load of 2844 kN when the displacement was around 115 ~ 135 mm. The yielding occurred when the pile displaced around 29 mm.

As introduced above, the plasticity index *PI* varied from 31% to 50% along the pile length, so the average rate parameter α as shown in Table 5.4 was used for the Brown's

method. For the ULM, the derived values were corrected with the rate effect factor of 0.47 and of 0.65 for the interest of comparison.

Table 5.4 Estimation of the rate parameter α from clayey soil, College Station, Texas.

Depth (m)	Plasticity index, *PI* (%)	Rate parameter, $\alpha = 0.03\ PI + 0.5$
0	0	0
1.5	37	1.61
3	35	1.55
4.6	35	1.55
6.1	32	1.46
7.6	31	1.43
9.1	48	1.94
9.5	50	2.00
Average		**1.65**

Parameters involving with the calculation are summarized in Table 5.5.

Table 5.5 Parameters used in the case study no.1.

Items	Value
Length of pile, L	10.7 m
Radius of pile, R	0.46 m
Density of pile material, ρ_p	2.4 ton/m^3
Young's modulus of pile material, E_p	27.60 GPa
Wave speed in pile, $c_p = \sqrt{E_p/\rho_p}$	3,391 m/s
Return period, $2L/c_p$	0.008 sec
Cross-sectional area of pile, $A_p = \pi \cdot R^2$	0.665 m^2
Impedance of pile $Z = A_p \cdot E_p/c_p$	5,410 kN.s/m
Mass of pile, $M = A_p \cdot L \cdot \rho_p$	17.1 tons

Similar to the earlier cases, the damping factors from the ULM and the DULM are shown in Figure 5.15. The average values of the ULM and DULM are 991 kN.s/m and

1583 kN.s/m, respectively. It can be seen that the latter is 60% higher than of the former. The reasons for this signification change are two folds; 1) the difference in marking the point of zero velocity (the unloading point) and 2) the difference in determining the resistance of soil (Eq. (4.1)).

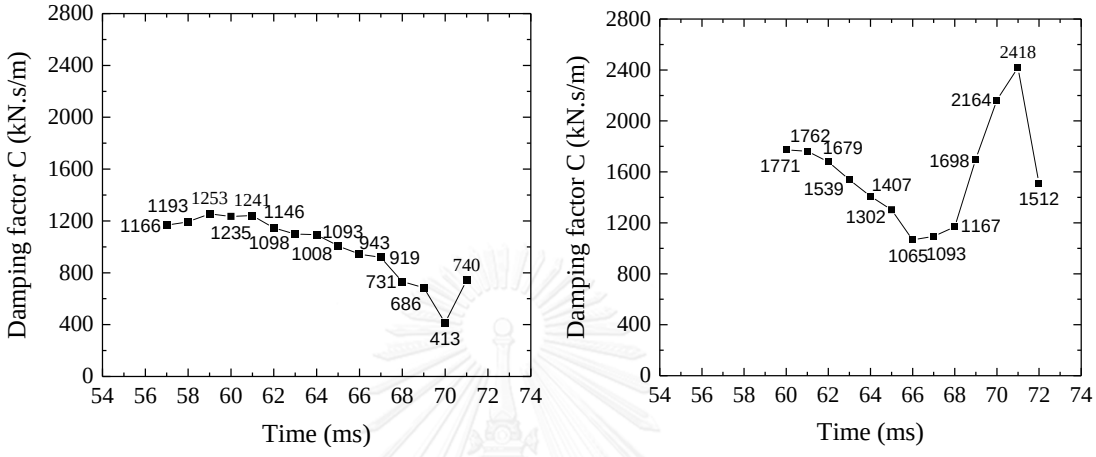

a) ULM b) DULM

Figure 5.15 Variation of the damping factor C.

Results from the ULM, DULM and load test results are shown in Figure 5.16. According to the previous studies, the DULM should be adjusted by the rate effect factor η. The optimum value of 0.65 was determined by trial and error and compared with suggested values in literatures which are in the range of 0.47 ~ 0.65. The adjusted results of the ULM and DULM as well as the result of nonlinear method are shown in Figure 5.16.

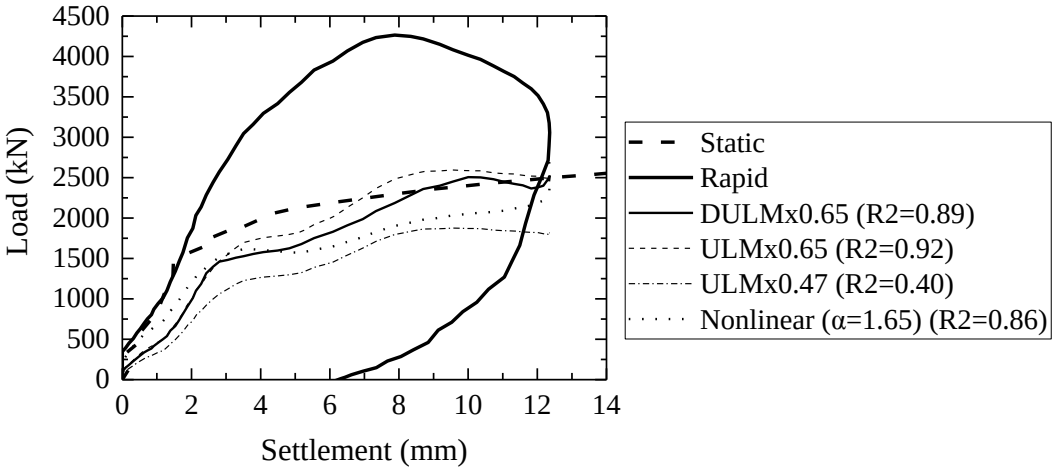

Figure 5.16 Comparison of predicted static capacity with measured, drilled shaft in clayey ground, College Station, Texas, USA.

The ULM modified with the rate effect factor of 0.47 (ULM x 0.47) showed the softest response. The performance of the nonlinear method was better than the ULM x 0.47 due to R^2(Nonlinear) = 0.86 > R^2(ULMx0.47) = 0.40, but it still underestimated the static line. Although the DULM x 0.65 and ULM x 0.65 are modified with the same value of the rate effect factor η, the estimation of the ULM x 0.65 was better than DULM x 0.65 because of R^2(ULMx0.65) = 0.92 > R^2(DULMx0.65) = 0.89.

5.3.2 Case study no.2, drilled pile, Rio Puerco, Gallup, N.M.

Brown (1994) reported a Statnamic test result on a drilled pile at Rio Puerco, Gallup, N.M. The pile was 0.76 m in diameter which was embedded 13.8 m in very stiff silty clayey soil.

The drilled pile was loaded under static loading 4 days prior to Statnamic loading. The test results are shown in Figure 5.17 and Figure 5.18.

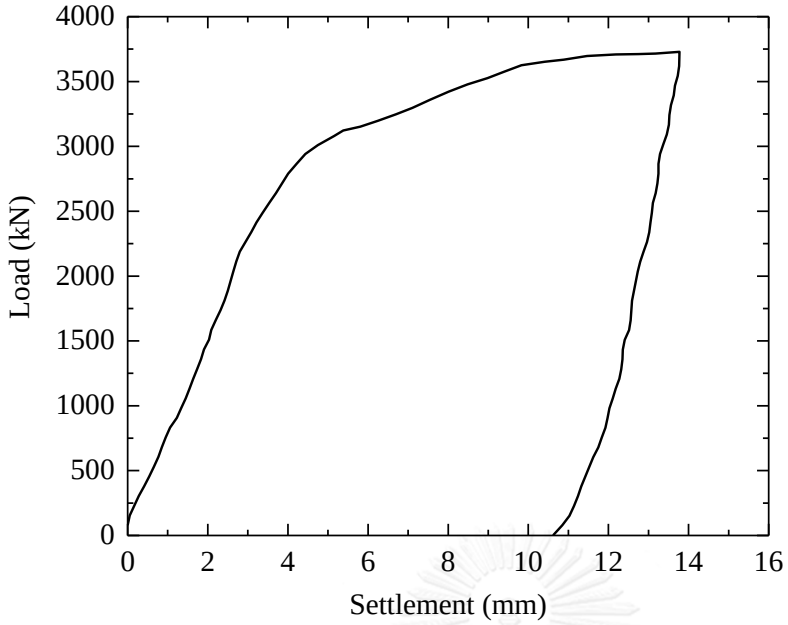

Figure 5.17 Static test result in clayey ground, drilled pile, Rio Puerco, Gallup, N.M. (Brown, 1994).

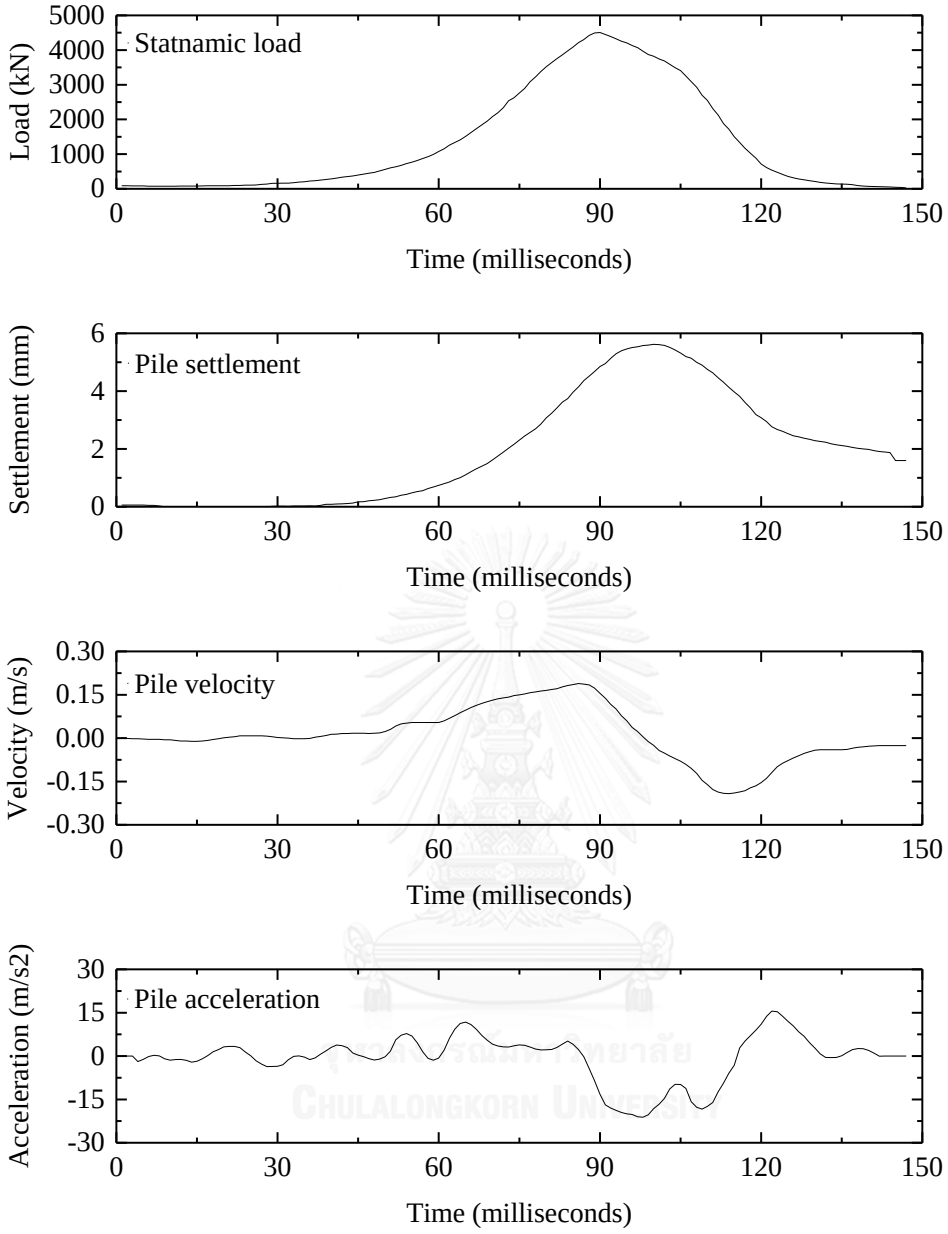

Figure 5.18 Statnamic test results in clayey ground, drilled pile, Rio Puerco, Gallup, N.M. (Brown, 1994).

Based on the result in Figure 5.17, the pile yielded at around 5 mm. The maximum test load was 3729 kN corresponding to the displacement of 13.8 mm or around 2% of pile diameter.

Brown (1994) did not show the plasticity index PI which can be used to calculate the rate parameter α. Therefore, the α of 1.0 was assumed for clayey soils as suggested by Randolph and Deeks (1992).

Parameters involving with the calculation are summarized in Table 5.6.

Table 5.6 Parameters used in the case study no.2.

Items	Value
Length of pile, L	13.8 m
Radius of pile, R	0.38 m
Density of pile material, ρ_p	2.4 ton/m^3
Young's modulus of pile material, E_p	30.00 GPa
Wave speed in pile, $c_p = \sqrt{E_p/\rho_p}$	3,536 m/s
Return period, $2L/c_p$	0.008 sec
Cross-sectional area of pile, $A_p = \pi \cdot R^2$	0.454 m^2
Impedance of pile, $Z = A_p \cdot E_p/c_p$	3,849 kN.s/m
Mass of pile, $M = A_p \cdot L \cdot \rho_p$	15.0 tons

Similar to the earlier cases, the damping factors from the ULM and the DULM are shown in Figure 5.19. The average values of the ULM and DULM are 3561 kN.s/m and 5350 kN.s/m, respectively. It can be seen that the latter is 50% higher than of the former. The reasons for this signification change are two folds; 1) the difference in marking the point of zero velocity (the unloading point) and 2) the difference in determining the resistance of soil (Eq. (4.1)).

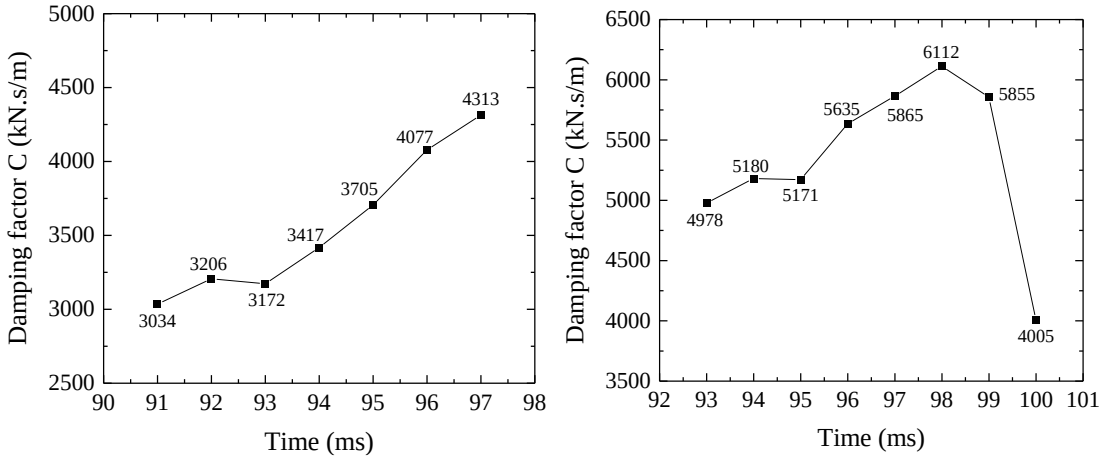

a) ULM b) DULM

Figure 5.19 Variation of the damping factor C.

Results from the ULM, DULM, nonlinear method and load test results are shown in Figure 5.20.

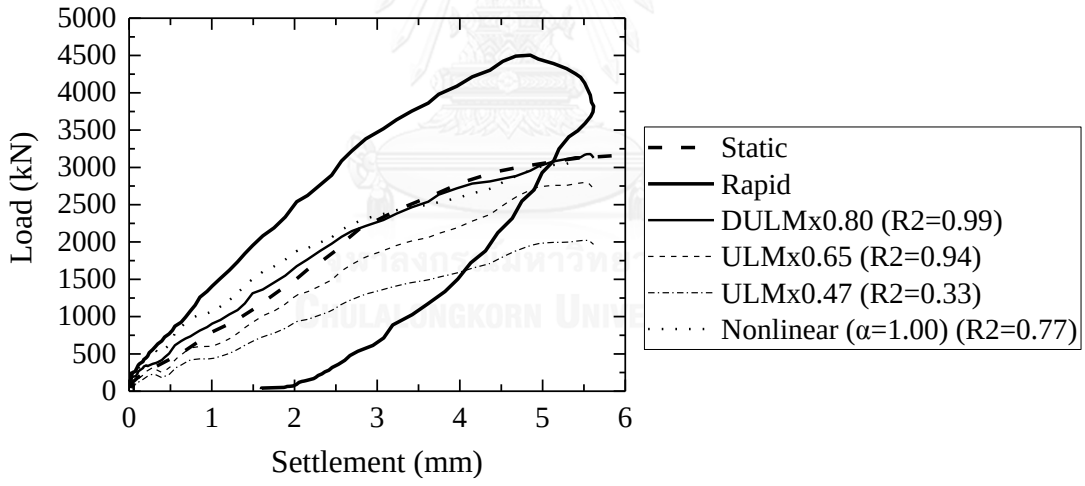

Figure 5.20 Comparison of predicted static capacity with measured, drilled shaft in clayey ground, Rio Puerco, Gallup, N.M.

Results calculated from the ULM combined with the rate effect factor of 0.47 and the nonlinear method according to R^2 of 0.33 and 0.77, respectively, were significantly lower than others. The result computed from the ULM x 0.65 (R^2 = 0.94) was slightly lower than the result of the DULM with the rate effect factor of 0.80 (R^2 = 0.99). Both of them gave good estimations of the static response.

5.3.3 Case study no.3, auger bored cast in-situ pile, Grimsby, UK

Brown (2004) carried out a Statnamic test on an auger bored cast in-situ pile in clayey soil. The site location was the Expanded Piling Company Limited's Cheapside head office, Waltham, Grimsby, United Kingdom. The soil description was firm to very stiff clay up to 20.35 m below ground surface. The plasticity index *PI* varied from 7% to 20%. The pile was 0.6 m in diameter and 12.24 m in length. It was bored to 11.76 m below ground level.

The pile was tested under rapid loading and followed by two types of static tests which were the constant rate of penetration test (CRP) at the rate of 0.01 mm/sec and the maintained load test (MLT). To avoid the influence of loading rate, MLT is used as the verification test in this study. The test results are shown in Figure 5.21 and Figure 5.22.

The pile plunging was observed at 15 mm under the load of 1800 kN. The settlement at the beginning of plunging was only 2.5 % of pile diameter.

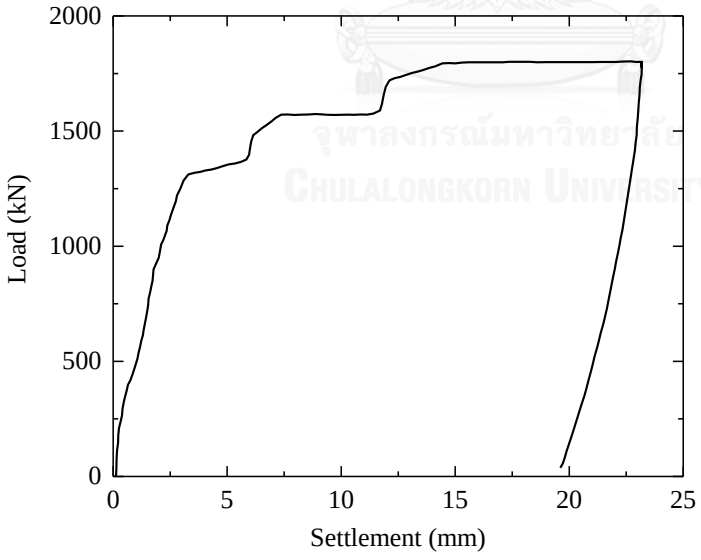

Figure 5.21 Static test result in clayey ground, auger bored cast in-situ pile, Grimsby, UK (Brown, 2004).

Before the static testing, the pile was tested under six rapid loading cycles. The magnitude of rapid loads increased from 1163 kN in the first cycle to 3062 kN in the final cycle.

Brown (2004) only showed the full data of the final rapid loading test which is used in this study. In this loading cycle, the maximum displacement was only 11 mm (or, 73% of 15 mm). Therefore, this settlement value is not enough to ensure the failure of pile during rapid testing.

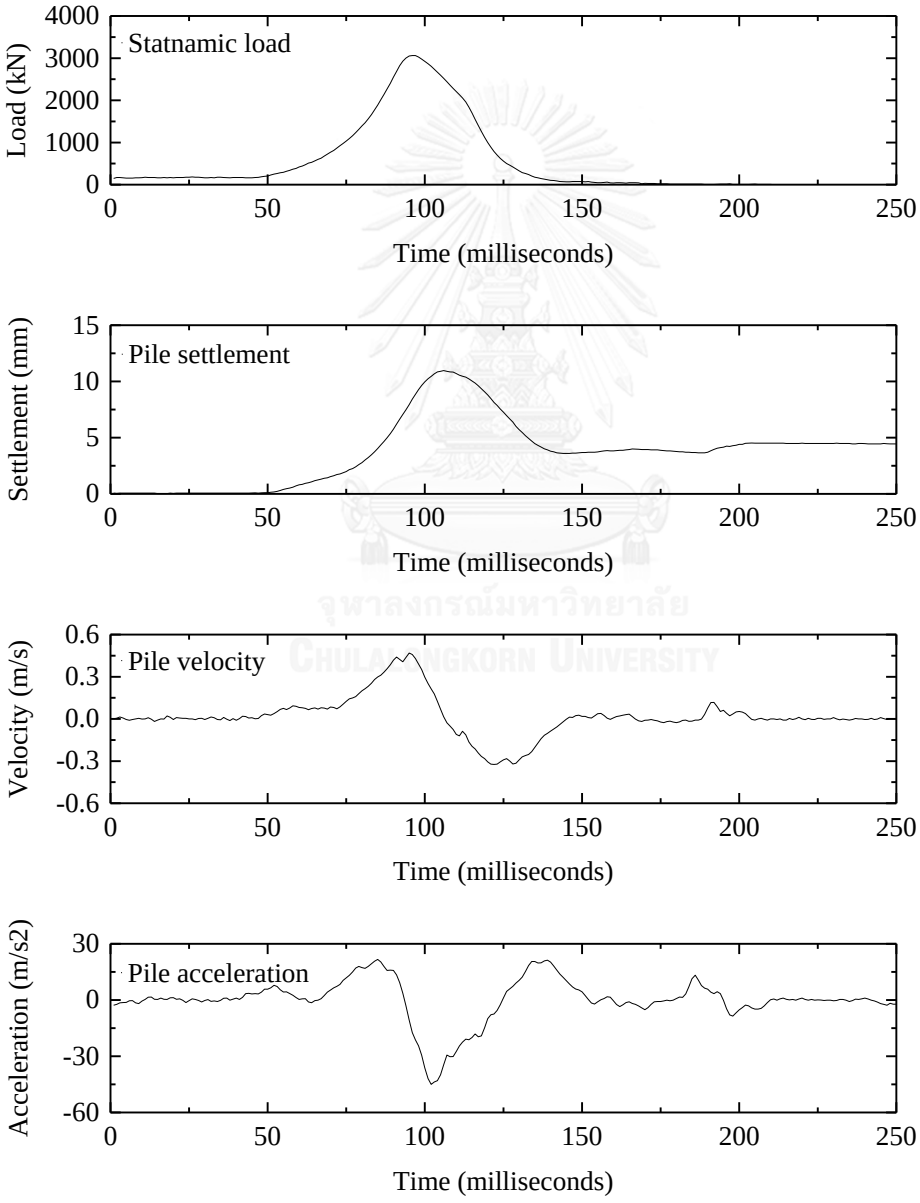

Figure 5.22 Statnamic test results in clayey ground, auger bored cast in-situ pile, Grimsby, UK (Brown, 2004).

As introduced above, the plasticity index *PI* varied from 7% to 20%, so the average rate parameter α as shown in Table 5.7 was used for the Brown's method. For the ULM, the derived values were corrected with the rate effect factor of 0.47 and 0.65 for the interest of comparison.

Table 5.7 Estimation of the rate parameter α *from clayey ground, Grimsby, UK.*

Plasticity index, *PI* (%)	Rate parameter, $\alpha = 0.03\ PI + 0.5$
7	0.71
20	1.10
Average	**0.91**

Parameters involving with the calculation are summarized in Table 5.8.

Table 5.8 Parameters used in the case study no.3.

Items	Value
Length of pile, *L*	12.24 m
Radius of pile, *R*	0.30 m
Density of pile material, ρ_p	2.4 ton/m^3
Young's modulus of pile material, E_p	31.37 GPa
Wave speed in pile, $c_p = \sqrt{E_p/\rho_p}$	3,615 m/s
Return period, $2L/c_p$	0.008 sec
Cross-sectional area of pile, $A_p = \pi \cdot R^2$	0.283 m^2
Impedance of pile $Z = A_p \cdot E_p/c_p$	2,453 kN.s/m
Mass of pile, $M = A_p \cdot L \cdot \rho_p$	8.3 tons

Similar to the earlier cases, the damping factors from the ULM and the DULM are shown in Figure 5.23. The average values of the ULM and DULM are 1452 kN.s/m and 3212 kN.s/m, respectively. It can be seen that the latter is around two times of the former. The reasons for this signification change are two folds; 1) the difference in

marking the point of zero velocity (the unloading point) and 2) the difference in determining the resistance of soil (Eq. (4.1)).

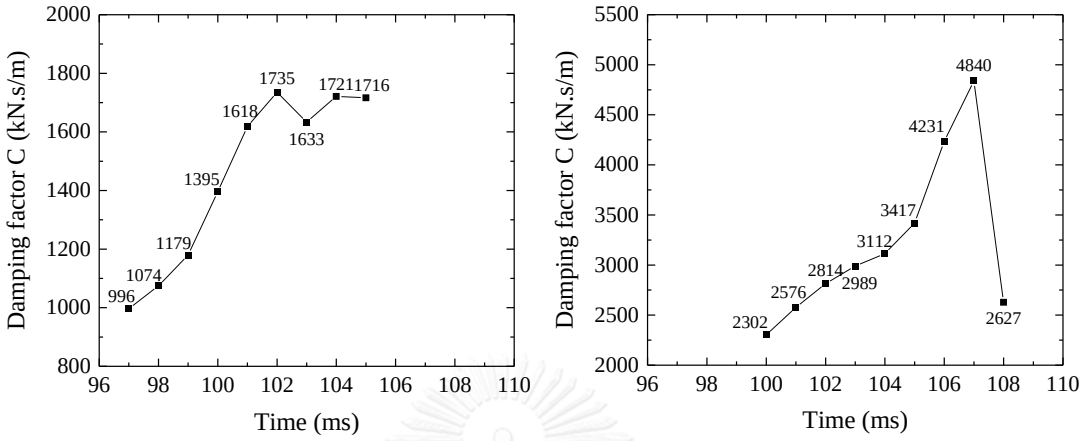

a) ULM b) DULM

Figure 5.23 Variation of the damping factor C.

Results from the ULM, DULM, the nonlinear method and load test results are shown in Figure 5.24. According to the previous studies, the DULM should be adjusted by the rate effect factor η. The optimum rate factor for the DULM was 0.75 which was estimated by the trial and error method.

As in the Figure 5.24, most derived static curves are quite linear and are not reasonable to compare with the measured static curve. In general, the estimation from the DULM x 0.75 shows the closest to the verified curve. The maximum force computed from the ULM x 0.47, ULM x 0.65, the nonlinear method and the DULM x 0.75 are 1251 kN, 1853 kN, 2080 kN and 1648 kN, which are equivalent to 80 %, 118%, 132% and 105% of the static force at the same displacement level, respectively.

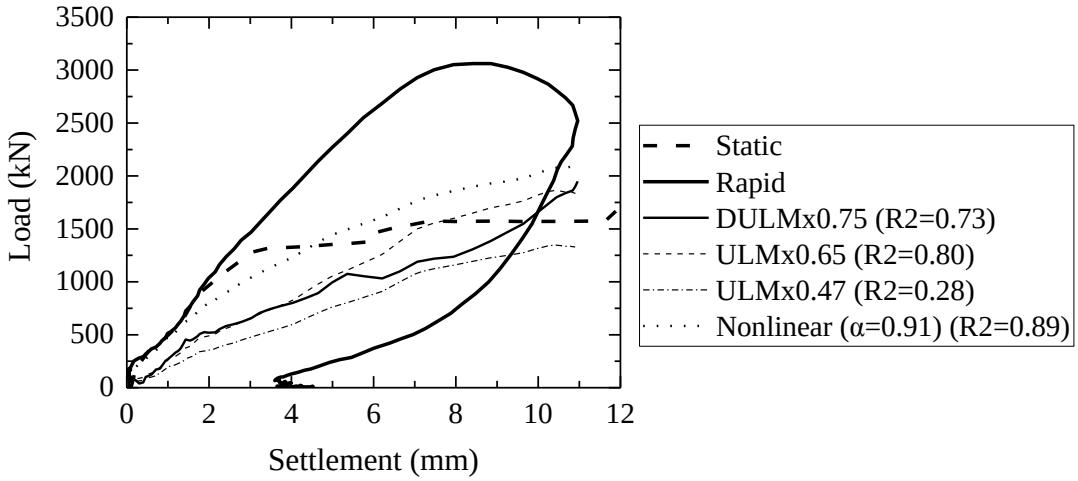

Figure 5.24 Comparison of predicted static capacity with measured, auger bored pile in clayey ground, Grimsby, UK.

The ULM modified with the rate effect factor of 0.47 (ULM x 0.47) showed the softest response with the lowest value of R^2. The result computed from the nonlinear method and ULM x 0.65 were better than one from the DULM x 0.75 due to the higher value of R^2.

5.3.4 Case study no.4, steel pipe pile, Salt Lake City, Utah

Garner (2007) conducted tests on steel pipe piles at South Temple and Salt Lake City, Utah. Static and rapid tests were carried out on different piles in the same site. The steel pipes had the inside diameter of 305 mm and the outside diameter of 324 mm. The void in the pipes were fully filled with concrete (Figure 5.25). They were driven to a depth of about 12.2 m. The ground mainly consisted of clay layers with the plasticity index *PI* varied between 5% and 43%.

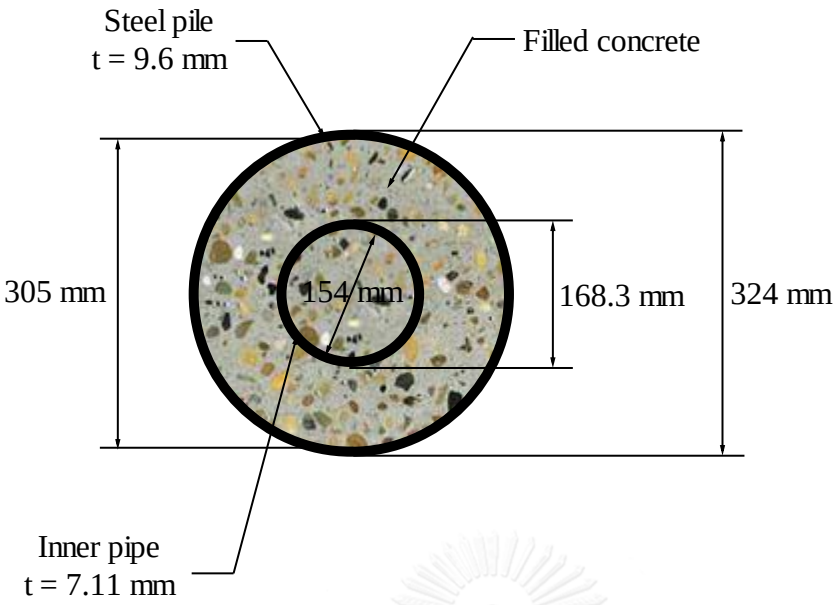

Figure 5.25 Cross-sectional area of the test pile (Garner, 2007).

Static tests were carried out at various rates of loading. The 54 minutes test (Figure 5.26) was selected as the verification test in this study. Since the displacement was mobilized up to 15 mm which was comparable to that occurred in the Statnamic test.

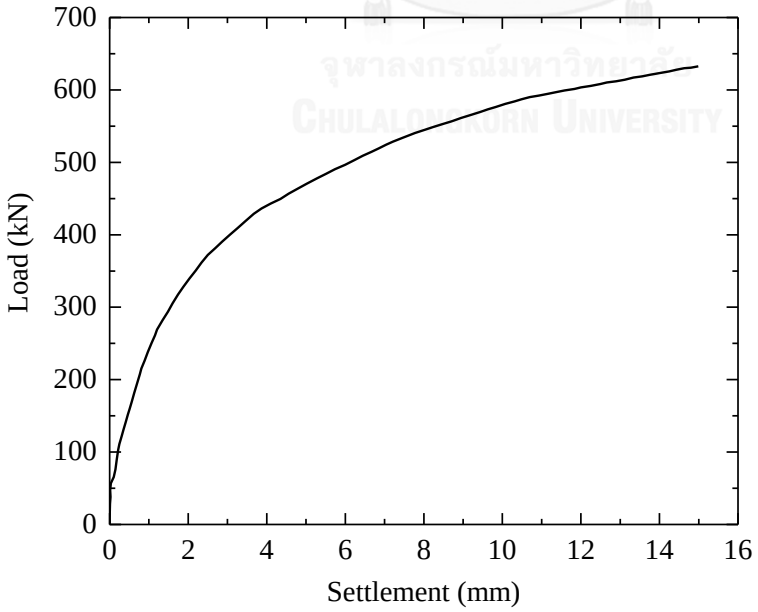

Figure 5.26 Static test result in clayey ground, steel pipe pile, Salt Lake City, Utah (Garner, 2007).

The Statnamic test was carried out on another pile in the same site. Two Statnamic loading cycles were performed for obtaining the results shown in Figure 5.27 and Figure 5.28.

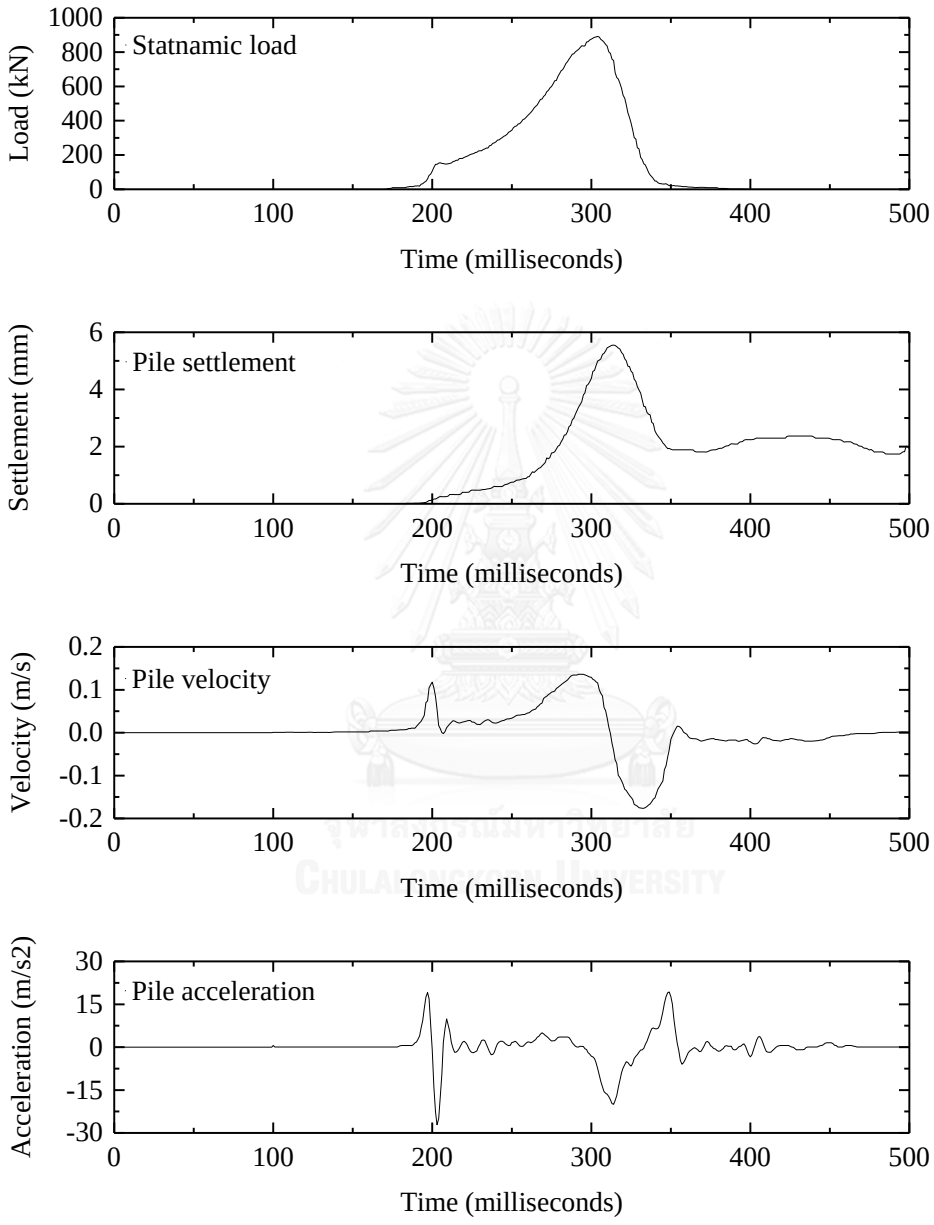

Figure 5.27 Statnamic test results in clayey ground (test #1), steel pipe pile, Salt Lake City, Utah (Garner, 2007).

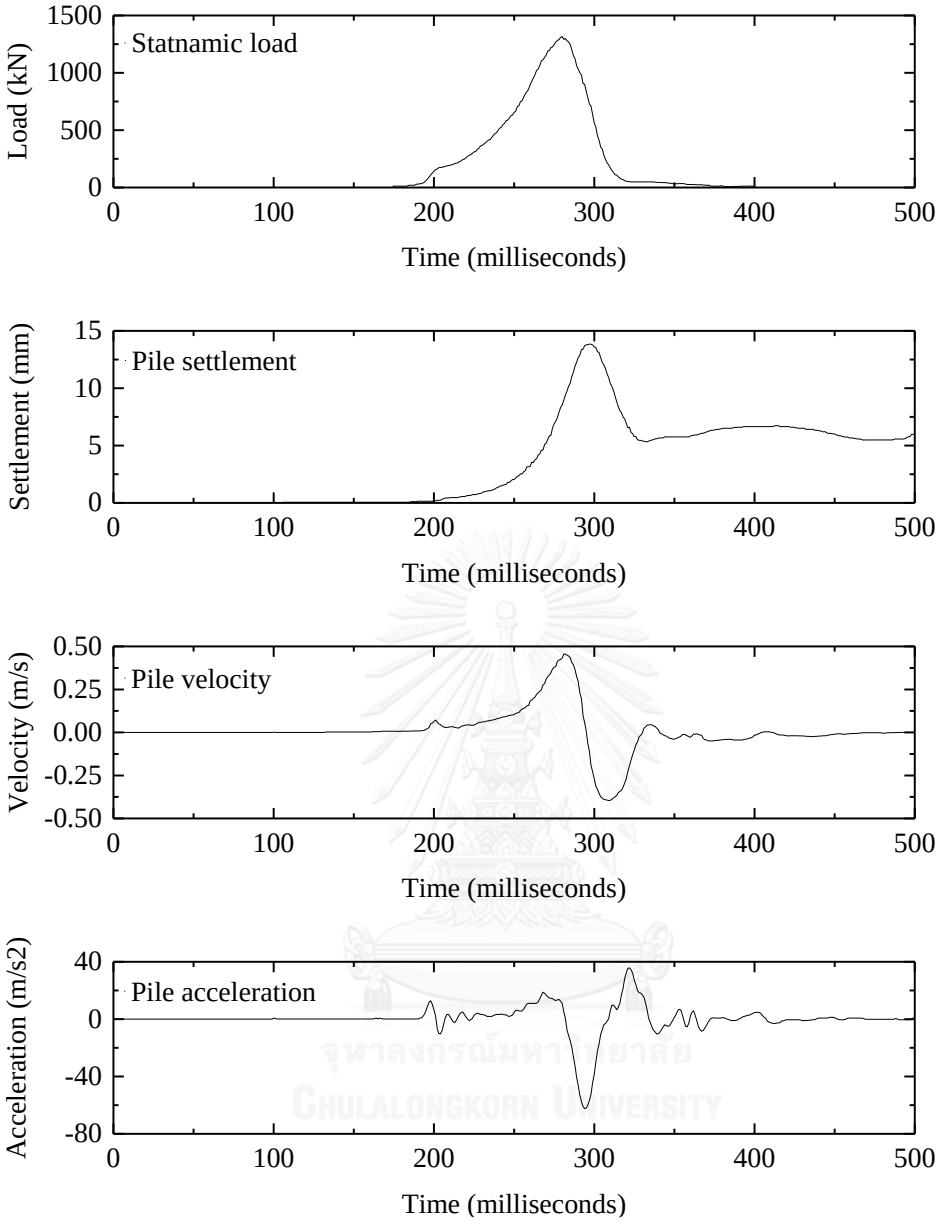

Figure 5.28 Statnamic test results in clayey ground (test #2), steel pipe pile, Salt Lake City, Utah (Garner, 2007).

As introduced above, the plasticity index *PI* varied from 5% to 43% along the pile length, so the average rate parameter α as shown in Table 5.9 was used for the Brown's method. For the ULM, the derived values were corrected with the rate effect factor of 0.47 and 0.65 for the interest of comparison.

Table 5.9 Estimation of the rate parameter α from the clayey soil, Salt Lake City, Utah..

Depth (m)	Plasticity index, *PI* (%)	Rate parameter, $\alpha = 0.03\ PI + 0.5$
0	0	0
0.08	43	1.79
0.1	27	1.31
0.2	22	1.16
0.4	32	1.46
0.5	11	0.83
0.7	25	1.25
1	13	0.89
1.1	15	0.95
1.3	5	0.65
1.6	20	1.10
1.7	16	0.98
1.8	13	0.89
1.9	12	0.86
2.5	15	0.95
2.7	13	0.89
3.6	14	0.92
5.4	30	1.40
6.3	24	1.22
8.2	19	1.07
8.9	30	1.40
10.3	36	1.58
Average		**1.12**

Parameters involving with the calculation are summarized in Table 5.10.

Table 5.10 Parameters used in the case study no.4.

Items	Value
Length of pile, L	12.2 m
Outer pile diameter, R_{out}	0.324 m
Inner pile diameter, R_{in}	0.305 m
Density of pile material, ρ_p	2.4 ton/m^3
Young's modulus of pile material, E_p	30.00 GPa
Wave speed in pile, $c_p = \sqrt{E_p/\rho_p}$	3,536 m/s
Return period, $2L/c_p$	0.008 sec
Cross-sectional area of outer pipe, A_{s1}	0.0094 m^2
Cross-sectional area of inner pipe, A_{s2}	0.0036 m^2
Total cross-sectional area of steel pipe, $A_s = A_{s1} + A_{s2}$	0.013 m^2
Elastic modulus of steel, E_s	200,000,000 kN/m^2
Total cross-sectional area of pile, $A = \pi \cdot R_{out}^2$	0.0824 m^2
Cross-sectional area of concrete, $A_c = A - A_s$	0.0694 m^2
Equivalent area of transformed concrete, $A_{eq} = A_c + A_s \cdot E_s/E_p$	0.1561 m^2
Impedance of pile, $Z = A_{eq} \cdot E_c/c_p$	1,325 kN.s/m
Mass of pile, $M = A_{eq} \cdot L \cdot \rho_p$	4.6 tons

Similar to the earlier cases, the damping factors from the ULM and the DULM are shown in Figure 5.29 and Figure 5.30. The average values of the ULM, DULM of test #1 and #2 are 679 kN.s/m, 1263 kN.s/m and 522 kN.s/m, 667 kN.s/m which the latter is 86% and 21% higher than of the former, respectively. The reasons for these signification changes are two folds; 1) the difference in marking the point of zero velocity (the unloading point) and 2) the difference in determining the resistance of soil (Eq. (4.1)).

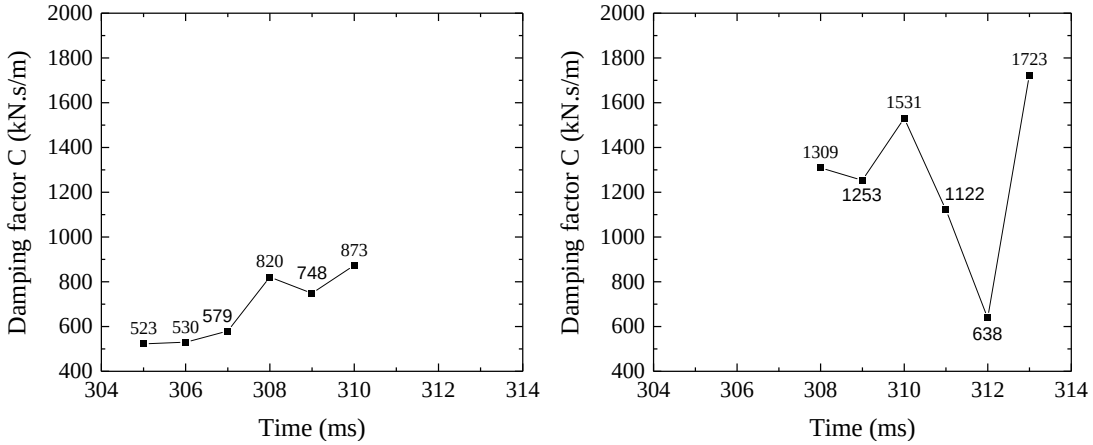

a) ULM b) DULM

Figure 5.29 Variation of the damping factor C (test #1).

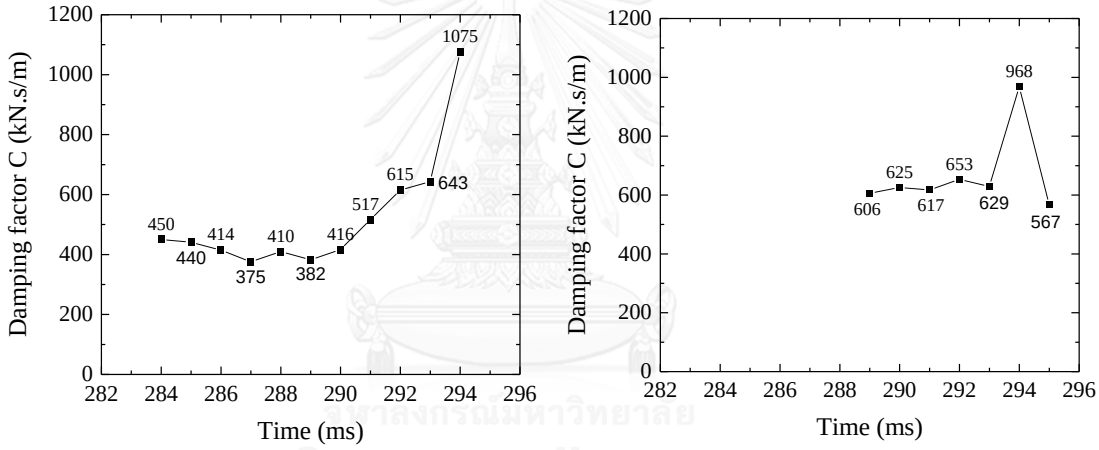

a) ULM b) DULM

Figure 5.30 Variation of the damping factor C (test #2).

According to the previous studies, the DULM should be adjusted by the rate effect factor η. The optimum value of 0.60 was determined by trial and error method. The adjusted results of the ULM and DULM as well as the result of nonlinear velocity are shown in Figure 5.31 and Figure 5.32.

Compare to the verified static results, the derived static results of the nonlinear method showed the softest response due to the lowest value of R^2 and the results computed from the ULM x 0.47 and ULM x 0.65 were improved but they were still far

from the static line. The DULM x 0.60 gave the best estimations comparing to other methods with the greatest values of R^2.

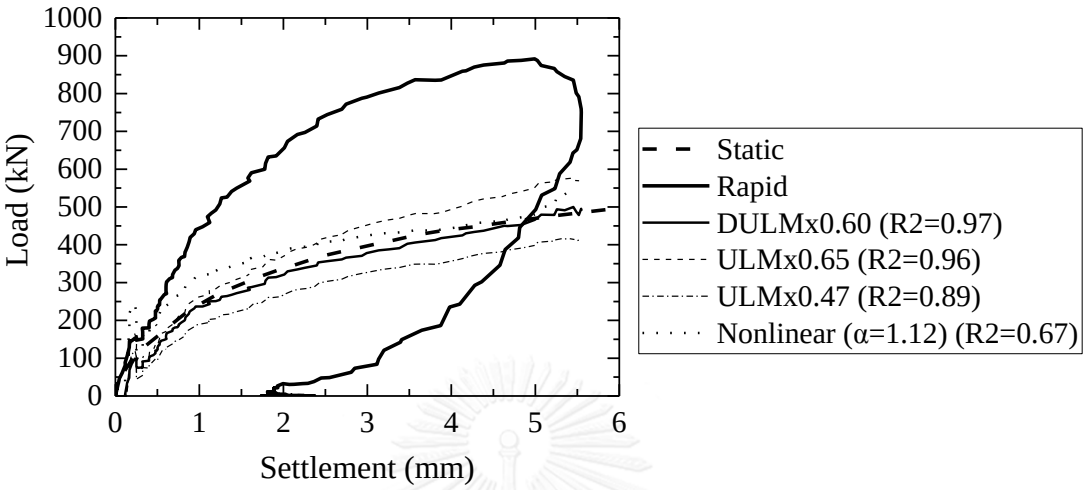

Figure 5.31 Comparison of predicted static capacity with measured, test #1, steel pipe pile in clayey ground, Salt Lake City, Utah.

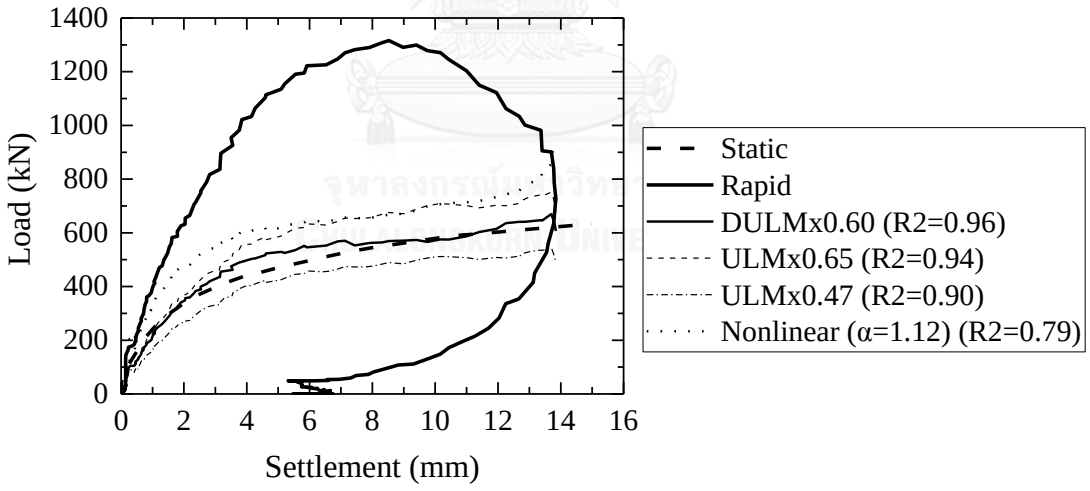

Figure 5.32 Comparison of predicted static capacity with measured, test #2, steel pipe pile in clayey ground, Salt Lake City, Utah.

5.3.5 Case study no.5, driven concrete pile, Waddinxveen, Dutch

Hölscher (2009) reported the tests on two driven concrete piles in the parking lot behind the IFCO building, Limaweg 17 at Waddinxveen, Dutch. The piles were square 0.35 x

0.35 m and 9.8 m long. They were embedded 57% in clay with peat and 43% in sand. The first pile (pile #1) was tested under rapid loading and followed by static loading. The second pile (pile #2) was tested in the reverse order.

As can be seen in Figure 5.33, the pile #1 and #2 began plunged under the maximum load of 1148 kN and 1123 kN, corresponding to displacement of 40 mm and 51 mm, respectively.

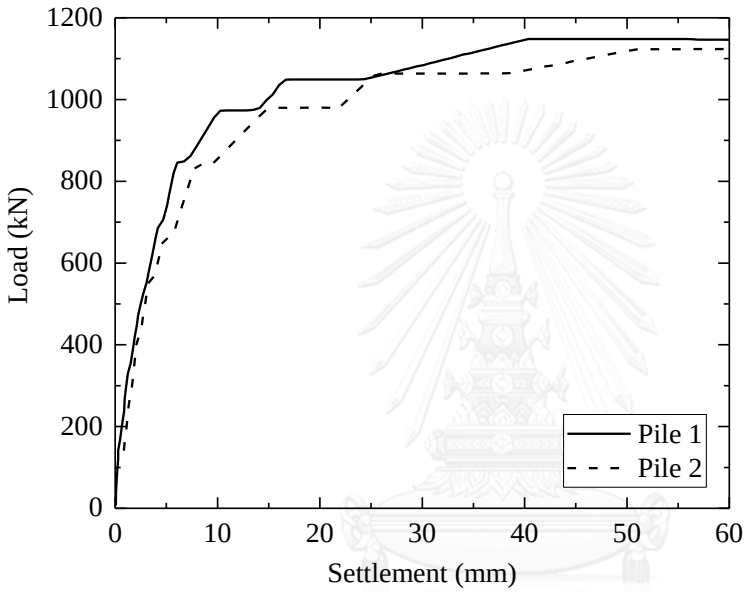

Figure 5.33 Static test results in clayey ground, driven concrete pile, Waddinxveen, Dutch (Hölscher, 2009).

The rapid tests on pile #1 were performed under six loading cycles and followed by static loading. Because the magnitude of loading in first three cycles were similar, only one of them was used in this study. For the second pile, four rapid load cycles were performed. However, the result from the first cycle was too small, only the remaining three tests were used in this study. The test results of pile #1 and pile #2 are shown from Figure 5.34 to Figure 5.37 and from Figure 5.38 to Figure 5.40, respectively.

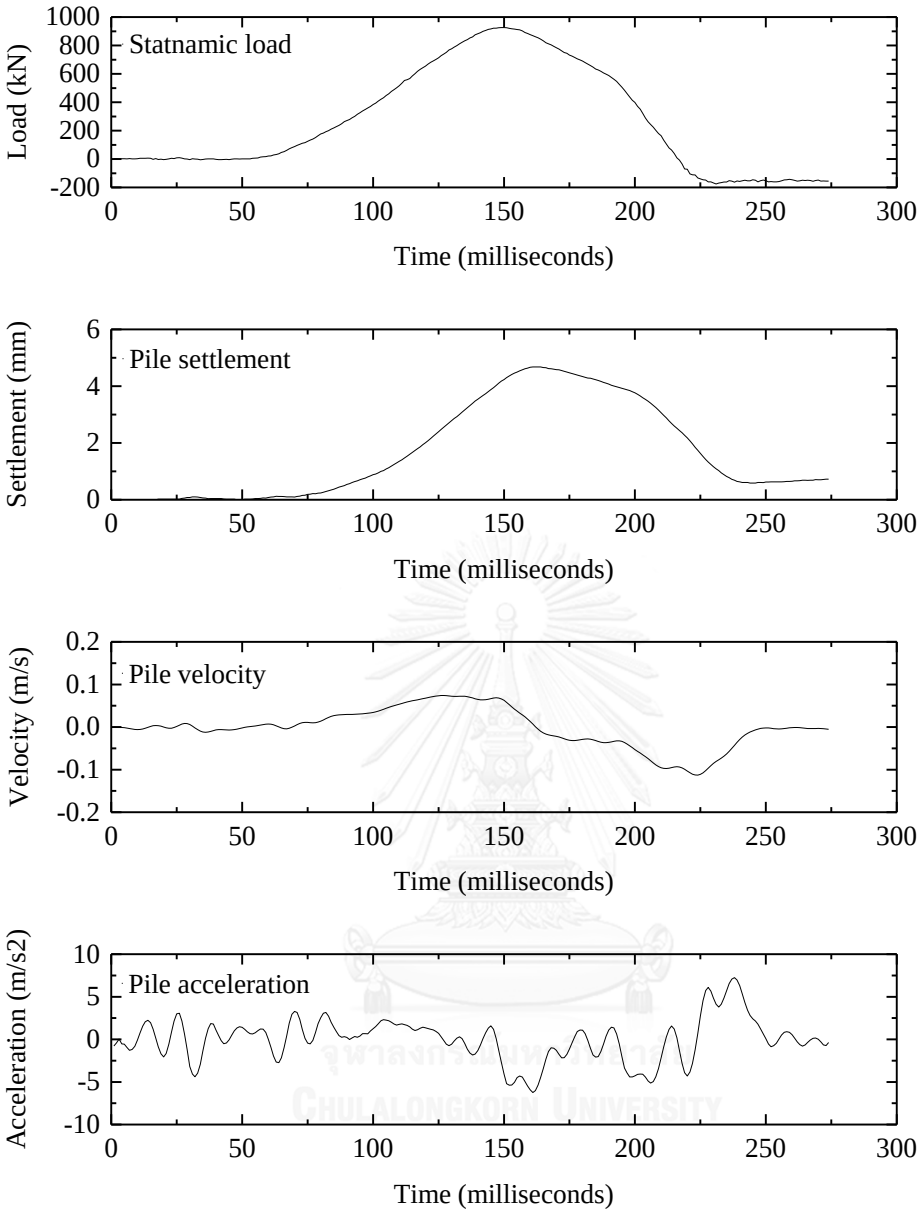

Figure 5.34 Statnamic test results in clayey ground (pile #1, loading cycle #2), driven concrete pile, Waddinxveen, Dutch (Hölscher, 2009).

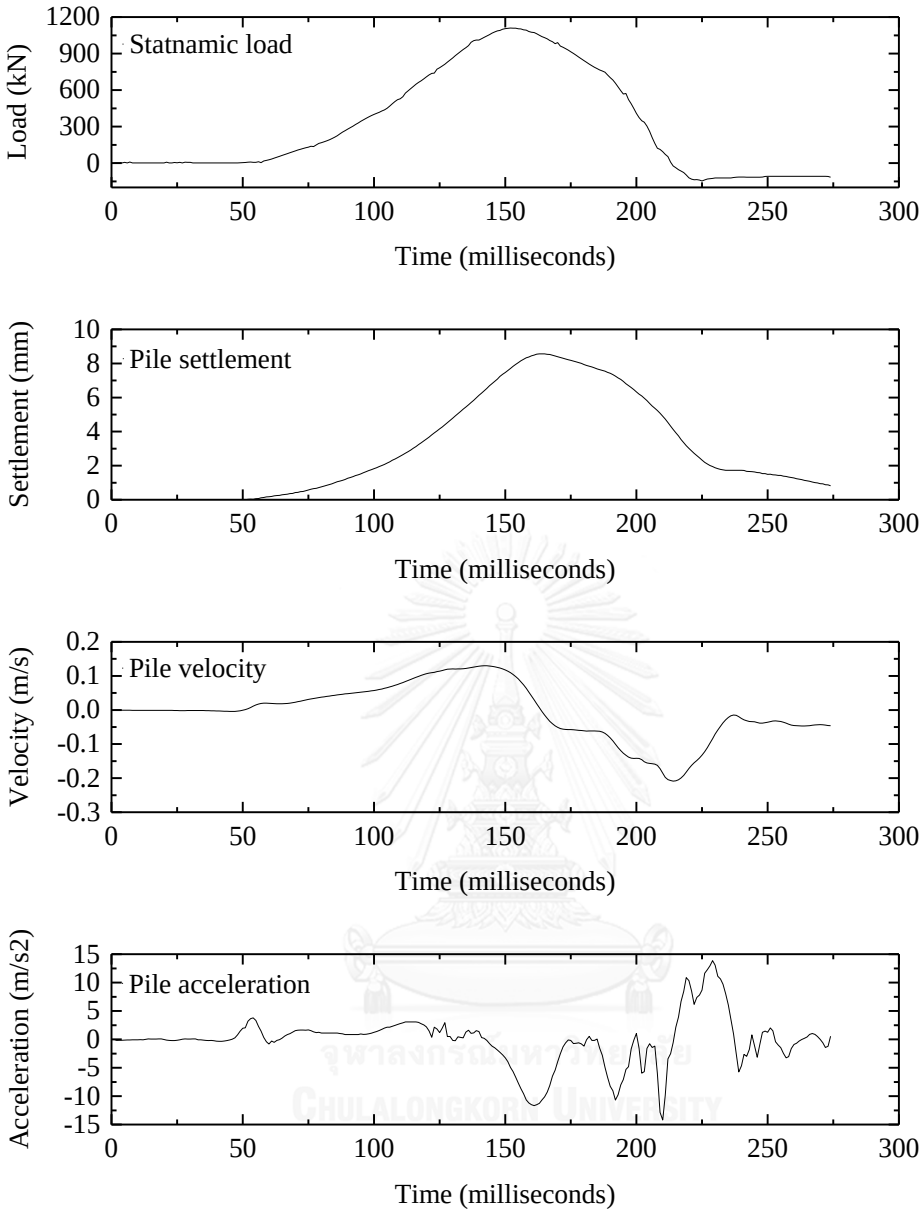

Figure 5.35 Statnamic test results in clayey ground (pile #1, loading cycle #4), driven concrete pile, Waddinxveen, Dutch (Hölscher, 2009).

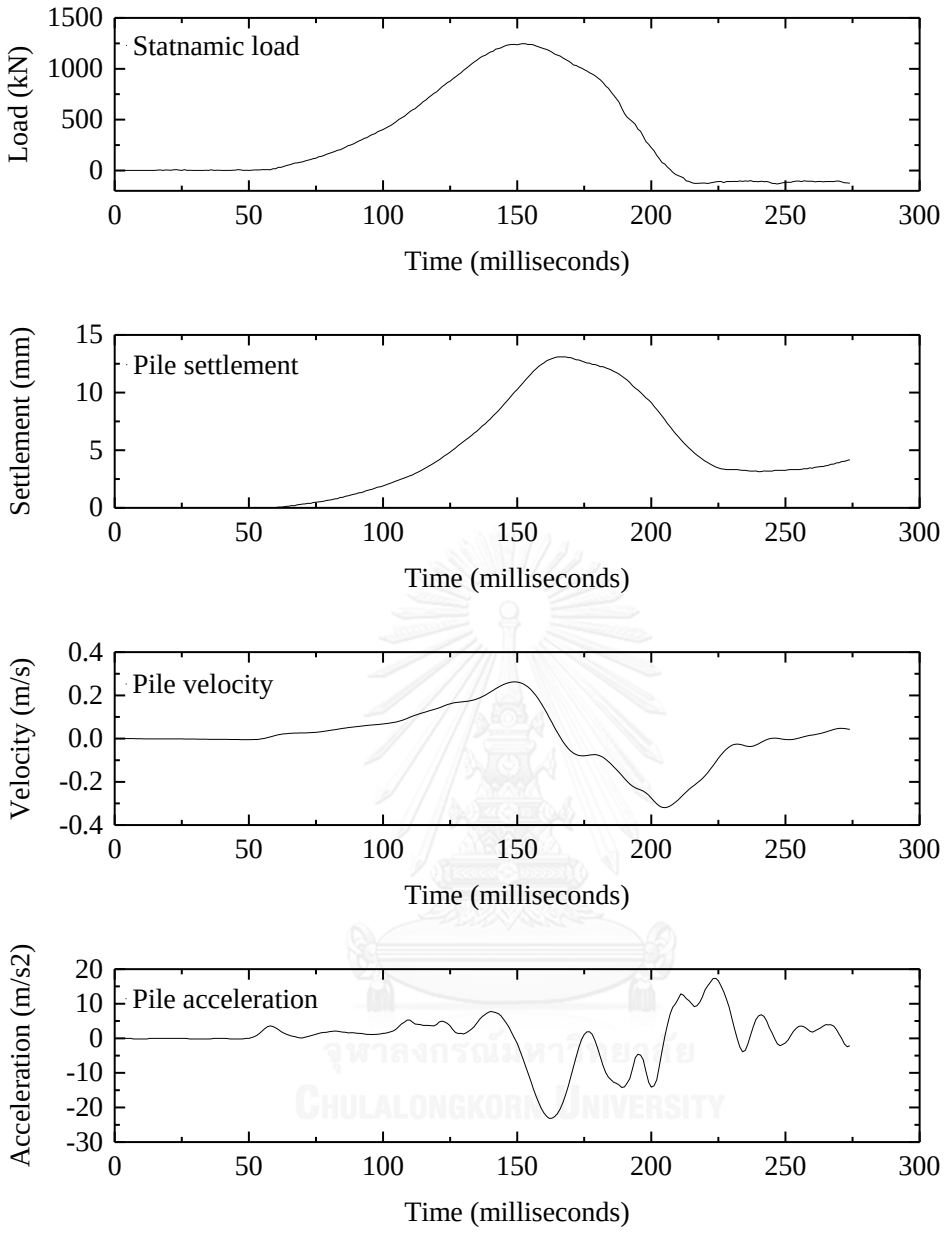

Figure 5.36 Statnamic test results in clayey ground (pile #1, loading cycle #5), driven concrete pile, Waddinxveen, Dutch (Hölscher, 2009).

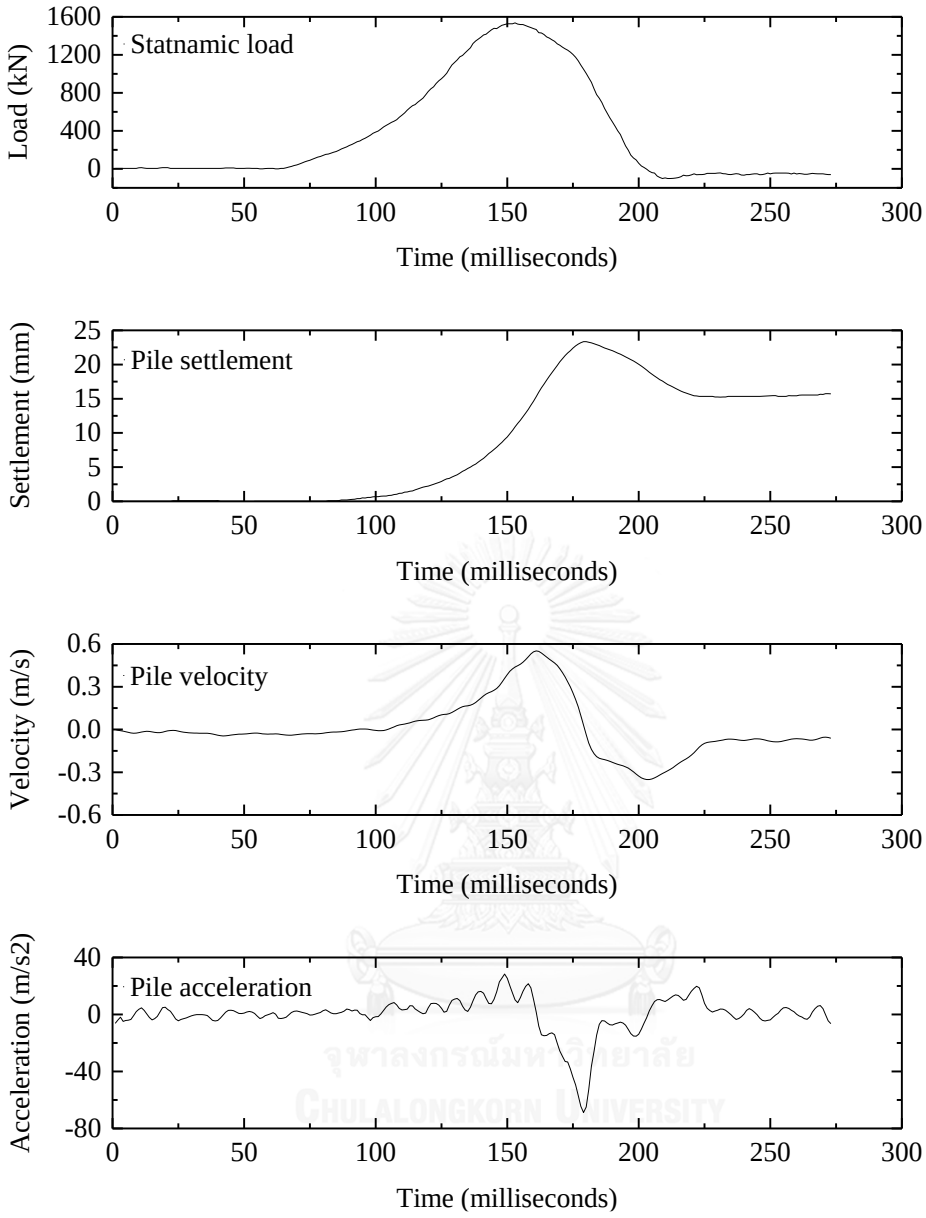

Figure 5.37 Statnamic test results in clayey ground (pile #1, loading cycle #6), driven concrete pile, Waddinxveen, Dutch (Hölscher, 2009).

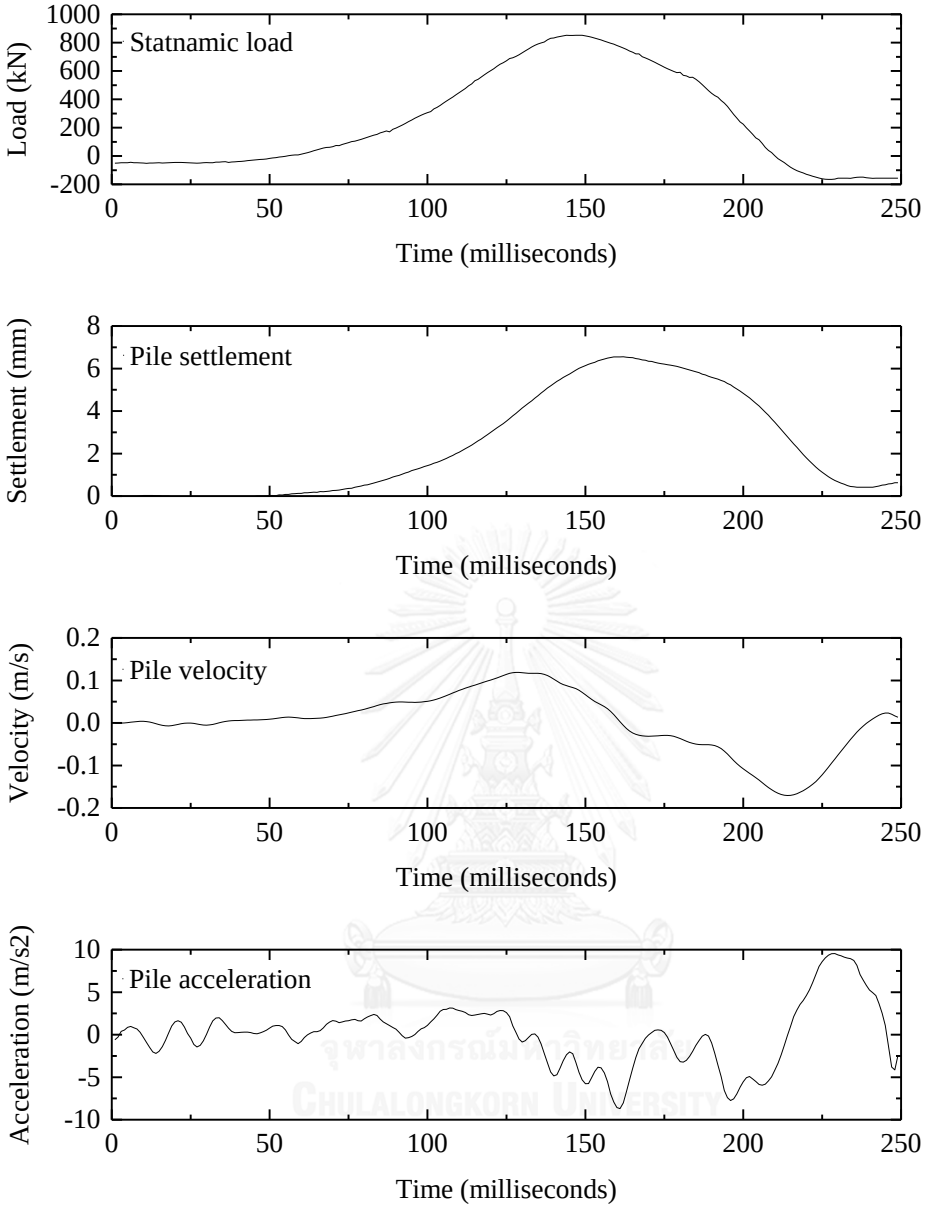

Figure 5.38 Statnamic test results in clayey ground (pile #2, loading cycle #2), driven concrete pile, Waddinxveen, Dutch (Hölscher, 2009).

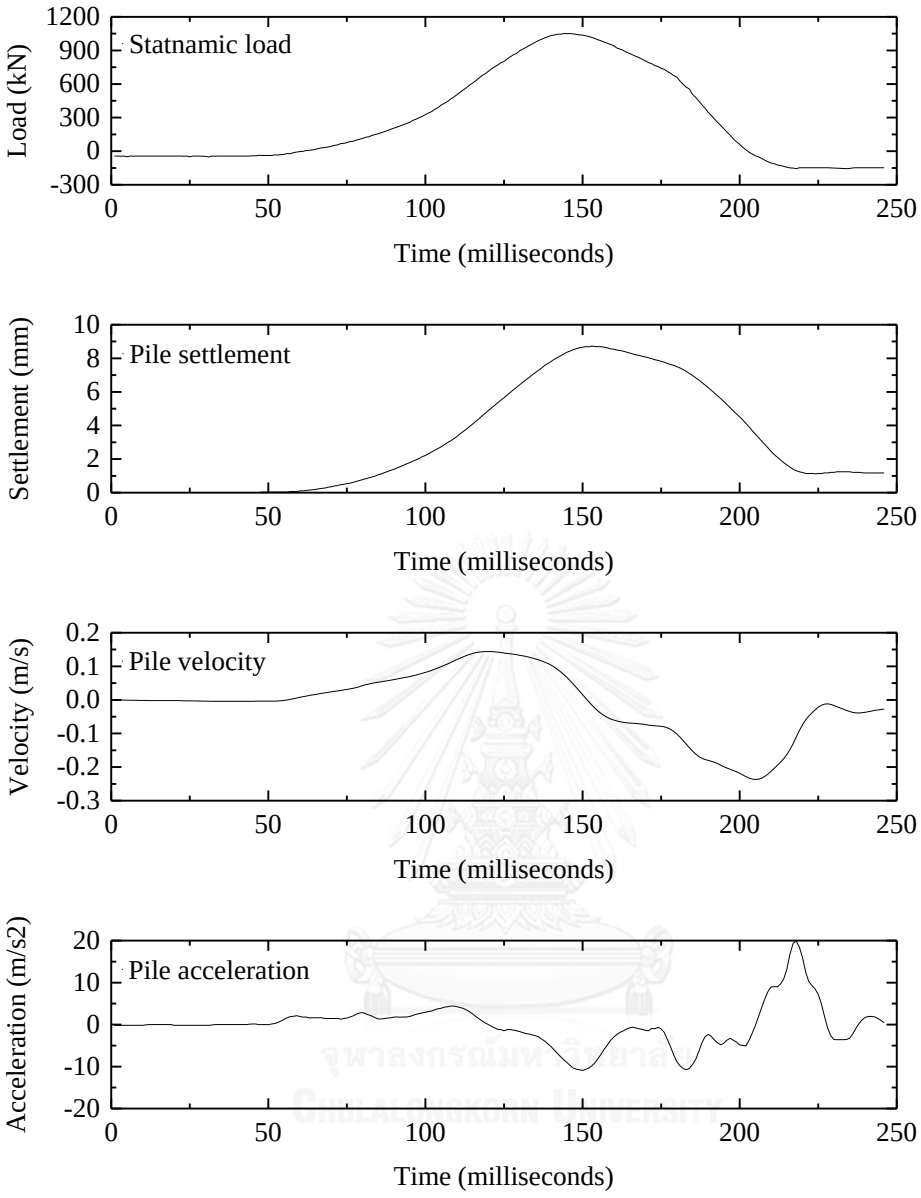

Figure 5.39 Statnamic test results in clayey ground (pile #2, loading cycle #3), driven concrete pile, Waddinxveen, Dutch (Hölscher, 2009).

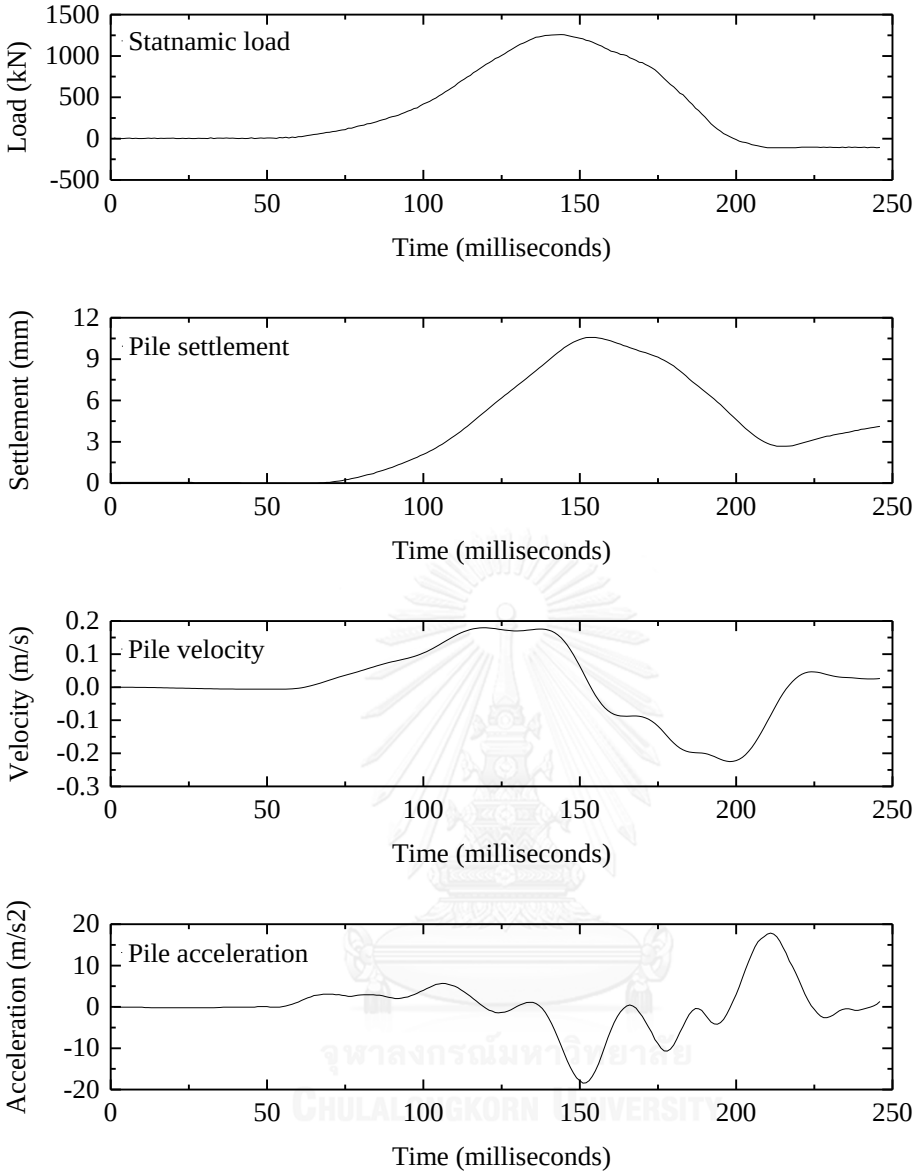

Figure 5.40 Statnamic test results in clayey ground (pile #2, loading cycle #4), driven concrete pile, Waddinxveen, Dutch (Hölscher, 2009).

Because Hölscher (2009) did not show the plasticity index *PI* which can be used to calculate the rate parameter α. Therefore, the α of 1.0 was assumed for clayey soils as suggested by Randolph and Deeks (1992).

Parameters involving with the calculation are summarized in Table 5.11.

Table 5.11 Parameters used in the case study no.5.

Items	Value
Length of pile, *L*	9.8 m
Edge of pile, *a*	0.35 m
Density of pile material, ρ_p	2.4 ton/m^3
Young's modulus of pile material, E_p	43.00 GPa
Wave speed in pile, $c_p = \sqrt{E_p/\rho_p}$	4,233 m/s
Return period, $2L/c_p$	0.006 sec
Cross-sectional area of pile, $A_p = a \times a$	0.123 m^2
Impedance of pile, $Z = A_p \cdot E_p/c_p$	1,244 kN.s/m
Mass of pile, $M = A_p \cdot L \cdot \rho_p$	2.9 tons

As presented above, there are four rapid loading cycles on pile #1 and three rapid tests on pile #2 which are selected to analyze in this study. Similar to the earlier cases, the damping factors of the ULM and the DULM in this case study are shown in Table 5.12 and from Figure 5.41 to Figure 5.47.

Table 5.12 The damping factor C of seven RLTs in the case study no.5.

Rapid test	*C* - ULM	*C* – DULM	Rapid test	*C* - ULM	*C* – DULM
	kN.s/m	*kN.s/m*		*kN.s/m*	*kN.s/m*
Pile 1, cycle 2	1198	1671	Pile 2, cycle 2	868	1317
cycle 4	635	935	cycle 3	355	673
cycle 5	526	767	cycle 4	442	645
cycle 6	372	526			

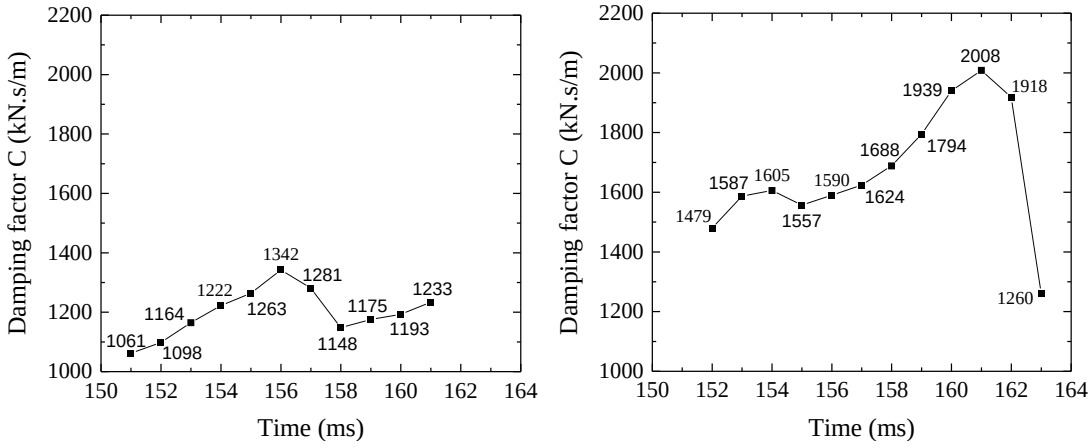

a) ULM b) DULM

Figure 5.41 Variation of the damping factor C (pile #1, loading cycle 2).

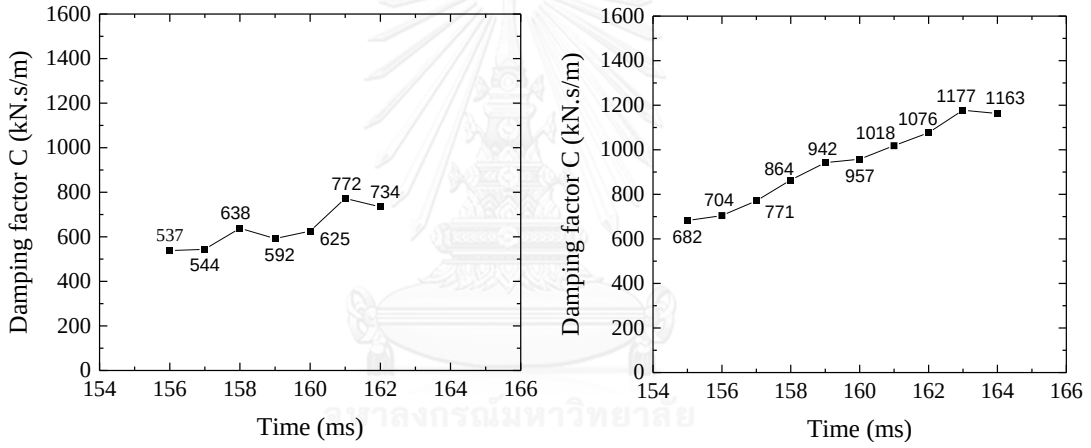

a) ULM b) DULM

Figure 5.42 Variation of the damping factor C (pile #1, loading cycle 4).

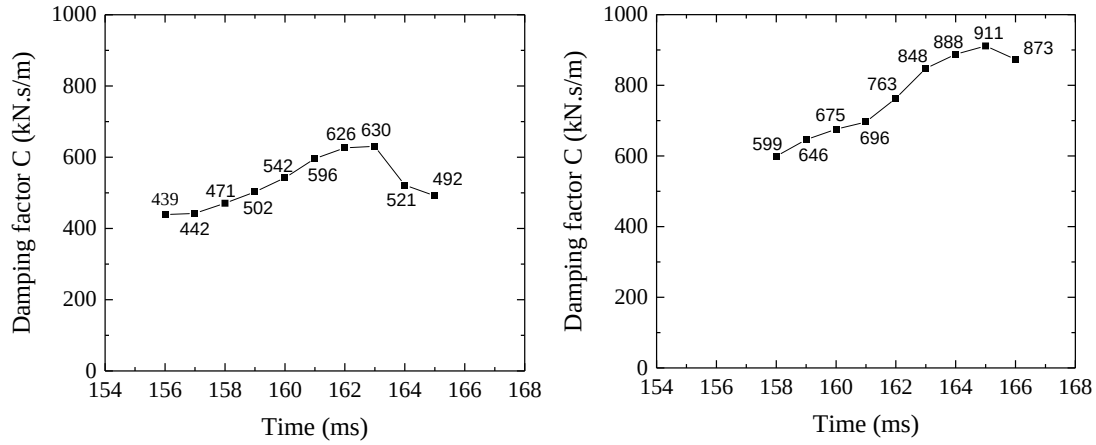

Figure 5.43 Variation of the damping factor C (pile #1, loading cycle 5).

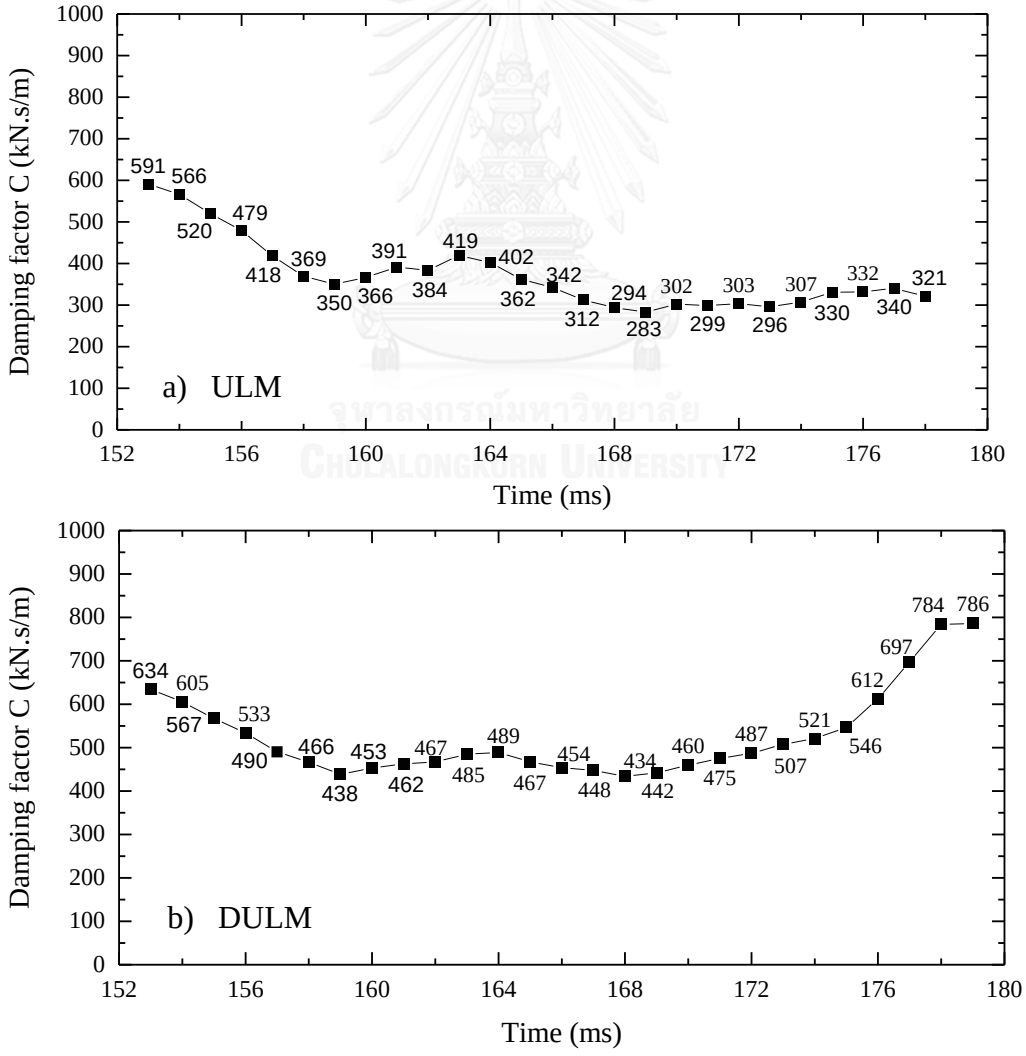

Figure 5.44 Variation of the damping factor C (pile #1, loading cycle 6).

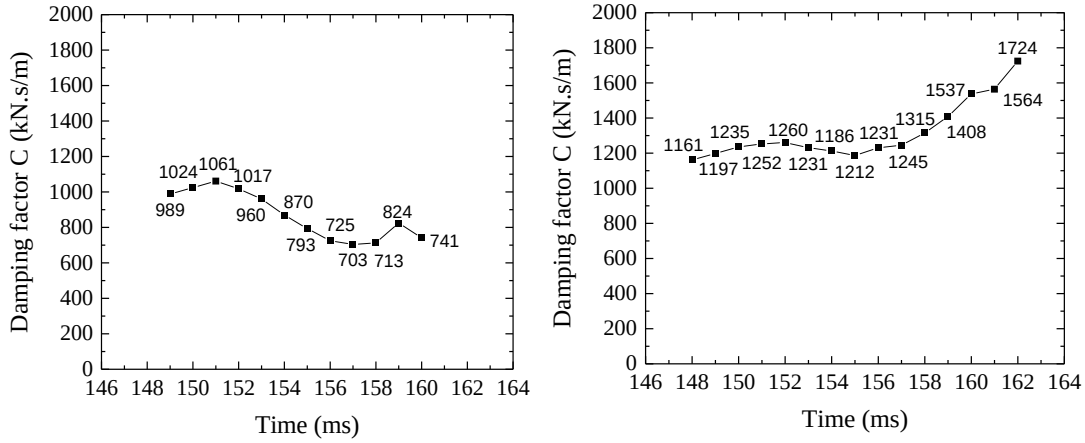

a) ULM b) DULM

Figure 5.45 Variation of the damping factor C (pile #2, loading cycle 2).

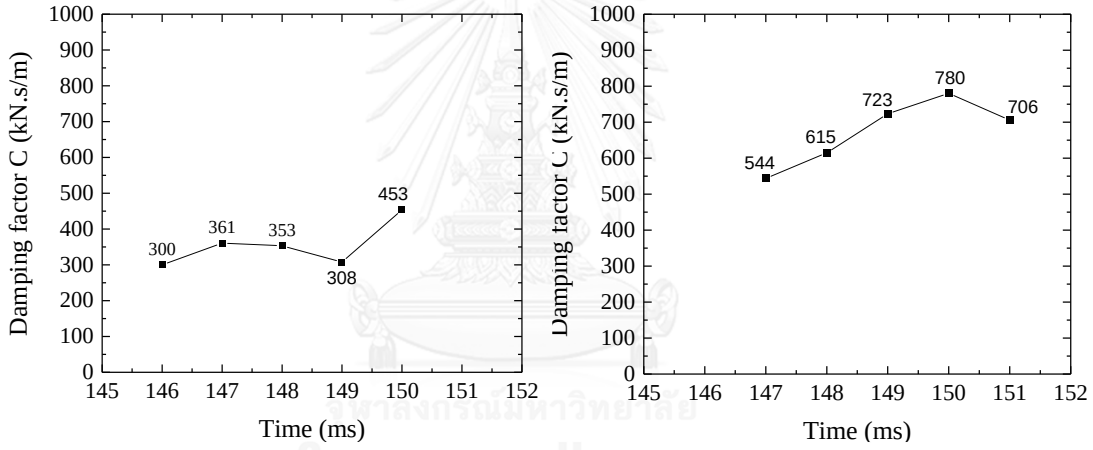

a) ULM b) DULM

Figure 5.46 Variation of the damping factor C (pile #2, loading cycle 3).

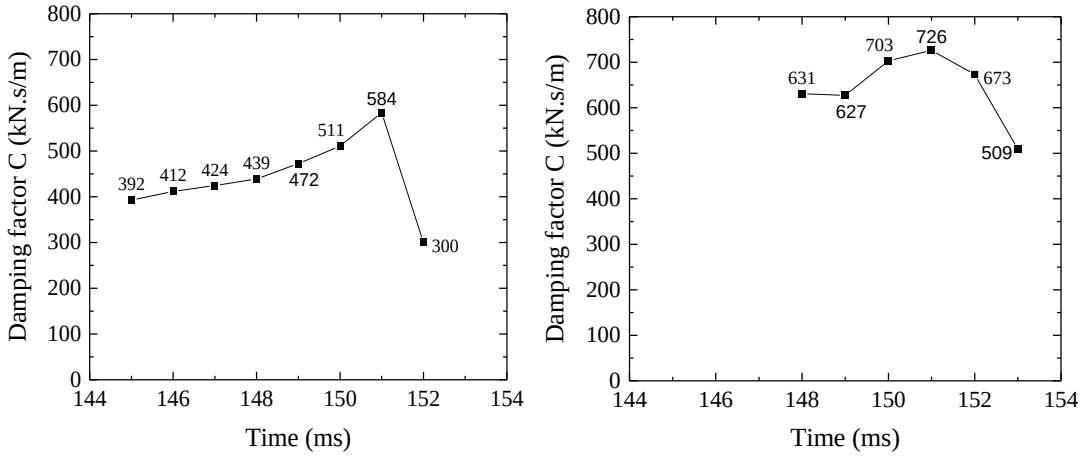

a) ULM b) DULM

Figure 5.47 Variation of the damping factor C (pile #2, loading cycle 4).

According to the previous studies, the DULM should be adjusted by the rate effect factor η. The optimum value varied in the range of 0.75 ~ 0.95 which were determined by trial and error method. The adjusted results of the ULM and DULM as well as the result of nonlinear velocity are shown from Figure 5.48 to Figure 5.54.

For pile #1 with loading cycle 6 (Figure 5.51), the derived static results of the ULM x 0.47, ULM x 0.65, the nonlinear method and the DULM x 0.90 were 581 kN, 807 kN, 905 kN and 1106 kN which were 51%, 70%, 79% and 96% smaller than the static one, respectively. The pile capacity derived from the DULM was the best estimation with an error 4% of the static one.

For pile #2 with loading cycle 4 (Figure 5.54), the derived static results of the ULM x 0.47, ULM x 0.65, the nonlinear method and the DULM x 0.75 were 540 kN, 773 kN, 791 kN and 884 kN which were around 47%, 67%, 69% and 77% smaller than the static one, respectively. The reason of the significant difference of the estimated result from the DULM with the static one is that the applied load was not large enough to get failure.

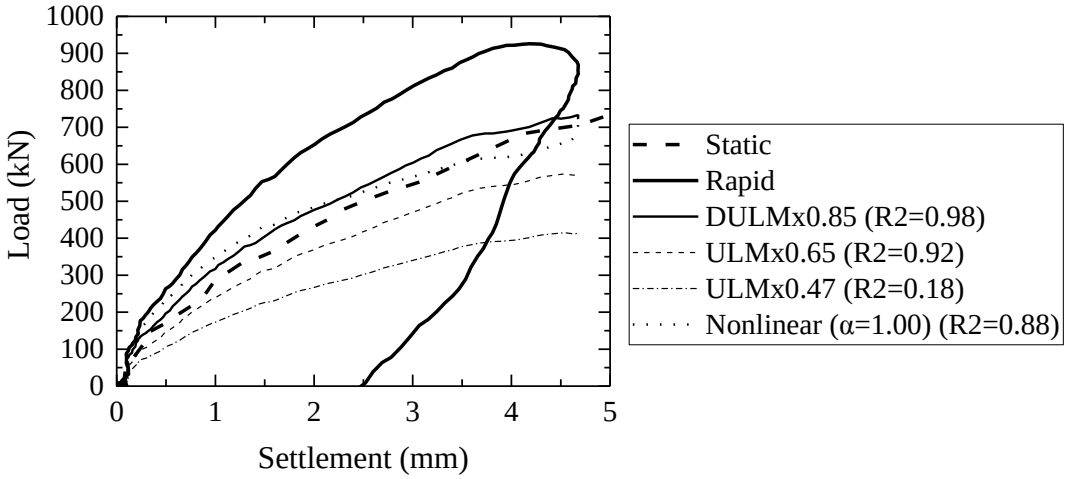

Figure 5.48 Comparison of predicted static capacity with measured (pile #1, loading cycle 2), driven concrete pile, Waddinxveen, Dutch.

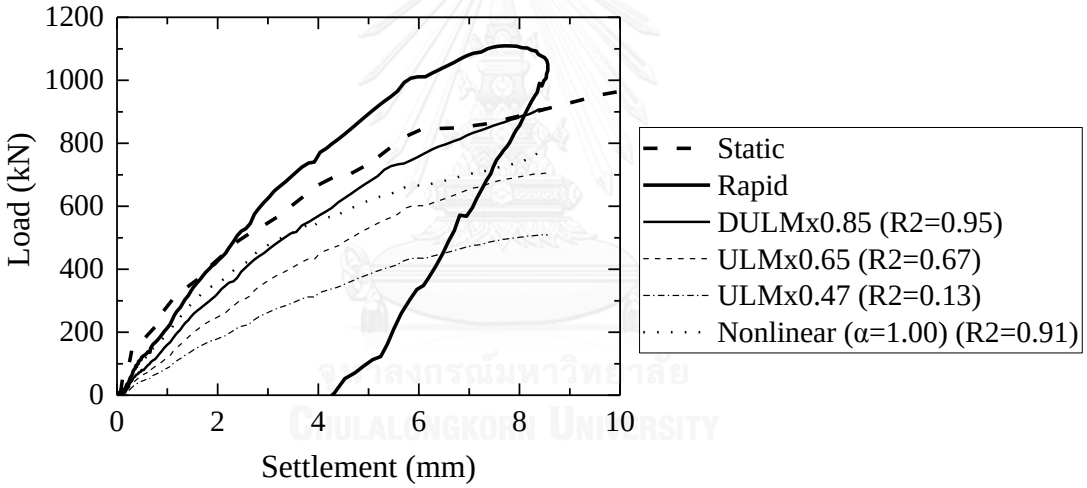

Figure 5.49 Comparison of predicted static capacity with measured (pile #1, loading cycle 4), driven concrete pile, Waddinxveen, Dutch.

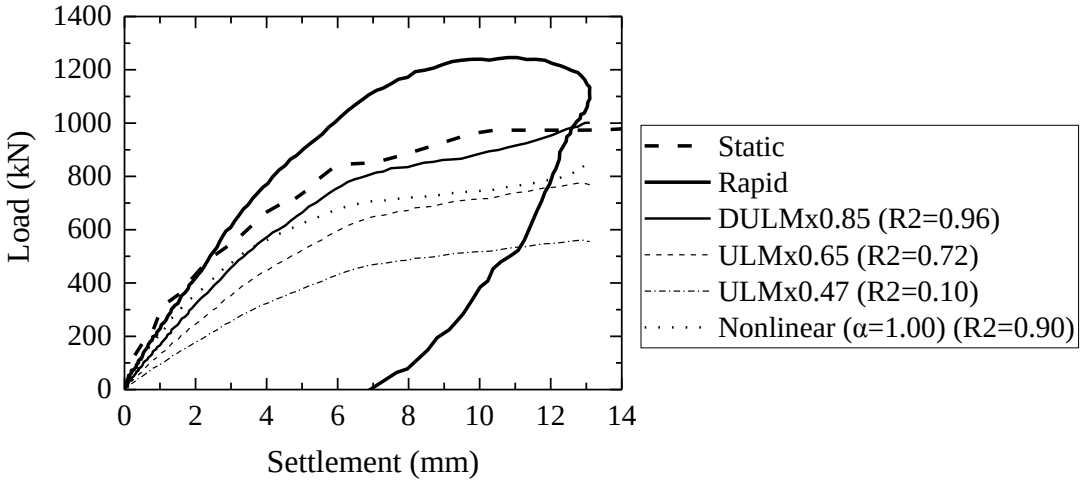

Figure 5.50 Comparison of predicted static capacity with measured (pile #1, loading cycle 5), driven concrete pile, Waddinxveen, Dutch.

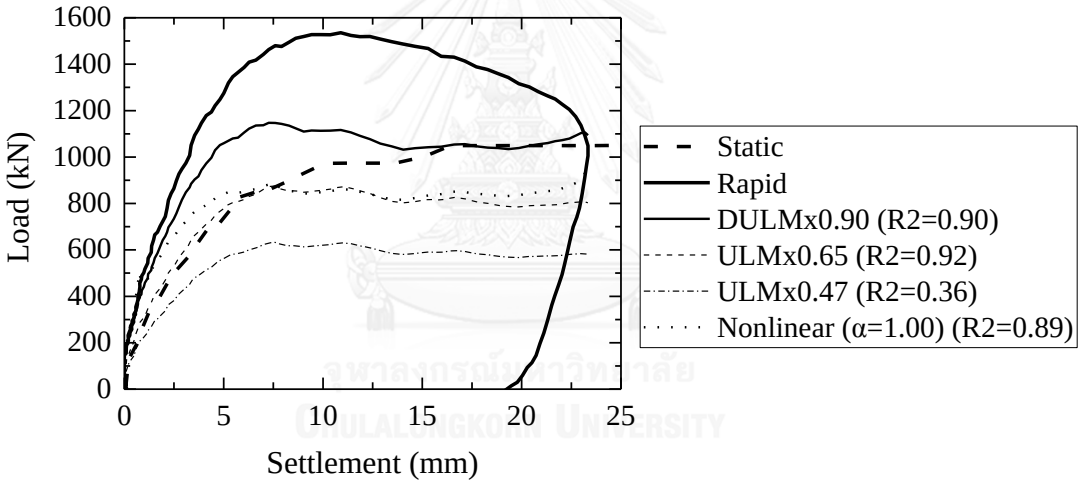

Figure 5.51 Comparison of predicted static capacity with measured (pile #1, loading cycle 6), driven concrete pile, Waddinxveen, Dutch.

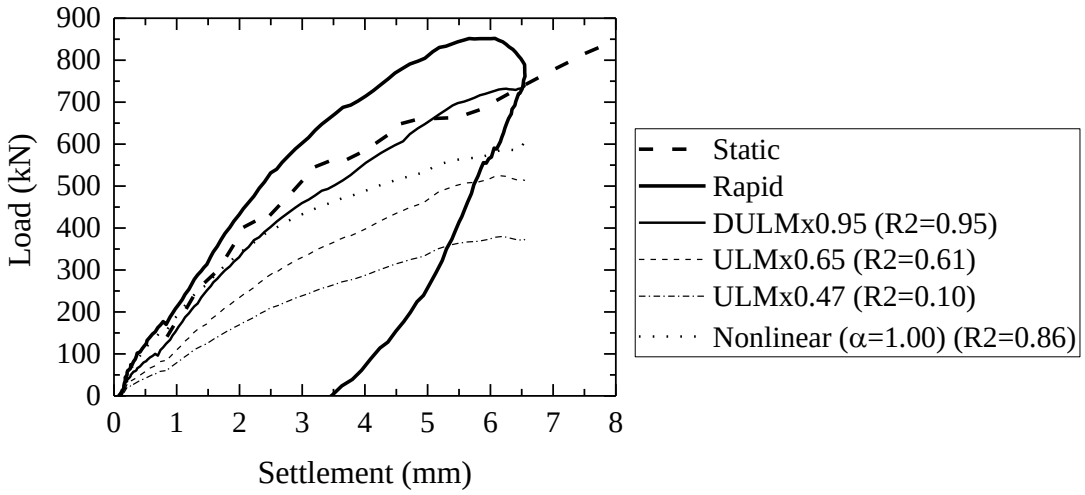

Figure 5.52 Comparison of predicted static capacity with measured (pile #2, loading cycle 2), driven concrete pile, Waddinxveen, Dutch.

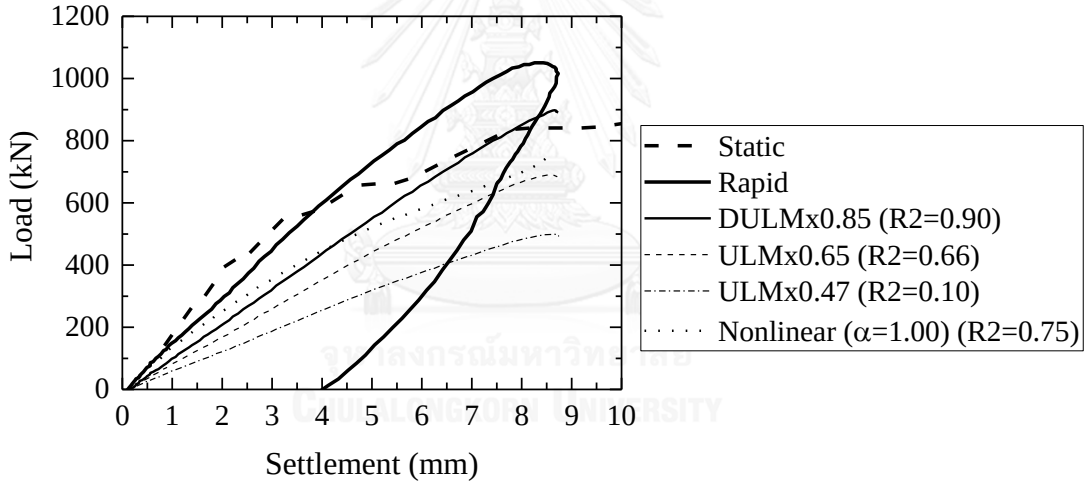

Figure 5.53 Comparison of predicted static capacity with measured (pile #2, loading cycle 3), driven concrete pile, Waddinxveen, Dutch.

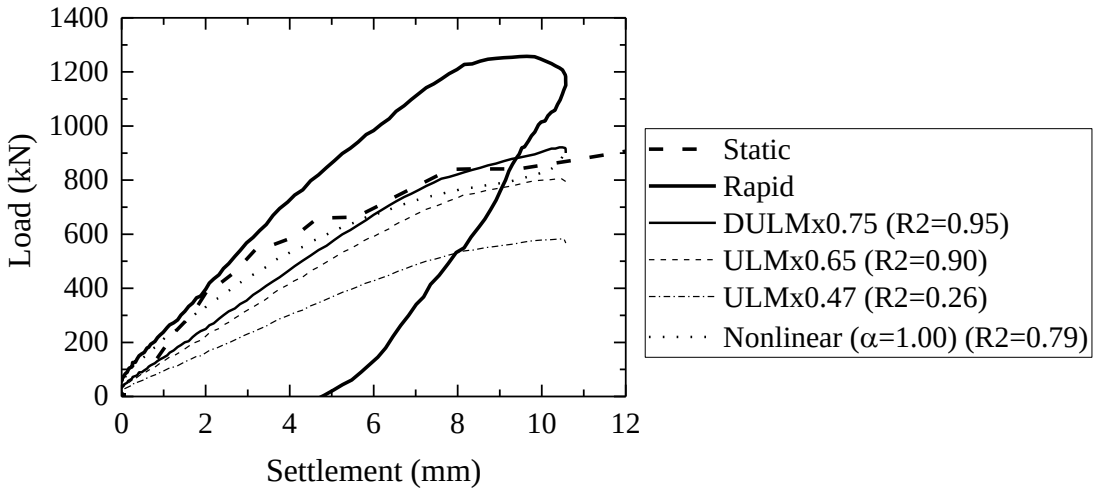

Figure 5.54 Comparison of predicted static capacity with measured (pile #2, loading cycle 4), driven concrete pile, Waddinxveen, Dutch.

Chapter 6: DISCUSSION ON THE RATE EFFECT FACTOR FOR THE ULM AND DULM

The optimum rate effect factors η determined by trial and error method for twelve rapid load tests in clayey ground are summarized in Table 6.1 and Figure 6.1.

Table 6.1 Summary the optimum rate effect factor from tests in clayey ground.

References	Location	Pile type	Rate effect factor, η
Brown (1994) & Ballouz et al. (1991)	Texas, USA	Drilled pile #7	0.65
	Gallup, N.M.	Drilled pile	0.80
Brown (2004)	Grimsby, UK	Auger bored pile	0.75
Garner (2007)	Salt Lake City, Utah	Steel pipe pile	Test 1, test 2: 0.60
Hölscher (2009)	Waddinxveen, Dutch	Driven concrete pile	Pile 1, cycles 2,4,5: 0.85 Pile 1, cycle 6: 0.90 Pile 2, cycle 2: 0.95 Pile 2, cycle 3: 0.85 Pile 2, cycle 4: 0.75
Average			**0.78**
Standard deviation			0.12
Coefficient of variation			0.15

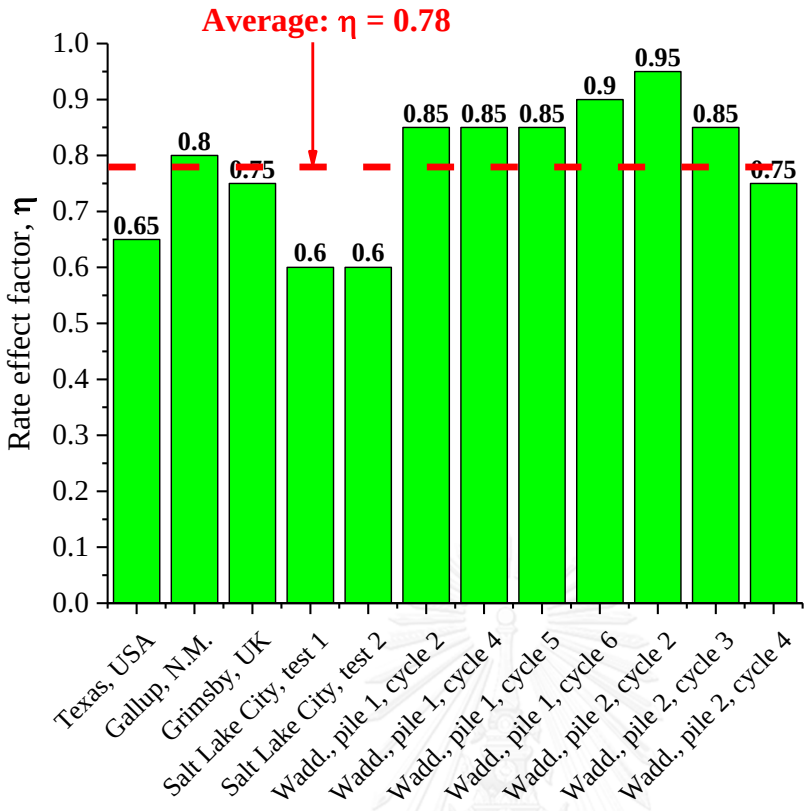

Figure 6.1 Optimum rate effect factors of twelve rapid tests in clayey ground.

The correlation between the static response from SLT and the derived static behavior by the different methods from the measured data of RLT is evaluated by means of the coefficient of determination which are summarized in Table 6.2 and Table 6.3 for sandy ground and clayey ground, respectively. The estimated results from the average rate effect factor, η = 0.78, and compared with other methods for clayey ground are plotted in Appendix.

Table 6.2 Summary the coefficient of determination from tests in sandy ground.

Case study	R^2 (DULM)	R^2 (ULM)
No.1	0.75	**0.78**
No.2	**0.96**	0.90
No.3	**0.97**	0.92

Table 6.3 Summary the coefficient of determination from tests in clayey ground.

Case study	R^2 (DULMx0.78)	R^2 (DULMxη_i)	R^2 (ULMx0.65)	R^2 (ULMx0.47)	R^2 (Nonlinear)
No.1	**0.93**	0.89	0.92	0.40	0.86
No.2	**0.99**	0.99	0.94	0.33	0.77
No.3	0.76	0.73	0.80	0.28	**0.89**
No.4(1)	0.93	**0.97**	0.96	0.89	0.67
No.4(2)	0.89	**0.96**	0.94	0.90	0.79
No.5(1)	**0.99**	0.98	0.92	0.18	0.88
No.5(2)	0.90	**0.95**	0.67	0.13	0.91
No.5(3)	0.91	**0.96**	0.72	0.10	0.90
No.5(4)	**0.94**	0.90	0.92	0.36	0.89
No.5(5)	0.83	**0.95**	0.61	0.10	0.86
No.5(6)	0.85	**0.90**	0.66	0.10	0.75
No.5(7)	**0.96**	0.95	0.90	0.26	0.79

Some conclusion can be made from the studies on twelve RLTs in clayey ground as follows;

1. The results obtained from the ULM x 0.47 showed the lowest estimation compared to verification tests and others due to the lowest values of R^2 in almost tests as indicated in Table 6.3.

2. Although the predictions by the ULM performed better when the η of 0.65 was used instead of 0.47 (R^2 of the ULMx0.65 are higher than ones of the ULMx0.47 as in Table 6.3), the estimated plots were still far from the measured static curves. Additionally, their results were not consistent among twelve studied cases. The estimated curves were higher in some cases and lower in other cases.

3. Even though the method suggested by Brown and Powell performed better than ULM corrected with the rate effect factor, they did not agree with verified results for all cases.

4. The DULM associated with rate effect factor η (in the range of 0.6 ~ 0.95) showed the closest estimation with the verification tests in twelve RLTs in clayey ground. In additional, the DULM together with the average η = 0.78 exhibited the better results in comparison with other methods as seen by the higher values of R^2 (Table 6.3).

Chapter 7: CONCLUSIONS AND RECOMMENDATIONS FOR FURTHER WORK

7.1 Conclusions

Although there have been many achievements for the estimation of pile behaviors, pile load testing is still essential for pile design. Compared to other techniques, rapid load testing provides many benefits but the methods to interpret test results have not been fully developed, especially for piles in clayey soils. To improve the interpretation of rapid test results for all pile types, a technique called the Unloading Point method associated with Time Delay (DULM) was developed and verified in this study.

Comparison of estimated static capacities were explained in Chapter 5, which lead to conclusions that follows;

1. The accuracy of analysis is considerably improved by the consideration of the velocity at the pile tip.

2. The resistance of ground during rapid loading can be determined by

$$F_{soil}\left(t+\frac{L}{c_p}\right)=\frac{1}{2}\left[F(t)+F\left(t+\frac{2L}{c_p}\right)\right]+\frac{M\cdot c_p}{2\cdot L}\left[v(t)-v\left(t+\frac{2L}{c_p}\right)\right]$$

Then, the pile tip velocity can be determined by

$$v_{toe}\left(t+\frac{L}{c_p}\right)=v(t)+\frac{c_p}{E_p\cdot A_p}\left[F(t)-F_{soil}(t)\right]$$

The equivalent static pile resistance needs to be analyzed by the Unloading Point method incorporating with the delayed response along pile length by an expression as follows;

$$F_s(t)=F_{soil}(t)-C_{av}\cdot v_{av}(t)$$

where the pile velocity, v_{av}, can be obtained from averaging of the top and toe velocity

$$v_{av}(t)=\frac{1}{2}\left[v(t)+v_{toe}(t)\right]$$

3. For rapid load testing in sandy soils:

    a. The results derived from the original Unloading Point method (ULM) were not consistent for all cases. Both of over-predicted and under-predicted results were observed in this study.

    b. The coefficient of determination, R^2, calculated from DULM are 0.96 and 0.97 higher than ones from the ULM as 0.90 and 0.92 in the case study no.2 and 3, respectively. Although the R^2 value of the ULM is 0.78 slightly higher than one of the DULM as 0.75 as in the case study no.1, it can be said that the DULM performed better than the ULM.

4. For rapid load testing in clayey soils:

    a. The results obtained from the ULM x 0.47 showed the lowest estimation compared to verification tests and others due to the smallest values of R^2 in almost tests.

    b. Although the predictions by the ULM performed better when the η of 0.65 was used instead of 0.47 (R^2 of the ULMx0.65 are higher than ones of the ULMx0.47), the estimated plots were still far from the measured static curves. Additionally, their results were not consistent among twelve studied cases. The estimated curves were higher in some cases and lower in other cases.

    c. Even though the method suggested by Brown and Powell performed better than ULM corrected with the rate effect factor, they did not agree with verified results for all cases.

    d. The DULM associated with rate effect factor η (in the range of 0.6 ~ 0.95) showed the closest estimation with the verification tests in twelve RLTs in clayey ground. In additional, the DULM together with the average η = 0.78 exhibited the better results in comparison with other methods as seen the higher values of R^2.

5. The prediction results showed that the proposed analysis technique is suitable for both of sandy and clayey soils.

6. The ultimate static capacity can be predicted accurately if the minimum applied rapid load is over a specific value, such as at least 1.7 times (Brown et al., 2006).

7.2 Recommendations for further work

1. The field study is based on a limit database of full scale rapid load testing to assess the static capacity of piles in sand and clay. Further research on different pile types and soil types should be performed to:

    a. Verify the consistent accuracy of the proposed technique for general condition.

    b. Validate rate parameter α for a variety of soils and pile types, and set-up the relationship between α and other fundamental soil properties such as the plasticity index *PI*, liquid limit *LL*, plastic limit *PL*, moisture content *w*, etc.

    c. Confirm rate effect factor η in the wider range of soil and pile types.

2. It is necessary to determine the minimum applied rapid load on the pile head that the pile top settles significantly to mobilize the full static resistance. Hence, the ultimate static capacity can be precisely predicted to check the designed capacity of pile foundation.

3. The calculated velocity at the pile tip should be verified by the measured value at the same position with the same testing condition.

4. The investigation has been made on the influence of soil inertia around the pile shaft and below the pile tip during rapid testing.

REFERENCES

ASTM-D1143 (2013) Standard Test Methods for Deep Foundations Under Static Axial Compressive Load.

ASTM-D7383-10 (2010) Standard Test Methods for Axial Compressive Force Pulse (Rapid) Testing of Deep Foundations, ASTM International, West Conshohocken, PA, www.astm.org.

Balderas-Meca, J. (2004) Rate effects in rapid loading of clay soils.) Ph. D. thesis, Department of Civil Structural Engineering, University of Sheffield, Sheffield, UK.

Ballouz, M., Nasr, G. & Briaud, J.-L. (1991) *Dynamic and static testing of nine drilled shafts at Texas A & M University geotechnical research sites*.

Bermingham, P. & Janes, M. (1989) An innovative approach to load testing of high capacity piles. In *Proceedings of the International Conference on Piling and Deep Foundations*.), Balkema, Rotterdam, London, vol. 1, pp. 409-413.

Bielefeld, M. W. & Middendorp, P. (1995) Statnamic simulation. In *Proceedings, Load Testing and the Influence of Stress Wave Phenomena, First International Statnamic Seminar, Vancouver*.), British Columbia, Canada.

Biggs, J. M. & Testa, B. (1964) *Introduction to structural dynamics.* McGraw-Hill New York.

Boonyatee, T. & Kimura, M. (2000) Keynote lecture: Three-dimensional finite element analysis of statnamic load test. In *Proceedings of Application of Stress-Wave Theory to Piles*. (Niyama, andBeim (eds)), Balkema, Rotterdam.

Brinch-Hansen, J. (1961) *The ultimate resistance of rigid piles against transversal forces.*

Brinkgreve, R., Kumarswamy, S. & Swolfs, W. M. (2016a) *Plaxis 2D - Material models manual.*

Brinkgreve, R., Kumarswamy, S. & Swolfs, W. M. (2016b) *Plaxis 2D - Reference manual.*

Brinkgreve, R. B. J., Kappert, M. H. & Bonnier, P. G. (2007) Hysteretic damping in a small-strain stiffness model. In *Proceeding of Numerical Models in Geomechanics*.), Rhodes, pp. 737-742.

Brown, D. A. (1994) Evaluation of static capacity of deep foundations from Statnamic testing. *Geotechnical Testing Journal, ASTM* **17(4)**:403-414.

Brown, M. (2004) *The rapid load testing of piles in fine grained soils*. Hyde, D. a. F. L.

Brown, M. J. & Hyde, A. F. L. (2008) Rate effects from pile shaft resistance measurements. *Canadian Geotechnical Journal* **45(3)**:425-431.

Brown, M. J., Hyde, A. F. L. & Anderson, W. F. (2006) Analysis of a rapid load test on an instrumented bored pile in clay. *Géotechnique* **56**:627-638.

Brown, M. J. & Powell, J. (2013) Comparison of Rapid load test analysis techniques in clay soils. *Journal of Geotechnical and Geoenvironmental Engineering* **139(1)**:152-161.

Brown, M. J. & Powell, J. J. M. (2012) Comparison of rapid load pile testing of driven and CFA piles installed in high OCR clay. *Soils and Foundations* **52(6)**:1033-1042.

Bs-8004 (1986) Code of practice for foundations. *British Standard, London*.

Cai, C., Zheng, H., Khan, M. & Hung, K. (2002) Modeling of material damping properties in ANSYS. In *CADFEM Users' Meeting & ANSYS Conference*.), pp. 9-11.

Cgs (2006) *Canadian foundation engineering manual*. 4th edn. Canadian Geotechnical Society. Canada.

Charatpangoon, B., Kiyono, J., Furukawa, A. & Hansapinyo, C. (2014) Dynamic analysis of earth dam damaged by the 2011 Off the Pacific Coast of Tohoku Earthquake. *Soil Dynamics and Earthquake Engineering* **64**:50-62.

Chew, S., Middendorp, P., Bakker, J. & Chuah, G. (2015) Recent advances of rapid load testing in Asia and Europe.).

Chin, F. (1970) Estimation of the ultimate load of piles not carried to failure. In *Proceedings of the 2nd Southeast Asian Conference on Soil Engineering*.), pp. 81-90.

Coyle, H. M., Bartoskewitz, R. E. & Berger, W. J. (1973) *Bearing capacity prediction by wave equation analysis - State of the art*. Report 125-8F.

Coyle, H. M. & Gibson, G. C. (1970) Empirical damping constants for sands and clays. *Journal of the Soil Mechanics and Foundations Division* **96(3)**:949-965.

Davisson, M. (1972) High capacity piles. *Proceedings, Soil Mechanics Lecture Series on Innovations in Foundation Construction*:81-112.

Deeks, A. & Randolph, M. (1993) Analytical modelling of hammer impact for pile driving. *International Journal for Numerical and Analytical Methods in Geomechanics* **17(5)**:279-302.

Ei-Naggar, M. H. & Novak, M. (1992) Analytical model for an innovative pile test. *Canadian Geotechnical Journal* **29(4)**:569-579.

Fakharian, K., Masouleh, S. F. & Mohammadlou, A. S. (2014) Comparison of end-of-drive and restrike signal matching analysis for a real case using continuum numerical modelling. *Soils and Foundations* **54(2)**:155-167.

Fellenius, B. H. (1980) The analysis of results from routine pile load tests. *Ground Engineering* **13(6)**:19-31.

Fleming, K., Weltman, A., Randolph, M. & Elson, K. (2009) *Piling engineering*. Third edn., CRC press.

Garner, M. P. (2007) *Loading rate effects on axial pile capacity in clays*.

Gibson, G. & Coyle, H. M. (1968) *Soil damping constants related to common soil properties in sands and clays*. College Station, Tex.

Goble, G., Rausche, F. & Likins, G. (1980) The analysis of pile driving - A state-of-the-arl. In *Proc. Int. Conf. on Stress-Wave Theory on Piles*.), Stockholm, pp. 131-161.

Goble, G. G., Likins Jr, G. & Rausche, F. (1975) *Bearing capacity of piles from dynamic measurements*.

Gonin, H., Coelus, G. & Leonard, M. (1984) Theory and performance of a new dynamic method of pile testing In *Proceedings of Proceedings of the 2nd International Conference on th Application of Stress Wave Theory to Piles*, pp. 403-410.

Hannigan, P. J., Goble, G. G., Thendean, G., Likins, G. E. & Rausche, F. (1997) *Design and construction of driven pile foundations-volume II*. Report FHWA-Hl-97-013, pp. 448.

Hardin, B. & Drnevich, V. P. (1972) Shear modulus and damping in soils: Design equations and curves. *Soil Mechanics and Foundation Division*.

Hashash, Y. M. & Park, D. (2002) Viscous damping formulation and high frequency motion propagation in non-linear site response analysis. *Soil Dynamics and Earthquake Engineering* **22(7)**:611-624.

Heerema, E. P. (1979) Relationship between wall friction, displacement velocity and horizontal stress in clay and in sand, for pile driveability analysis. *Ground Engineering* **12(1)**:55-65.

Holeyman, A. E. (1992) Keynote lecture: Technology of pile dynamic testing. In *Proceedings of the Fourth International Conference on the Application of Stress-Wave Theory to Piles*. (Barends, F. (ed)), Balkema, Rotterdam, pp. 195-215.

Hölscher, P. (2009) *Field test rapid load testing Waddinxveen*.

Horikoshi, K., Kato, K. & Matsumoto, T. (1998) Finite element analysis of Statnamic loading test of pile. In *Proceedings of 2nd International Statnamic Seminar*.), Tokyo, Japan, pp. 295-302.

Horvath, R. G., Bermingham, P. & Middendorp, P. (1993) The equilibrium point method of analysis for the Statnamic loading test with supporting case histories. In *Proceedings, 18th Annual Conference of the Deep Foundations Institute, Pittsburgh, Pa., October*.), pp. 18-20.

Hudson, M., Idriss, I. & Beikae, M. (1994) *User's Manual for QUAD4M*.

Huy, N. (2010) *Literature review Quasi-static and Dynamic pile load tests: Primarily report on non-static pile load tests.*

Hyde, A., Robinson, S. & Anderson, W. (1998) Rate effects in clay soils and their relevance to Statnamic pile testing. In *STATNAMIC Loading Test, Proc. of 2nd International Statnamic Seminar*.), pp. 303-309.

Hyde, A. F. & Brown, M. J. (2008) Load transfer in rapid load pile tests in clays. In *Rapid Load Testing on Piles*.), pp. 37.

Ice (2007) *Specification for piling and embedded retaining walls*. The Institution of Civil Engineers. London, UK, Thomas Telford Publishing.

JGS-1815 (2002) Draft of "Method for Rapid load test of single piles". Proceedings of the Second International Statnamic Seminar, Tokyo, October 1998 pp. 237-242, Committee on Standardization of Pile Loading Tests, The Japanese Geotechnical Society, Japan.

Justason, M., Mullins, A., Robertson, D. & Knight, W. (1998) A comparison of static and Statnamic load tests in sand: a case study of the Bayou Chico bridge in Pensacola, Florida In *Proceedings of the 7th International Conference and Exhibition on Piling and Deep Foundations, Deep Foundations Institute, Vienna, Austria* vol. 5, pp. 2-5.22.

Justason, M. D. (1997) *Report of load testing at the Taipei municipal incinerator expansion project. Taipei city, Taipei*.

Kramer, S. L. (1996) *Geotechnical earthquake engineering.* Prentice Hall Upper Saddle River, NJ.

Lai-Bing, C. (2000) Analysis of bearing capacity of rock-socketed piles by high strain dynamic testing. *Industrial Construction* **10**:016.

Lanzo, G., Vucetic, M. & Doroudian, M. (1997) Reduction of shear modulus at small strains in simple shear. *Journal of Geotechnical and Geoenvironmental Engineering* **123(11)**:1035-1042.

Lee Leon Lowery, J., Hirsch, T. J. & C. H. Samson, J. (1967) *Report: Pile driving analysis - Simulation of hammers, cushions, piles, and soil*. The Texas Highway Department in coorperation with the U. S. Department of Transportation, Federal Highway Administration, Bereau of Public Roads.

Litkouhi, S. & Poskitt, T. J. (1980) Damping constants for pile driveability calculations. *Géotechnique* **30(1)**:77-86.

Long, M. (2007) Comparing dynamic and static test results of bored piles.

Massarsch, K. (1993) Static and dynamic soil displacements caused by pile driving. *Australian Geomechanics***(24)**.

Matsumoto, T. (1998) A FEM analysis of a STATNAMIC test on open-ended steel pipe pile In *Proceedings of Proceedings of the 2nd International Statnamic Seminar* (Kusakabe, O., Kuwabara, F., andMatsumoto, T. (eds)), pp. 287-294.

Matsumoto, T., Fujita, K., Kusakabe, O., Okahara, M., Kawabata, N. & Nishimura, S. (2000) Dynamic load testing and Statnamic load testing for acceptance and design of driven piles in Japan. In *Proc. of Application of Stress-Wave Theory to Piles (Quality Assurance on Land and Offshore Piling)*. (Beim, J., andNiyama, S. (eds)) CRC Press, Balkema, pp. 335-344.

Matsumoto, T., Matsuzawa, K. & Kitiyodom, P. (2008) A role of pile load test–Pile load test as element test for design of foundation system. In *Proceedings of the 8th International Conference on the Application of Stress-Wave Theory to Piles*.) IOS Press, Portugal, pp. 39-58.

Matsumoto, T., Wakisaka, T., Wang, F. W., Takeda, K. & Yabuuchi, N. (2004) Development of a rapid pile load test method using a falling mass attached with spring and damper In *Proceedings of Proceedings of the 7th International Conference on the Application of Stress Wave Theory to Piles*, pp. 351-358.

Matsuzawa, K., Nakashima, Y. & Matsumoto, T. (2008) Spring hammer rapid load test method and its validation. In *Proceedings of the Second BGA International Conference on Foundations*. (Brown, M. J., Bransby, M. F., Brennan, A. J., andKnappett, J. A. (eds)).

Mcvay, M., Kuo, C. L. & Guisinger, A. L. (2003) *Calibrating resistance factors for load and resistance factor design for Statnamic load testing*. Florida Department of Transportation, Research Management Center, University of Florida.

Middendorp, P. (2000) Statnamic the engineering of art In *Proceedings of the 6th International Conference on the Application of Stress Wave Theory to Piles, Sao Paulo, Brazil*, pp. 1-12.

Middendorp, P. (2004) Thirty years of experience with the wave equation solution based on the method of characteristics. In *7th International Conference on the Application of Stres Wave Theory to Piles, 2004, Kuala Lumur, Malaysia*.).

Middendorp, P., Beck, C. & Lambo, A. (2008) Verification of Statnamic load testing with static load testing in a cohesive soil type in Germany. In *Proceedings of the 8th International Conference on the Application of Stress Wave Theory to Piles*.), Amsterdam, Netherlands pp. 531-538

Middendorp, P., Bermingham, P. & Kuiper, B. (1992) Statnamic load testing of foundation piles. In *Proceedings of the 4th International Conference on the Application of Stress Wave Theory to Piles*.), pp. 581-588.

Middendorp, P. & Bielefeld, M. W. (1995) Statnamic load testing and the influence of stress wave phenomena. In *Proceedings of the First International Statnamic Seminar*.), Vancouver, Canada, pp. 207-220.

Middendorp, P., Van Ginneken, G. & Van Foeken, R. (2000) The advantages and disadvantages of dynamic load testing and statnamic load testing. In *6th International Conference on the Application of Stress Wave Theory to Piles*.), Sao Paulo, Brazil.

Miyasaka, T., Kuwabara, F., Likins, G. & Rausche, F. (2008) Rapid load test on high bearing capacity piles. In *Proceedings of the 8th International Conference on the Application of Stress Wave Theory to Piles*. (Santos, J. A. (ed)), Lisbon, Portugal, pp. 501-506.

Mullins, G., Lewis, C. L. & Justason, M. D. (2002) Advancements in Statnamic data regression techniques. *Deep Foundations*:915-930.

Nguyen, D. H. (2005) Statnamic testing of piles in clay. In *Department of Civil and Structural Engineering*.) Sheffield, University of Sheffield, vol. PhD, pp. 308.

Nishimura, S. & Matsumoto, T. (1998) Wave propagation analysis during Statnamic loading of a steel pipe. *Proceeding of 1st International Statnamic Seminar, Vancouver*:23-33.

Ochiai, H., Kusakabe, O., Sumi, K., Matsumnoto, T. & Nishimura, S. (1997) Dynamic and Statnamic load tests on offshore steel pipe piles with regard to failure mechanisms of pile-soil interfaces at external and internal shafts. In *Proceedings of International Conference on Foundation Failures*.), Singapore, pp. 327-338.

Osterberg, J. O. (1998) The Osterberg load test method for bored and driven piles the first ten years. In *Proceedings of the Seventh International Conference & Exhibition on Piling and Deep Foundations*.), pp. 1-17.

Paikowsky, S. G. (2006) *Innovative load testing systems*.

Phillips, C. & Hashash, Y. M. (2009) Damping formulation for nonlinear 1D site response analyses. *Soil Dynamics and Earthquake Engineering* **29(7)**:1143-1158.

Poulos, H. (2000) Pile testing–from the designer's viewpoint. *Keynote Lecture, Statnamic Loading Test* **98(0)**:3-21.

Powell, J. J. M. & Brown, M. J. (2006) Statnamic pile testing for foundation re-use In *Proceedings of International Conference on the Re-use of Foundations for Urban Sites*, pp. 223-236.

Randolph, M. F. (1991) Chapter 6 - Analysis of the dynamics of pile driving. In *Developments in soil mechanics and foundation engineering*. (Banerjee, P. K., andButterfield, R. (eds)), vol. 4, pp. 223-272.

Randolph, M. F. (2003) Science and empiricism in pile foundation design. *Géotechnique* **53**:847-875.

Randolph, M. F. & Deeks, A. J. (1992) Keynote lecture: Dynamic and static soil models for axial pile response In *Proceedings of the 4th International Conference on the Application of Stress Wave Theory to Piles* (Barends, F. B. J. (ed)), pp. 3-14.

Randolph, M. F. & Simons, H. (1986) An improved soil model for one-dimensional pile driving analysis.

Rausche, F. (2000) Keynote lecture: Pile driving equipment: Capabilities and properties. *Proceedings of the Sixth International Conference on the Application of Stress-Wave Theory to Piles*:75-89.

Rausche, F., Goble, G. & Likins, G. (1985) Dynamic determination of pile capacity. *Journal of Geotechnical Engineering* **111(3)**:367-383.

Rausche, F., Goble, G. & Likins, G. (1992) Investigation of dynamic soil resistance on piles using GRLWEAP. In *Proceedings of the Fourth International Conference on the Application of Stress-Wave Theory to Piles*.), pp. 137-142.

Rausche, F., Goble, G. G. & Likins, G. (2010) *GRLWEAP 2010 Background Report*.

Rausche, F., Goble, G. G. & Likins, G. E. (1988) Recent WEAP developments. *Proceedings of 3rd International Conference on Application of Stress-Wave Theory to Piles*:164-173.

Rausche, F., Robinson, B. & Liang, L. (2000) Automatic signal matching with CAPWAP. In *Proceedings of Sixth International Conference on the Application of Stress-Wave Theory to Piles*.), Sao Paulo, Brazil.

Richart, F. E., Hall, J. R. & Woods, R. D. (1970) Vibrations of soils and foundations.

Salgado, R., Loukidis, D., Abou-Jaoude, G. & Zhang, Y. (2015) The role of soil stiffness non-linearity in 1D pile driving simulations. *Géotechnique* **65(3)**:169-187.

Schellingerhout, A. J. G. & Revoort, E. (1996) Pseudo static pile load tester In *Proceedings of Proceedings of the 5th International Conference on the Application of Stress Wave Theory to Piles*, pp. 1031-1037.

Schmertmann, J. H. & Hayes, J. A. (1997) The Osterberg cell and bored pile testing – A symbiosis. In *Proceedings: 3rd International Geotechnical Engineering Conference, Cairo University, Cairo, Egypt*.).

Schmuker, C. (2005) Comparison of static load tests and Statnamic load test. *German: Vergleich statischer und statnamischer Pfahlprobebelastungen), MSc-Thesis Biberach University, Germany*.

Smith, E. A. (1960) Pile-driving analysis by the wave equation. *American Society of Civil Engineers Transactions* **127**:1145-1193.

Tien, N. T. (1987) Dynamic and static behaviour of driven piles. In *Publication of: Swedish Geotechnical Institute*.) Swedish Geotechnical Institute, pp. 239.

Turner, J. P. (2006) *Rock-socketed shafts for highway structure foundations.* Transportation Research Board.

Van Ginneken, G. J. J. & Middendorp, P. (2000) Introducing statnamic load testing in Europe: Case studies in the Netherlands. In *Proceedings of the 6th International Conference on the Application of Stress-Wave Theory to Piles : Quality Assurance on Land and Offshore Piling*. (Niyama, S., andBeim, J. (eds)), A.A. Balkema, Rotterdam.

Weaver, T. & Rollins, K. (2010) Reduction Factor for the Unloading Point Method at Clay Soil Sites. *Journal of Geotechnical and Geoenvironmental Engineering* **136(4)**:643-646.

Wilson, E. (2005) Dynamic analysis by numerical integration. *Technical reports. San Francisco, California: Computers and Structures Inc*.

Yamashita, K., Tsubakihara, Y. & Kakurai, M. (1995) Method for estimating static load-settlement relation by rapid pile load tests. In *Proceedings - Seventh International Conference & Exhibition on Piling and Deep Foundations (DFI).*), Vienna, Austria, pp. 1.29.1-1.29.6.

Yoshida, N. (2015) *Seismic Ground Response Analysis.* Springer.

Zhang, L., Mcvay, M. C. & Ng, C. W. (2001) A possible physical meaning of Case damping in pile dynamics. *Canadian Geotechnical Journal* **38(1)**:83-94.

REFERENCES

APPENDIX: THE COMPARISON OF PREDICTED STATIC CAPACITY WITH MEASURED

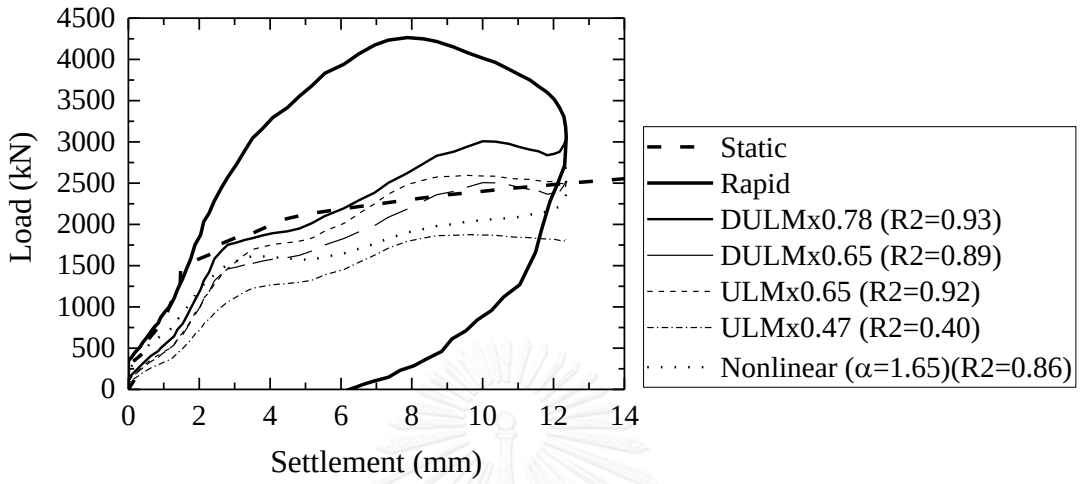

Figure 1 Comparison of predicted static capacity with measured, drilled shaft in clayey ground, College Station, Texas, USA.

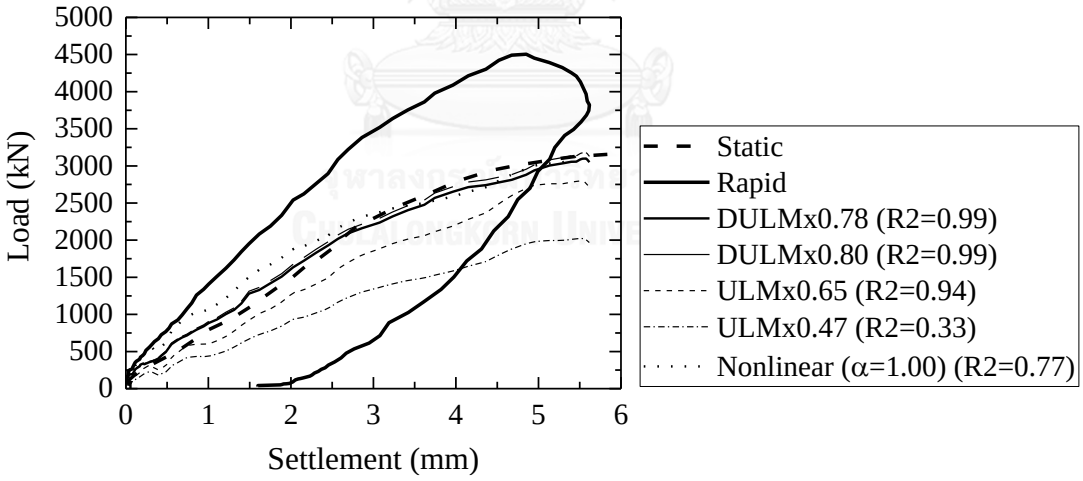

Figure 2 Comparison of predicted static capacity with measured, drilled shaft in clayey ground, Rio Puerco, Gallup, N.M.

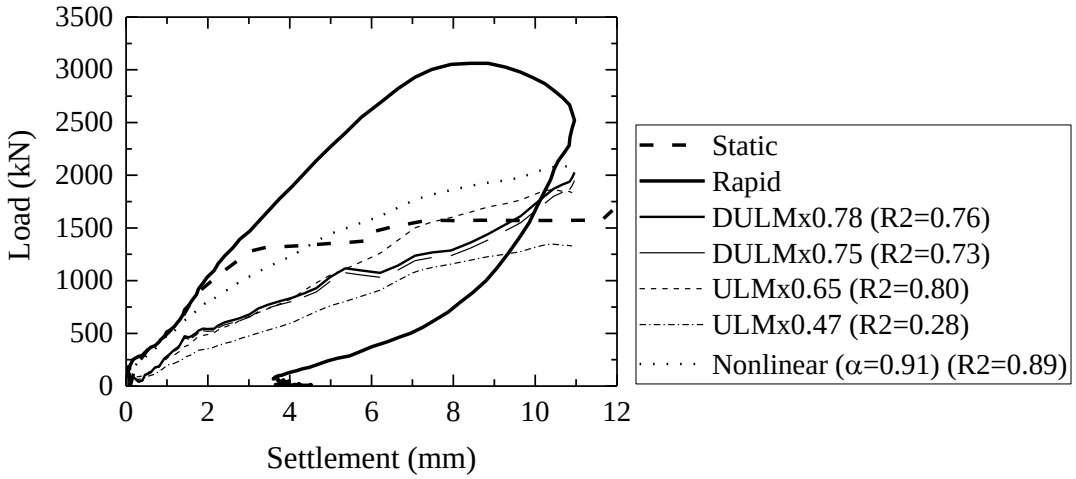

Figure 3 Comparison of predicted static capacity with measured, auger bored pile in clayey ground, Grimsby, UK.

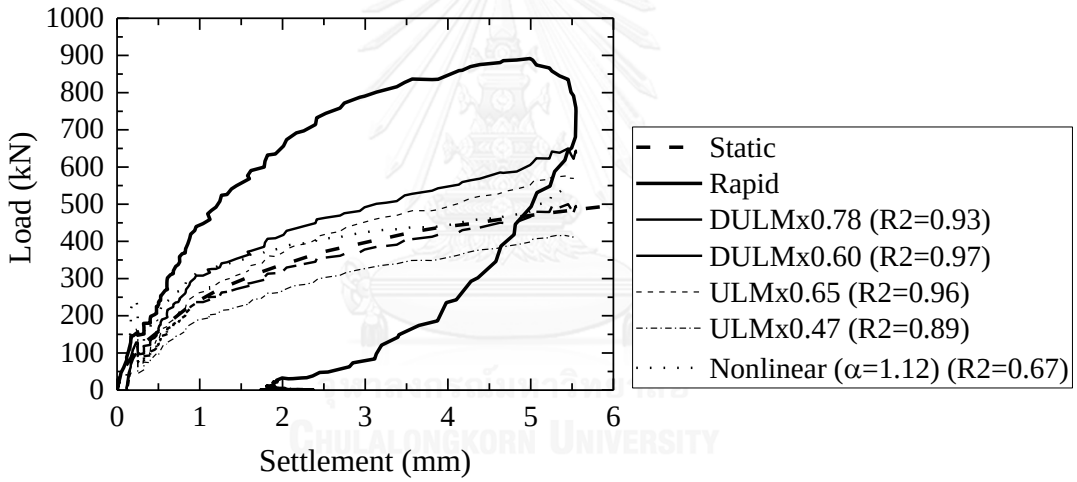

Figure 4 Comparison of predicted static capacity with measured, test #1, steel pipe pile in clayey ground, Salt Lake City, Utah.

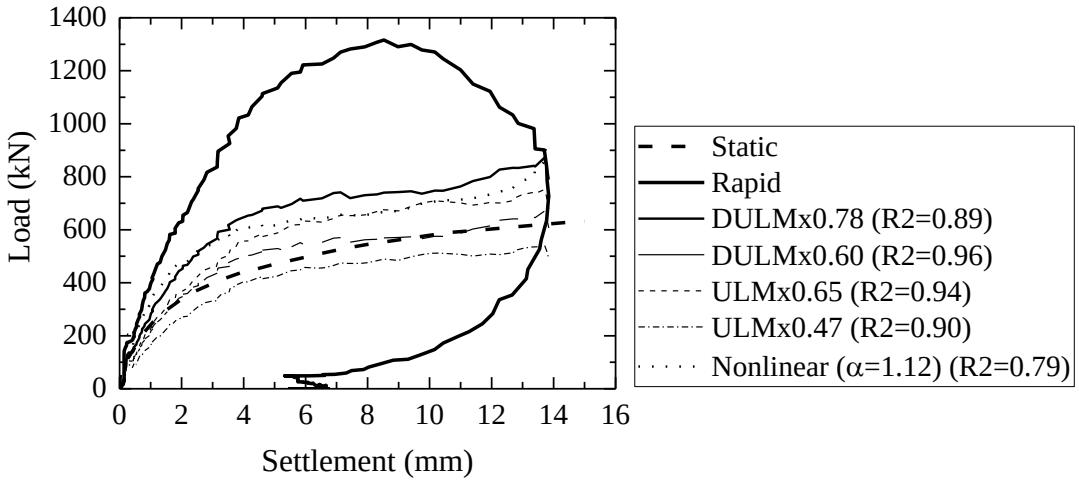

Figure 5 Comparison of predicted static capacity with measured, test #2, steel pipe pile in clayey ground, Salt Lake City, Utah.

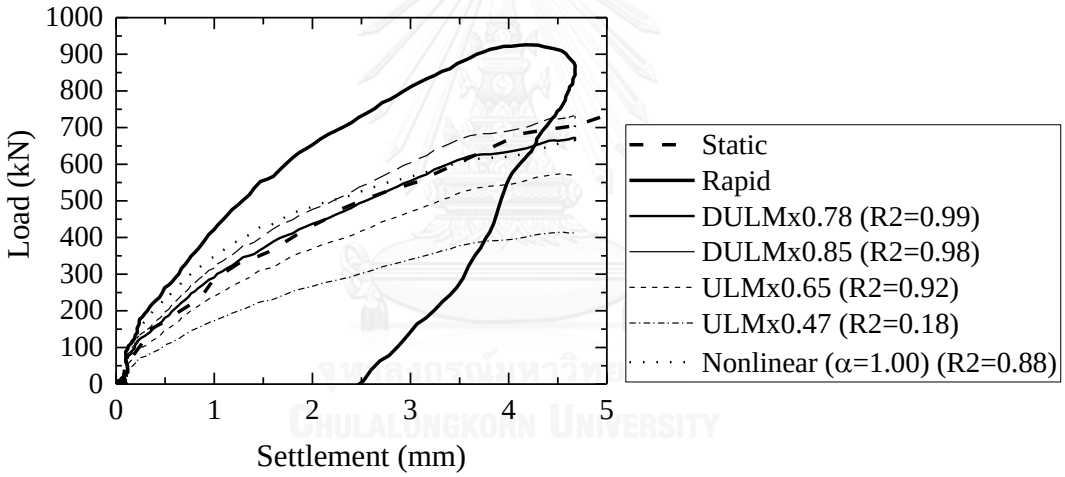

Figure 6 Comparison of predicted static capacity with measured (pile #1, loading cycle 2), driven concrete pile, Waddinxveen, Dutch.

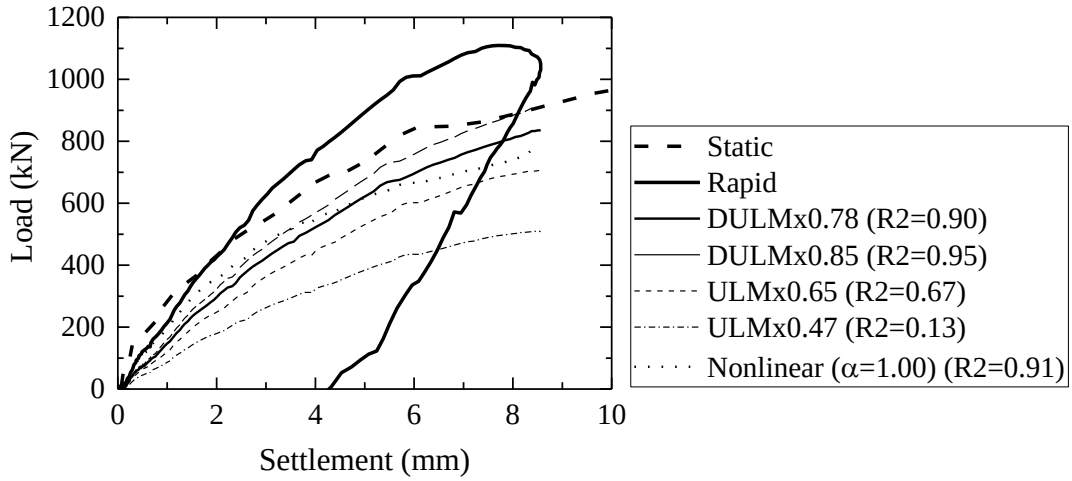

Figure 7 Comparison of predicted static capacity with measured (pile #1, loading cycle 4), driven concrete pile, Waddinxveen, Dutch.

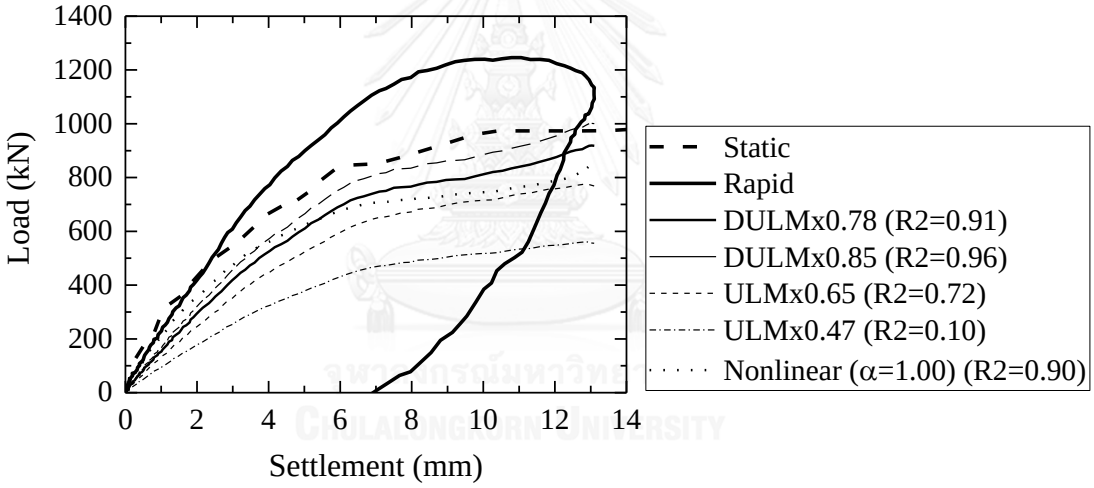

Figure 8 Comparison of predicted static capacity with measured (pile #1, loading cycle 5), driven concrete pile, Waddinxveen, Dutch.

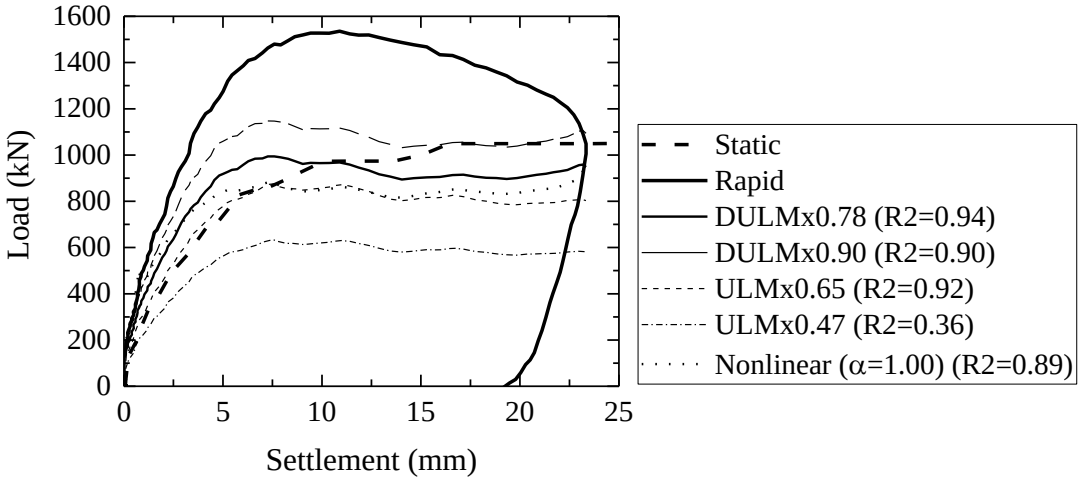

Figure 9 Comparison of predicted static capacity with measured (pile #1, loading cycle 6), driven concrete pile, Waddinxveen, Dutch.

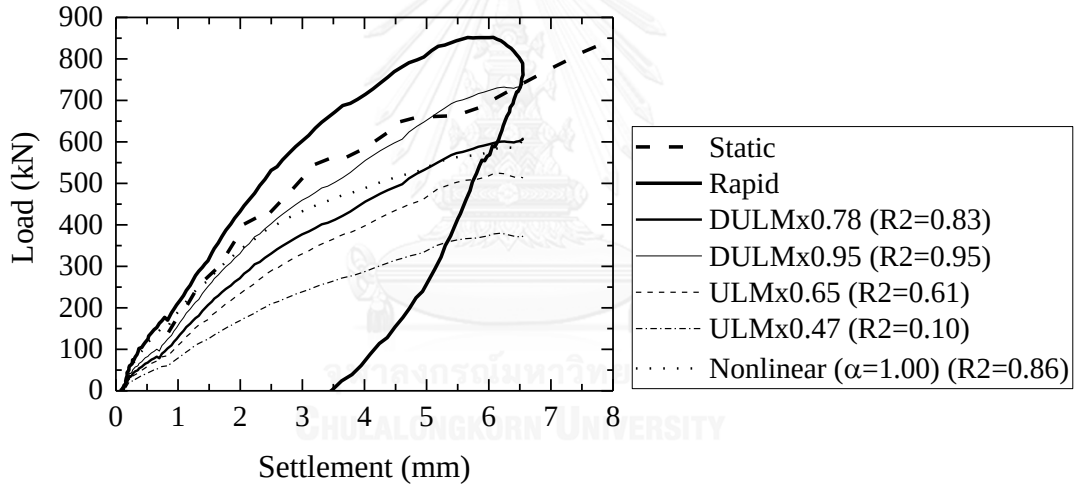

Figure10 Comparison of predicted static capacity with measured (pile #2, loading cycle 2), driven concrete pile, Waddinxveen, Dutch.

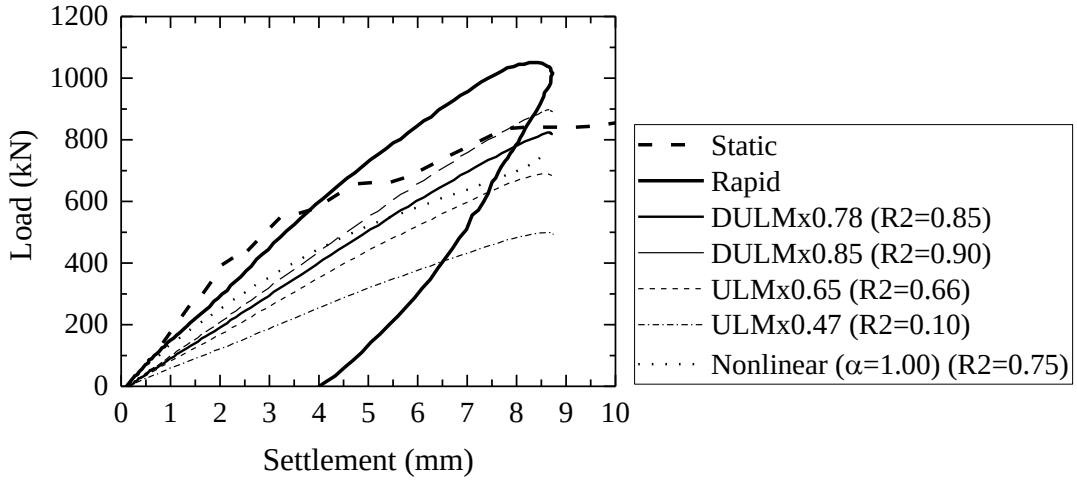

Figure11 Comparison of predicted static capacity with measured (pile #2, loading cycle 3), driven concrete pile, Waddinxveen, Dutch.

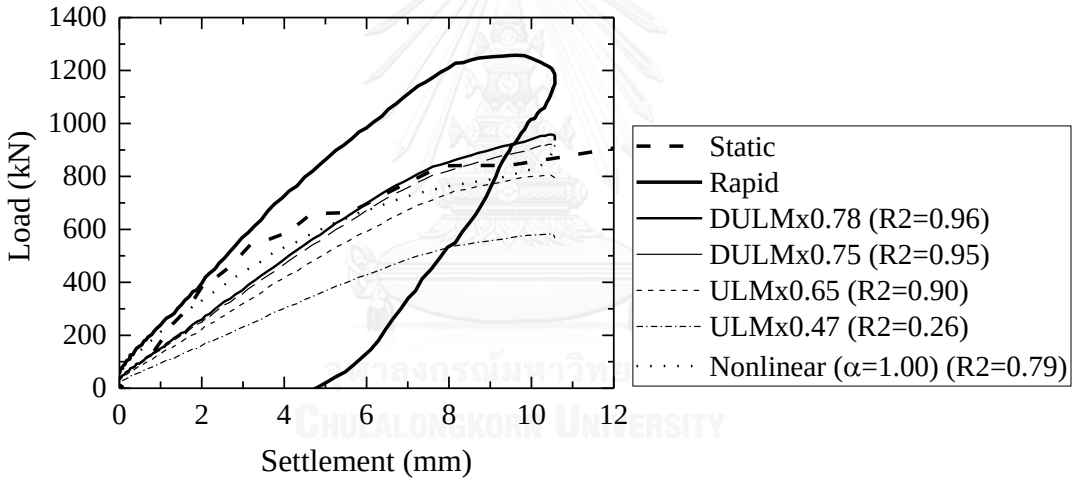

Figure12 Comparison of predicted static capacity with measured (pile #2, loading cycle 4), driven concrete pile, Waddinxveen, Dutch.

VITA

Lam Van Duc graduated with a bachelor degree in Civil Engineering and received a master degree in Geotechnical Engineering from Ho Chi Minh City University of Technology in 2010 and 2012, respectively. Since June 2013, he joined a Ph.D. program in Geotechnical Engineering at Chulalongkorn University supported by Chulalongkorn University. During his Ph.D. study, he has already submitted two papers for International Conference and one article for Géotechnique Letters Journal with his advisor. One of the papers received the Student Award for Outstanding Young Researcher from the Twenty-Seventh KKHTCNN Symposium on Civil Engineering in Shanghai, China.

His research interests include numerical analysis in geomechanics and pile load tests. He is a member of Vietnamese Geotechnical Society (VSSMGE).